音響OFDMを用いた水中通信の高性能化に関する研究

メタデータ	言語: 出版者: 琉球大学 公開日: 2016-11-07 キーワード (Ja): キーワード (En): 作成者: Tran, Hai Minh, チャン, ハイ ミン メールアドレス: 所属:
URL	http://hdl.handle.net/20.500.12000/35705

UNIVERSITY OF THE RYUKYUS

Underwater Wireless Communication using Acoustic OFDM

Tran Minh Hai

Graduate School of Engineering and Science

A thesis submitted to University of the Ryukyus
in partial fulfilment of the requirements for the degree of
Doctor of Engineering

August 2016

Acknowledgments

This thesis could not start without support from Prof. Tomohisa Wada who let me join the project on Underwater Wireless Communication (UAC). Performing experiments in Okinawa with researchers, Dr. Suzuki Taisaku, Dr. Rie Saotome has become the most memorable experiences with me. In Shizuoka, the huge barge where we can view Fuji mountain when doing experiments, that is the most beautiful bay I ever seen, and OKISEATEC company provides such great facilities. Without experiments, my understanding on acoustic OFDM systems is very vague and meaningless. It is a little stressful due to mismatches between equations, simulations and experiments, however, investigating the reasons behind the mismatches brings me insight knowledge. Most importantly, technical challenges arise during experiments are interesting research topics, and system performance evaluated through experiments is reliable. Once again, I would like to express my gratitude to my sensei, prof. Wada, Dr. Suzuki, Dr. Saotome and OKISEATEC company.

Abstract

In this thesis, we design and experiment an acoustic OFDM system for underwater wireless communication. (1) We disclose experimental results on Underwater Acoustic Communication (UAC) using acoustic OFDM, with data taken in sea in Okinawa and Shizuoka through many experiments since Oct. 2013. (2) We propose a symbol-by-symbol Doppler estimation and compensation for acoustic OFDM systems. The proposed system is robust to time varying Doppler rate and outperforms the conventional re-sampling method when velocity changes roughly over OFDM symbols. Overall, the proposed system utilizes a center frequency of 24kHz, and a bandwidth around 8kHz. The sub-carrier space is 93.75Hz and 46.875Hz for mode 2 and mode 3, respectively. The number of sub-carrier of mode 2 and mode 3 are 81 and 161, respectively. Experimental results taken in Okinawa, Shizuoka, Japan, show our system using QPSK, 16QAM, and 64QAM achieved a data throughput of 7.5Kbit/sec with a transmitter moving at maximum 2m/s, in a complicated trajectory, over 30m vertically. (3) In addition, we propose an iterative channel estimation and ICI cancellation for mobile OFDM receivers. This method is applicable to mobile OFDM systems, in which there are many multipath and each path has a different Doppler shift, provided that the maximum Dopller shift is less than 10% of the sub-carrier space.

Contents

Acknowledgments i
Abstract ii

List of Abbrevations viii

1 Introduction **1**
1.1 Review of Existing Systems 1
1.2 Target Application/Motivation 2
1.3 Contribution 3
1.4 Organization 4

2 Background **5**
2.1 Underwater Acoustic Transmission Channel 5
2.2 Basics of OFDM 7
2.2.1 Generation of OFDM Signal 7
2.2.2 Impact of Static Multipath Channel 8
2.2.3 Impact of Time Varying Channel 11
2.2.4 A Primitive OFDM Receiver 13
2.3 Impacts of Doppler Effect on Acoustic OFDM Systems 14
2.3.1 Time Compression/Expansion Caused by Doppler 14
2.3.2 Non-uniform Doppler shift Caused by Doppler 16

3 The Proposed Transceiver Architecture **18**
3.1 Overview 18
3.2 Transmitter 19
3.2.1 Data Frame Structure 19
3.2.2 Pilot Structure 20
3.2.3 Turbo Encoder 21
3.3 Receiver Architecture 22
3.3.1 Time and Frequency Synchronization 22
3.3.2 Review of Doppler Shift/Rate Estimation 22
3.3.3 Diversity Receiver 23
3.3.4 Impulsive Noise Cancellation 24
3.3.5 Turbo Decoder 24

4 Doppler Rate Estimation and Non-Uniform Doppler Compensation **27**
4.1 Introduction 27
4.2 Estimation of Doppler Rate/Doppler Shift 28
4.2.1 Existing Methods for Estimating Doppler 28
4.2.1.1 Using Cyclic Prefix 28
4.2.1.2 Linear Frequency Modulation (Chirp) Signal 30
4.2.2 Proposed Method for Estimating Doppler 31
4.2.2.1 Rough Estimation by Monitoring the drift of Power Delay Profile . . 31

4.2.2.2 Fine Estimation by using Continual Pilots . . . 32
4.2.2.3 Multi-Resampler . . . 33
4.3 Compensation Impacts of Doppler . . . 36
4.3.1 Existing Methods for Compensating Doppler . . . 36
4.3.1.1 Re-sampling in Time Domain . . . 36
4.3.1.2 A Simple Non-Uniform Phase Rotation . . . 38
4.3.2 Proposed non-uniform ICI cancellation . . . 39

5 Time Varying Channel Estimation and ICI Cancellation 41
5.1 Analysis of Time Varying Channel in OFDM . . . 41
5.2 Conventional Channel Estimation . . . 45
5.2.1 Interpolation using FIR Filter . . . 45
5.2.2 LMMSE Based Interpolation . . . 47
5.3 Proposed Channel Estimation and ICI Cancellation . . . 48
5.3.1 Iterative Channel Estimation and ICI Cancellation . . . 50
5.3.2 SALSA De-noising Channel Estimation . . . 50
5.3.3 Path-Searching Channel Estimation . . . 52
5.3.4 Combination of Path-Searching and Slope-Based ICI Cancellation . . . 57

6 Simulation and Experimental Results 59
6.1 Introduction . . . 59
6.2 Simulation Results . . . 60
6.2.1 Comparison Methods for Synchronization . . . 60
6.2.2 Comparison Methods for Doppler Rate/Shift Estimation . . . 60
6.2.3 Comparison Methods for compensation of non-uniform Doppler . . . 64
6.2.4 Comparison Methods for Channel Estimation and ICI Cancellation . . . 66
6.3 Experiments in Okinawa, Japan . . . 68
6.3.1 Experiments in Henoko Okinawa . . . 68
6.3.2 Experiments in Oujima Okinawa . . . 72
6.4 Experiments in Shizuoka, Japan . . . 73
6.4.1 Experiment Site and Setting . . . 73
6.4.2 Experimental Results . . . 78

7 Conclusion 85

Bibliography 86

List of Figures

1.1 An example of target application . . . 2
1.2 Thesis Organization . . . 3

2.1 sound absorption in the sea-water Michael&James model [1], temperature = 20^0C, pH =8, depth =1km, salinity = 35ppt . . . 5
2.2 freq. offset and time comp./exp. caused by Doppler, $fc = 24kHz, Fs = 96kHz, N_{sb} =$ 1536 samples . . . 6
2.3 a primitive ofdm transmitter . . . 7
2.4 OFDM implementation by DFT-spread . . . 8
2.5 Multipath channel . . . 9
2.6 8-FFT OFDM . . . 9
2.7 a premitive ofdm receiver . . . 13
2.8 Doppler effect . . . 14
2.9 expanded received signal due to Doppler . . . 15
2.10 tail of an OFDM symbol, expanded received signal due to Doppler . . . 15
2.11 non-uniform Doppler shift, $N_c = 81, f_0 = 93.75Hz, f_c = 24kHz$ . . . 16

3.1 Proposed Transceiver Architecture . . . 18
3.2 Data Frame Structure . . . 20
3.3 Pilot Pattern . . . 20
3.4 Turbo Encoder . . . 21
3.5 4-Diversity Receiver . . . 23
3.6 QPSK soft-demaping . . . 24
3.7 Turbo Decoding . . . 25

4.1 Power Delay Profile of TU Extended Model [10] . . . 29
4.2 ISI Power Over Samples of Guard Interval = 160 samples Ts . . . 29
4.3 Doppler rate estimation using Chirp pre/postample . . . 30
4.4 Proposed Doppler Estimation . . . 31
4.5 Drift of Power Delay Profile over ofdm symbols . . . 31
4.6 Proposed Multi-Resampler . . . 35
4.7 sinc interpolation for arbitrary rate re-sampling . . . 37
4.8 a bank of 64 FIR filters . . . 38

5.1 time varying channel impulse response of 1^{st} tap, $f_d = dop \times f_0$, 1280 samples/an OFDM symbol . . . 41
5.2 time varying channel transfer function of 10^{th} sub-carrier, $f_d = dop \times f_0$, two paths has same dop, 1280 samples/an OFDM symbol . . . 42
5.3 time varying channel transfer function of 10^{th} sub-carrier, $dop1 = dop, dop2 = dop \times cos(\pi/3)$, 1280 samples/an OFDM symbol . . . 42
5.4 raised cosine taps $f_{cut} = 0.5, \beta = 0.35$ . . . 46
5.5 transfer function of rs $f_{cut} = 0.5, \beta = 0.35$ . . . 47
5.6 LMMSE channel interpolation . . . 47

5.7 $|I(k \leftarrow l)|$ . . . 49
5.8 CNR due to ICI $10log(\frac{P_{sub}}{P_{ICI}})$ . . . 49
5.9 iterative channel estimation and ici cancellation . . . 50
5.10 improved channel estimation by de-noising . . . 51

6.1 LFM simulation . . . 61
6.2 LFM airtest . . . 61
6.3 two identical symbols airtest . . . 62
6.4 experiment setting/senario . . . 63
6.5 Doppler estimation (simulation) . . . 63
6.6 multi-resampler simulation . . . 64
6.7 multi-resampler simulation zoom in . . . 64
6.8 multi-resampler simulation . . . 65
6.9 compare our non-uniform doppler comp. vs. the simple phase rotation [2] . . . 65
6.10 comparison of channel estimation methods 1 . . . 67
6.11 comparison of channel estimation methods 2 . . . 68
6.12 SALAS de-noising BER 16QAM . . . 69
6.13 SALAS de-noising BER QAM . . . 69
6.14 transceiver for henoko experiment . . . 70
6.15 henoko experiment site . . . 70
6.16 henoko rx sign . . . 71
6.17 henoko delay profile . . . 71
6.18 henoko constellation 1 . . . 71
6.19 henoko constellation 2 . . . 72
6.20 Henoko Mode2 QPSK move 0.3 . . . 72
6.21 Henoko Mode 2 QPSK moving 0.9knot . . . 73
6.22 Henoko Mode2 QPSK no moving . . . 73
6.23 Henoko Mode3 QPSK moving 0.6knot . . . 74
6.24 Henoko Mode3 QPSK no moving . . . 74
6.25 Oujima experiment site . . . 75
6.26 Oujima experiment site . . . 75
6.27 Oujima rx signal . . . 75
6.28 Oujima delay profile . . . 76
6.29 Oujima constellation . . . 76
6.30 Oujima BER . . . 76
6.31 experiment site . . . 77
6.32 OKISEATEC Barge . . . 77
6.33 OKISEATEC moon pool . . . 77
6.34 performing experiments . . . 78
6.35 shizuoka experiment setting . . . 78
6.36 transceiver architecture for experiments in Shizuoka . . . 79
6.37 Shizuoka Doppler estimation . . . 79
6.38 Constellation . . . 80
6.39 Shizuoka Mode2 64QAM adaptive Doppler compensation . . . 81
6.40 Shizuoka Mode2 64QAM adaptive Doppler compensation . . . 81
6.41 Shizuoka Mode2 64QAM adaptive Doppler compensation . . . 82
6.42 Shizuoka Mode3 4QAM adaptive Doppler compensation . . . 82
6.43 Shizuoka Mode3 16QAM adaptive Doppler compensation . . . 83
6.44 Shizuoka Mode3 64QAM adaptive Doppler compensation . . . 83
6.45 compare our non-uniform Doppler comp. vs. re-sampling . . . 84
6.46 compare our non-uniform Doppler comp. vs. re-sampling . . . 84

List of Tables

1.1 Acoustic communication system in the past 10 years 1
1.2 Acoustic OFDM system in the past 10 years 1
1.3 Industrial acoustic communication systems 2

6.1 system parameters 60
6.2 parameters for multi-resampler 62
6.3 parameters for channel estimation and ICI cancellation 66
6.4 System parameters for SALAS de-noising simulation 67

List of Abbrevations

ADC	Analogue to Digital Converter
AWGN	Additive White Gaussian Noise
BER	Bit Error Rate
CFO	Carrier Frequency Offset
CIR	Channel Impulse Response
CNR	Carrier to Noise Ratio
CP	Cyclic Prefix
DAC	Digital to Analogue Converter
DFT	Discrete Fourier Transform
FEC	Forward Error Correction
Freq-IMP	Frequency Impulsive Noise Cancellation
FFT	Fast Fourier Transform
GI	Guard Interval
ICI	Inter Carrier Interference
I-ICI	Inverse Matrix Inter-Carrier Interference Cancellation
J-ICI	Jacobi Inter-Carrier Interference Cancellation
IFFT	Inverse Fast Fourier Transform
ISI	Inter Symbol Interference
LFM	Linear Frequency Modulation
LLR	Log-Likelihood Ratio
LMMSE	Linear Minimum Mean Square Error
MIMO	Multiple Input Multiple Output
ML	Maximum Likelihood
MRC	Maximum Ratio Combination
OFDM	Orthogonal Frequency Division Multiplexing
PDP	Power Delay Profile
QAM	Quadrature Amplitude Modulation
QPSK	Quadrature Phase Shift Keying
RS Filter	Raised Cosine Filter
SALSA	Split Augmented Lagrangian Shrinkage Algorithm
S-ICI	Slope Inter-Carrier Interference Cancellation
SIR	Signal to Interference Ratio
SOVA	Soft Output Viterbi Algorithm
SNR	Signal to Noise Ratio
SP	Scattered Pilot

T-IMP	Time Impulsive Noise Cancellation
UAC	Underwater Acoustic Communication
2D-DFT	Two Dimension Discrete Fourier Transform

Chapter 1

Introduction

1.1 Review of Existing Systems

In this chapter, we will review several Underwater Acoustic Communication (UAC) systems developed over the past decades. Depending target applications several acoustic systems were developed, and features of those systems are shown in Table 1.1, 1.2 and 1.3. As shown in Table 1.2, in recent 5 years, OFDM has been considered as a promising for acoustic communication, and several groups have putted great efforts developing and experimenting acoustic OFDM. These systems also consider Doppler estimation and compensation. The Doppler effect is a great challenge, so the moving speed can be

Table 1.1: Acoustic communication system in the past 10 years

developed by	application	channel	modulation	band	data rate
Oki Elec.,Ind. Comp. [3]	robot communication control	60m	16-QAM	BW 1MHz,	500kbps
JAMSTEC [4]	image transmission	6500m Vertical	4-DPSK	BW 8 kHz carrier 20kHz	16kbps
JAMSTEC [5, 6]	very long range communication	600km	Time-reversal, 16QAM, BPSK		450-550bps
WHOI [7, 8]	under ice, arctic, communication navigation	70-90km Vertical	FM sweep	BW 32Hz carrier 700Hz	5-10bps

Table 1.2: Acoustic OFDM system in the past 10 years

developed by	modulation	distance	moving speed	band	data rate
Newcastle University [9]	OFDM	200∼1000m	0.35m/s	BW: 4kHz, carrier 12kHz	∼ 3kbps
Northeastern University [10]	OFDM	3.5∼7km	0.5∼2m/s	BW 4883Hz, carrier 12.5 kHz	∼4.3-8.7kbps
Connecticut University [11]	OFDM	450∼1500m	1.5m/s	W 62.5kHz, carrier 110kHz	∼125.7kbps
Connecticut University [12]	OFDM	100∼600m	5.14m/s	BW 12kHz carrier 27kHz	10.52∼14.55kbps

TABLE 1.3: Industrial acoustic communication systems

developed by	product id	modulation	distance	band	data rate
Evologics [13]	S2CR S2CM	Sweep-Spread Carrier Signal	0.3-8km	7-17,kHz, 13-24,kHz, 18-34kHz, 42-65kHz, 48-78kHz	9.2-62.5kpbs
Teledyne [14]	ATM-900	OFDM	2-6km	9-14kHz, 16-21kHz, 22-27 kHz	14-15kpbs
Aquasent [15]	AM-OFDM-13A, AM-D2000	OFDM	0.2∼2km	9-15 kHz, 21-27kHz	1,500-9,375bps

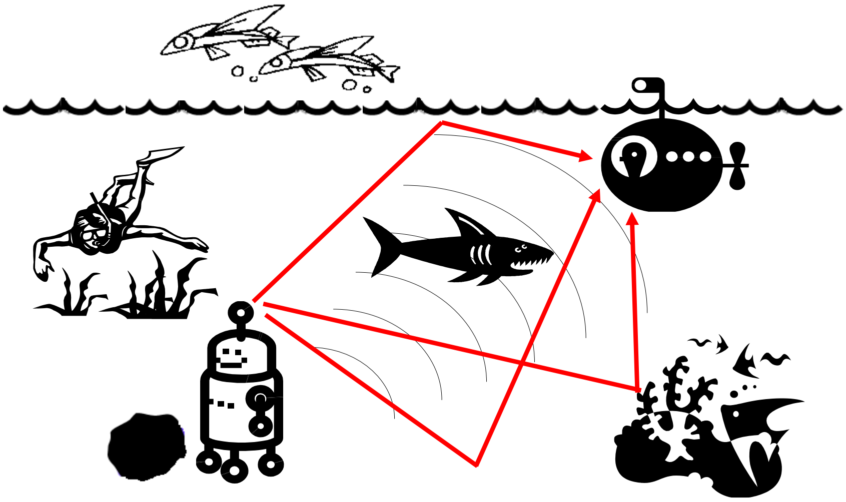

FIGURE 1.1: An example of target application

supported in state-of-the-art system is quite limited. Papers [11, 12] achieves the most impressive results when it can operates under a moving speed of 5.14m/s. However, it is noted that those papers utilize an array of 12 receiver elements, the modulation is QPSK and require high computation cost consiting of resampling in time domain, 2D sparse channel estimation [16] (2D dictionary).

1.2 Target Application/Motivation

Though demands for underwater wireless communication currently is not huge as radio wireless communication in the air, UAC promises to support and facilitate new industries, applications, such as deep sea mining, deep sea data collecting, sub-marine communication, navigation and so on. Therefore, research on UAC is a promising topic. In fact, recently researchers have been putting great effort in acoustic OFDM that is considered a strong solution considering both data speed and hardware implementation feasibility. Our studies on acoustic OFDM provide a platform to implement different acoustic OFDM systems specializing to different applications. In addition, we particularly focus on the communication in vertical direction such as supporting communication between a robot at the sea bottom and a ship in the sea surface. Figure 1.1 shows this target application.

1.3 Contribution

The contributions of this thesis are:

(1) Disclose experiments results on UAC using acoustic OFDM, with data taken in sea in Okinawa and Shizuoka through many experiments.

(2) Propose methods for estimation of time vary Doppler rate/shift. A method for estimation and compensat ion of Doppler (rate/shift) symbol-by-symbol in acoustic OFDM systems is published in [17, 18, 19].

(3) Propose methods for channel estimation and ICI cancellation. An iterative channel estimation and ICI cancellation is published in [20, 21]. ICI (inter-carrier interference caused by Doppler effect in UAC (Underwater Acoustic Communication) is more severe than in radio wireless systems, therefore, methods for channel estimation under high ICI and methods for ICI cancellation play an important role in acoustic OFDM systems.

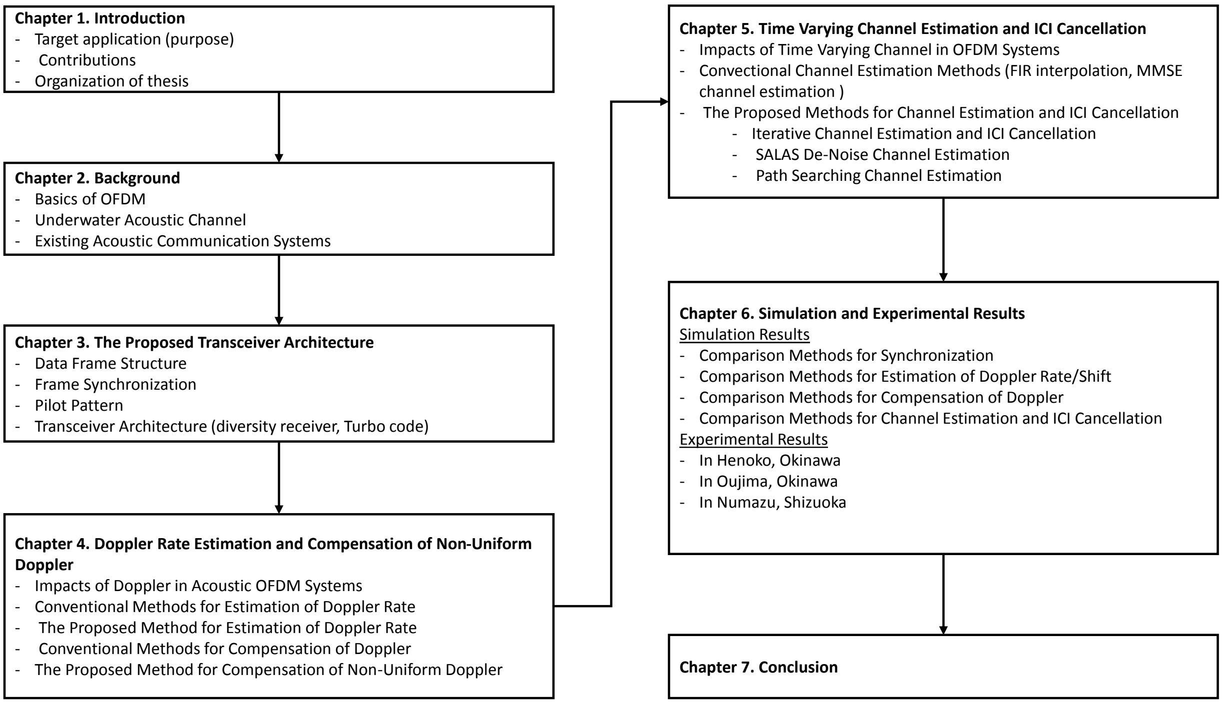

FIGURE 1.2: Thesis Organization

1.4 Organization

The thesis is organized as follow. Chapter 2 presents our proposed transceiver architecture. Chapter 3 explains impacts of channel on acoustic OFDM systems. In this chapter, we will model the acoustic transmission channel consisting multipath and Doppler effect. Also, we figure out impacts of Doppler on acoustic OFDM system. Chapter 4 is the highlights of this thesis, in which, we review state-of-the-art methods for Doppler estimation and compensation, and propose our solutions. Chapter 5 shows simulation results, and compare our methods against existing methods for Doppler estimation and compensation, channel estimation and ICI cancellation. Chapter 6 presents experimental results including three main parts. The first part show results taken in a non-reflection pool to verify our system compared with theoretical performance of OFDM systems. The second part shows experimental results taken in sea in Okinawa. The final part is experimental results taken in sea in Shizuoka.

Chapter 2

Background

In this chapter, we discuss characteristics of underwater acoustic channel and its impacts on acoustic OFDM systems. Our interest is channel for short and medium range communication (several hundered meters to several kilometers) in shallow sea. So the frequnce band of interest is around 25kHz. According to [1, 22], the attenuation of sound in the water is a function of frequency as figure2.1.

2.1 Underwater Acoustic Transmission Channel

The first characteristic is frequency-dependent acoustic attenuation. This characteristic is shown in figure 2.1. Overall, the low frequency can propagate over very long distance, however, low frequency

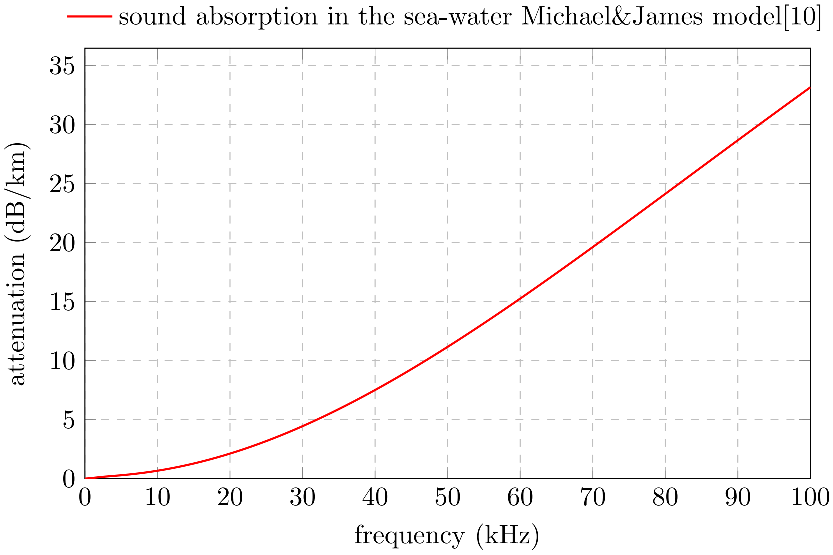

Figure 2.1: sound absorption in the sea-water Michael&James model [1], temperature = 20^0C, pH =8, depth =1km, salinity = 35ppt

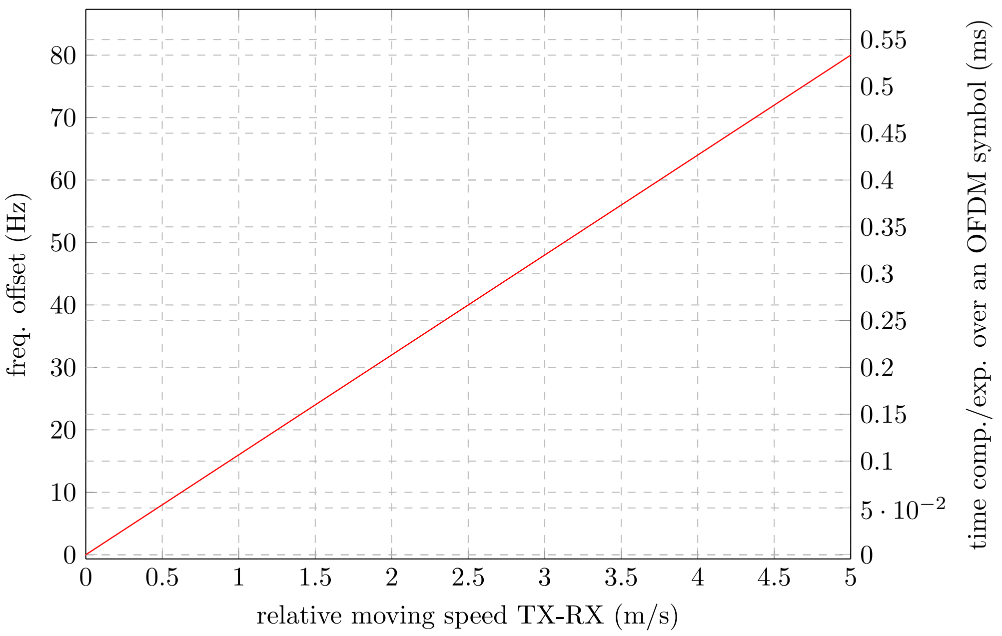

FIGURE 2.2: freq. offset and time comp./exp. caused by Doppler, $fc = 24kHz, Fs = 96kHz, N_{sb} =$ 1536 samples

range only support low data rate. In contrast, high frequency attenuates quickly over short distance, but enables high data rate. For short and medium range communication (from several hundred meters to several kilometers), carrier frequency around 24kHz to 27kHz is preferred.

Second, UAC (Underwater Acoustic Communication)channel also experiences multipath as radio in the air. However, due to slow propagation speed of sound 1500(m/s), the delay spread is severe than in radio wireless. For example, the difference in distance between a light of sight path and a delay path is 7.5m. This delay happens a transducer operates around 3 to 4m depth, and the delay path is due to surface reflection. So the equivalent delay is 5ms which is 31.25% of an OFDM symbol length in our system (16ms). On the other hand, in LTE-4G system, the extended CP (Cyclic Prefix) is 25% of an OFDM symbol.

Third, the slow propagation speed 1500m/s also causes severe Doppler effect. For example, considering an acoustic OFDM system operating at carrier frequency of 24kHz, a relative moving between transmitter and receiver of 1.5m/s causes a Doppler shift of 24Hz which is 25% of a sub-carrier (96.375Hz) in our system. State-of-the-art OFDM radio wireless system currently support a maximum Doppler spread about 10% of a sub-carrier space. For example, LTE-4G operates around 2GHz, and supports a receiver moving at 500km/h which causes Doppler shift of 920Hz or 6.1% of a sub-carrier ($f_0 = 15kHz$).

In addition, acoustic OFDM systems usually are wideband systems since bandwidth is compatible to carrier frequency. For instance, our system bandwidth is around 8kHz which is 1/3 of carrier frequency 24kHz. Therefore, each sub-carrier experiences a difference amount of frequency offset caused by Doppler. This is called non-uniform Doppler in [2, 11, 12, 17, 18, 19]. In the time domain, the time compression/expansion due to Doppler is significant. For example, under a moving speed of 1.5m/s, the time compression/expansion due to Doppler is 1 sample period (an OFDM symbol consist of 1536 samples). Different from familiar radio OFDM systems, the non-uniform Doppler and the time compression/expansion are new challenges in acoustic OFDM systems. Frequency offset and time compression/expansion caused by Doppler are shown in figure 2.2.

2.2 Basics of OFDM

2.2.1 Generation of OFDM Signal

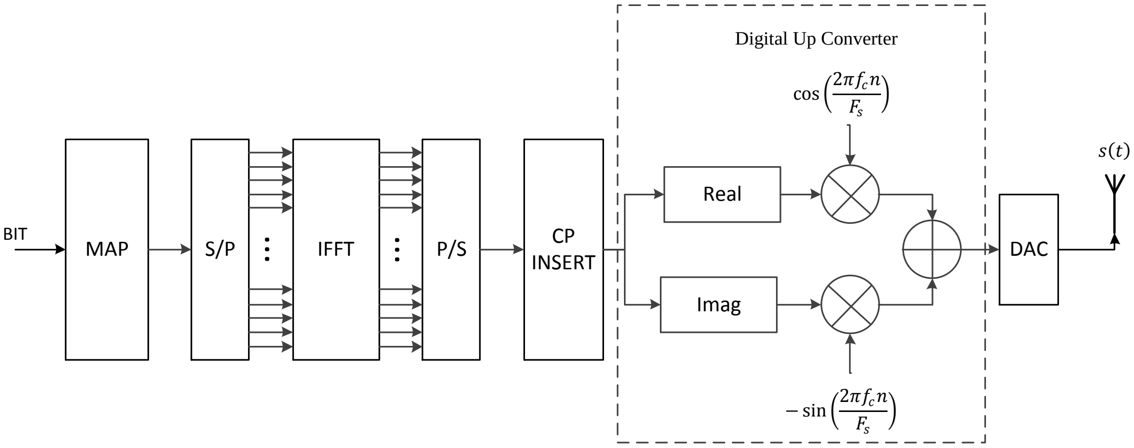

Figure 2.3: a primitive ofdm transmitter

Figure 2.3 is diagram of a primitive OFDM transmitter. The OFDM signal is a case of multi-carrier modulation and the complex baseband OFDM signal can be written as

$$S_B(t) = \sum_{k=0}^{N_c-1} D_k e^{j2\pi(kf_0)t} \tag{2.1}$$

Here, N_c is the number of sub-carriers carrying digital modulation symbol D_k. Since direct implementation of this equation needs N_c oscillators, it is not easy to implement. The breakthrough is implementation of OFDM by FFT. If the signal $S_B(t)$ is sampled within a period $1/f_0 = T_0$ with a sampling speed of $F_s = Nf_0$, then equation (2) is re-written as

$$S_B(n) = \sum_{k=0}^{N-1} D_k e^{\frac{j2\pi kn}{N}} \tag{2.2}$$

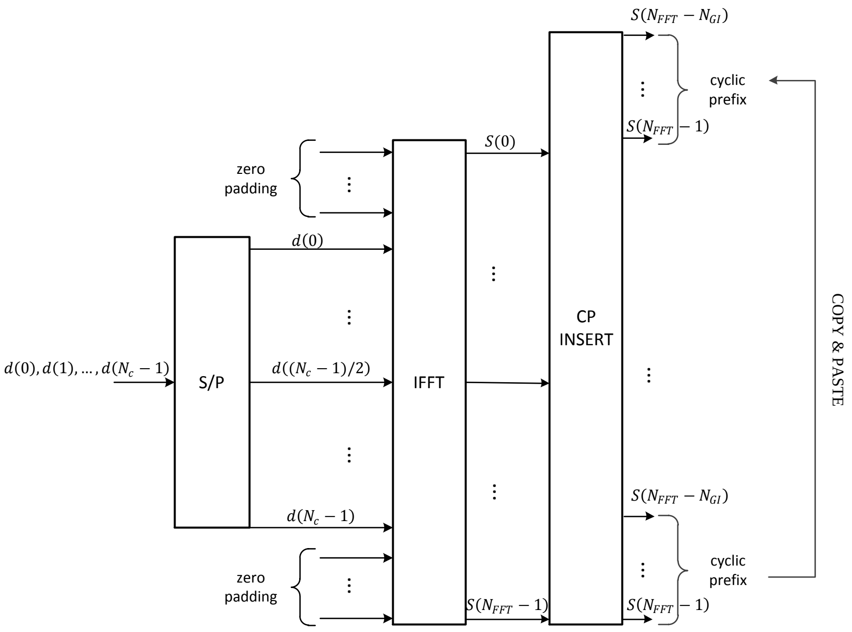

Figure 2.4: OFDM implementation by DFT-spread

This equation is the same as IFFT of sequence D_k. It is noted that N is FFT point and N_c is the number of sub-carrier actually carrying information D_k. $(N - N_c)$ are zero padded, and this scheme is called DFT-spread as shown in figure 2.4. After cyclic prefix (CP) insertion, up-conversion and digital to analog conversion the transmitted can be written as

$$S(t) = Real\left\{ \sum_{k=0}^{N-1} D_k e^{j2\pi(f_c + kf_0)t} \right\}, -T_{GI} \leq t \leq T_0 \tag{2.3}$$

Here, T_{GI} is guard interval (GI)length, and total of samples of an OFDM symbol is $(N + N_{GI})$.

2.2.2 Impact of Static Multipath Channel

The transmitted signal goes through mutlipath channel as illustrated in figure 2.5. To mitigate impacts of multipath channel, guard interval is inserted in OFDM symbols. The guard interval is generated by copy portion of an OFDM symbol at the end, and paste to the head of an OFDM symbol as in figure 2.4. This scheme is called cyclic prefix. The cyclic prefix has twofold, one is preventing inter-symbol-interference (ISI) and the other is ensuring impact of multipath channel can be represented by an circular matrix in time domain. Then, in frequency domain, the circular matrix turns into a diagonal matrix. Therefore, channel estimation and equalization can be done in frequency domain conveniently.

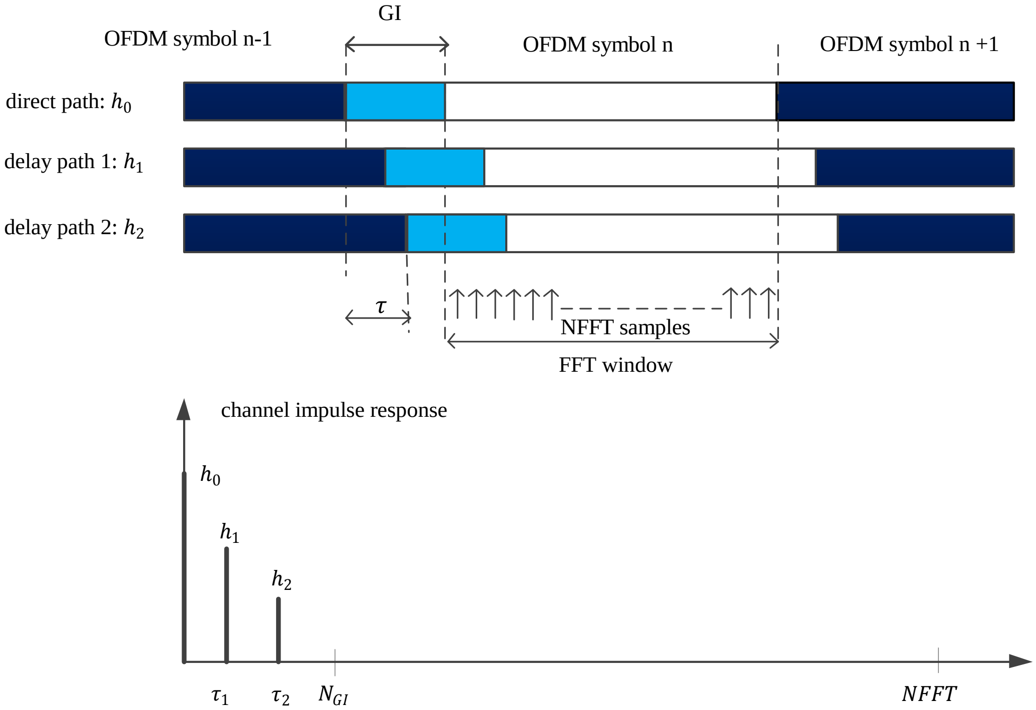

FIGURE 2.5: Multipath channel

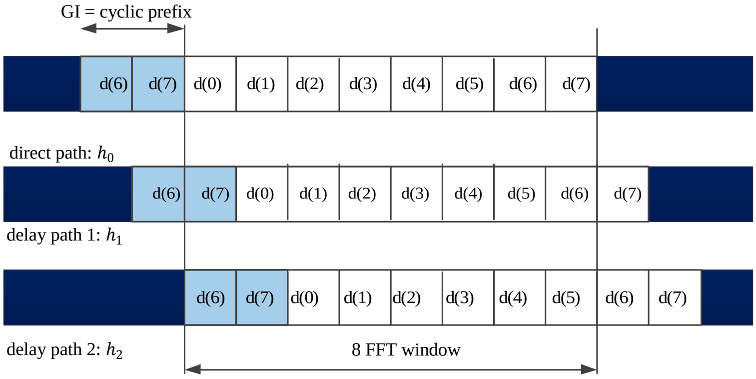

FIGURE 2.6: 8-FFT OFDM

Let's consider and example of an 8-point FFT OFDM is shown in figure 2.6. The matrix equation of (2.4) shows time domain signal $y[n]$ is output of the multipath channel and $d[n]$ is input of the channel. Here, $w[n]$ is time domain additive noise.

$$\begin{bmatrix} y(0)\\ y(1)\\ y(2)\\ y(3)\\ y(4)\\ y(5)\\ y(6)\\ y(7) \end{bmatrix} = \underbrace{\begin{bmatrix} h_0 & 0 & 0 & 0 & 0 & 0 & h_2 & h_1\\ h_1 & h_0 & 0 & 0 & 0 & 0 & 0 & h_2\\ h_2 & h_1 & h_0 & 0 & 0 & 0 & 0 & 0\\ 0 & h_2 & h_1 & h_0 & 0 & 0 & 0 & 0\\ 0 & 0 & h_2 & h_1 & h_0 & 0 & 0 & 0\\ 0 & 0 & 0 & h_2 & h_1 & h_0 & 0 & 0\\ 0 & 0 & 0 & 0 & h_2 & h_1 & h_0 & 0\\ 0 & 0 & 0 & 0 & 0 & h_2 & h_1 & h_0 \end{bmatrix}}_{h-channel impulse response-circular matrix} \times \begin{bmatrix} d(0)\\ d(1)\\ d(2)\\ d(3)\\ d(4)\\ d(5)\\ d(6)\\ d(7) \end{bmatrix} + \begin{bmatrix} w(0)\\ w(1)\\ w(2)\\ w(3)\\ w(4)\\ w(5)\\ w(6)\\ w(7) \end{bmatrix} \tag{2.4}$$

Using FFT matrix $[F]_{N\times N}$, the equation (2.4) can be transformed into frequency domain as follows.

$$[F][y] = \Big([F][h][F]^{-1}\Big)[F][d] \tag{2.5}$$

$$[Y] = [H][D] \tag{2.6}$$

$$[H] = [F][h][F]^{-1} \tag{2.7}$$

$$\begin{bmatrix} Y(0)\\ Y(1)\\ Y(2)\\ Y(3)\\ Y(4)\\ Y(5)\\ Y(6)\\ Y(7) \end{bmatrix} = \underbrace{\begin{bmatrix} H_0 & 0 & 0 & 0 & 0 & 0 & 0 & 0\\ 0 & H_1 & 0 & 0 & 0 & 0 & 0 & 0\\ 0 & 0 & H_2 & 0 & 0 & 0 & 0 & 0\\ 0 & 0 & 0 & H_3 & 0 & 0 & 0 & 0\\ 0 & 0 & 0 & 0 & H_4 & 0 & 0 & 0\\ 0 & 0 & 0 & 0 & 0 & H_5 & 0 & 0\\ 0 & 0 & 0 & 0 & 0 & 0 & H_6 & 0\\ 0 & 0 & 0 & 0 & 0 & 0 & 0 & H_7 \end{bmatrix}}_{H-channel transfer function-diagonal matrix} \times \begin{bmatrix} D(0)\\ D(1)\\ D(2)\\ D(3)\\ D(4)\\ D(5)\\ D(6)\\ D(7) \end{bmatrix} + \begin{bmatrix} W(0)\\ W(1)\\ W(2)\\ W(3)\\ W(4)\\ W(5)\\ W(6)\\ W(7) \end{bmatrix} \tag{2.8}$$

Here, Y and D is received and transmitted data symbol in frequency domain. W denotes random noise in frequency domain, and H is channel transfer function. Therefore, using cyclic prefix channel transfer function H becomes a diagonal matrix.

Assuming frequency domain noise W is negligible, and $\hat{H}$ is the estimated channel transfer function, the transmitted data symbol can be recovered as follows

$$\begin{bmatrix}\hat{D}(0)\\ \hat{D}(1)\\ \hat{D}(2)\\ \hat{D}(3)\\ \hat{D}(4)\\ \hat{D}(5)\\ \hat{D}(6)\\ \hat{D}(7)\end{bmatrix} = \underbrace{\begin{bmatrix}\frac{1}{\hat{H}_0} & 0 & 0 & 0 & 0 & 0 & 0 & 0\\ 0 & \frac{1}{\hat{H}_1} & 0 & 0 & 0 & 0 & 0 & 0\\ 0 & 0 & \frac{1}{\hat{H}_2} & 0 & 0 & 0 & 0 & 0\\ 0 & 0 & 0 & \frac{1}{\hat{H}_3} & 0 & 0 & 0 & 0\\ 0 & 0 & 0 & 0 & \frac{1}{\hat{H}_4} & 0 & 0 & 0\\ 0 & 0 & 0 & 0 & 0 & \frac{1}{\hat{H}_5} & 0 & 0\\ 0 & 0 & 0 & 0 & 0 & 0 & \frac{1}{\hat{H}_6} & 0\\ 0 & 0 & 0 & 0 & 0 & 0 & 0 & \frac{1}{\hat{H}_7}\end{bmatrix}}_{\hat{H}-estimated-channeltransferfunction} \times \begin{bmatrix}Y(0)\\ Y(1)\\ Y(2)\\ Y(3)\\ Y(4)\\ Y(5)\\ Y(6)\\ Y(7)\end{bmatrix} \tag{2.9}$$

2.2.3 Impact of Time Varying Channel

Due to relative moving between transmitter and receiver, or dynamic of channel itself, the channel impulse response $[h]$ changes within an OFDM symbol. As a result, the channel matrix $[h]$ is not a circular matrix, and channel transfer function matrix $[H]$ is not a diagonal matrix. For example, assuming that $[h]$ change linearly within an OFDM symbol as

$$h_i(n) = \bar{h_i} + \delta_i n, \quad \frac{-N}{2} \leq n \leq \frac{N}{2} \tag{2.10}$$

Here, $h_i(n)$ is time varying path i, and slope δ_i quantifies how fast the path changes in time.

$$\delta_i \approx \frac{2\pi f_{di}}{N} \tag{2.11}$$

Here, f_{di} is the Doppler shift of path i. The channel impulse response matrix is re-written as

$$\begin{aligned}
&\underbrace{\begin{bmatrix}
\bar{h}_0 & 0 & 0 & 0 & 0 & 0 & \bar{h}_2 & \bar{h}_1 \\
\bar{h}_1 & \bar{h}_0 & 0 & 0 & 0 & 0 & 0 & \bar{h}_2 \\
\bar{h}_2 & \bar{h}_1 & \bar{h}_0 & 0 & 0 & 0 & 0 & 0 \\
0 & \bar{h}_2 & \bar{h}_1 & \bar{h}_0 & 0 & 0 & 0 & 0 \\
0 & 0 & \bar{h}_2 & \bar{h}_1 & \bar{h}_0 & 0 & 0 & 0 \\
0 & 0 & 0 & \bar{h}_2 & \bar{h}_1 & \bar{h}_0 & 0 & 0 \\
0 & 0 & 0 & 0 & \bar{h}_2 & \bar{h}_1 & \bar{h}_0 & 0 \\
0 & 0 & 0 & 0 & 0 & \bar{h}_2 & \bar{h}_1 & \bar{h}_0
\end{bmatrix}}_{\bar{h}-circularmatrix} \\
&+\underbrace{\begin{bmatrix}
-3.5\delta_0 & 0 & 0 & 0 & 0 & 0 & -3.5\delta_2 & -3.5\delta_1 \\
-2.5\delta_1 & -2.5\delta_0 & 0 & 0 & 0 & 0 & 0 & -2.5\delta_2 \\
-1.5\delta_2 & -1.5\delta_1 & -1.5\delta_0 & 0 & 0 & 0 & 0 & 0 \\
0 & -0.5\delta_2 & -0.5\delta_1 & -0.5\delta_0 & 0 & 0 & 0 & 0 \\
0 & 0 & 0.5\delta_2 & 0.5\delta_1 & 0.5\delta_0 & 0 & 0 & 0 \\
0 & 0 & 0 & 1.5\delta_2 & 1.5\delta_1 & 1.5\delta_0 & 0 & 0 \\
0 & 0 & 0 & 0 & 2.5\delta_2 & 2.5\delta_1 & 2.5\delta_0 & 0 \\
0 & 0 & 0 & 0 & 0 & 3.5\delta_2 & 3.5\delta_1 & 3.5\delta_0
\end{bmatrix}}_{slope[\delta]-non-circularmatrix}
\end{aligned} \tag{2.12}$$

In frequency domain, received signal is written as

$$[Y] = [F]\Bigg([\bar{h}] + [\delta]\Bigg)[F]^{-1}[D] \tag{2.13}$$

The conventional channel transfer function is

$$[H] = [F]\Bigg([\bar{h}] + \Bigg)[F]^{-1} \tag{2.14}$$

The slope $[\delta]$ shows how fast the channel changes in time domain, and ICI power distribution across sub-carrier is represented the ICI matrix as

$$[I] = [F][\delta][F^{-1}] \tag{2.15}$$

Finally, the received data symbol $[Y]$ can be written as

$$[Y]([H] + [I])[D] \tag{2.16}$$

2.2.4 A Primitive OFDM Receiver

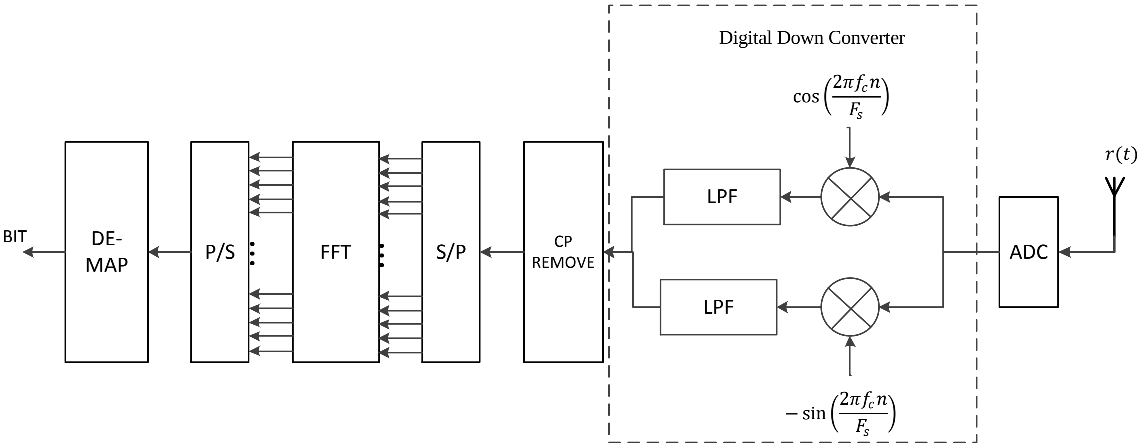

FIGURE 2.7: a premitive ofdm receiver

As shown in figure 2.7, after sampling (ADC), down-conversion, and cp removal, OFDM demodulation is performed by FFT. Under the assumption that delay spread of channel is smaller than guard interval, and the channel is unchanged within an OFDM symbol, after FFT demodulation, the signal can be written as

$$Y(k) = H(k)D(k) + W(k) \tag{2.17}$$

Here, $H(k)$ is channel transfer function caused by multipath channel. $W(k)$ is random noise. Assuming that the channel consist of L delay paths (no-changed within an OFDM symbol), the relationship between $H(k)$ and $h(\tau)$ is

$$[H] = [F][h] \tag{2.18}$$

Here, $[F]_{N\times N}$ is FFT matrix. Preferably, channel estimation and equalization in OFDM system are performed in the frequency domain due to its convenient. Channel transfer function at pilot positions are computed as

$$\hat{H}(k_p) = \frac{Y(k_p)}{X(k_p)} \tag{2.19}$$

Here, k_p is pilot index, $X(k_p)$ and $Y(k_p)$ are pilot symbols and received pilot, respectively.

$$\hat{H}(k_p) = H(k_p) + \frac{W(k_p)}{X(k_p)} \tag{2.20}$$

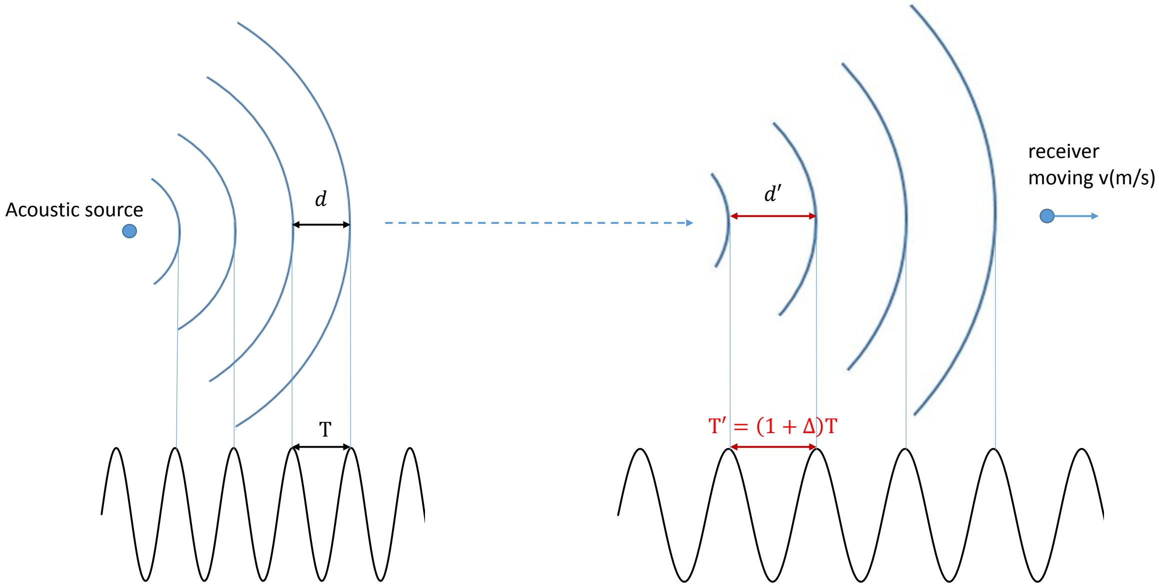

Figure 2.8: Doppler effect

Channel transfer function at all sub-carrier index k can be found through interpolating $\hat{H}(k_p)$ as in [23, 24, 25, 26].

2.3 Impacts of Doppler Effect on Acoustic OFDM Systems

Overall, Doppler effect causes two challenges in acoustic OFDM systems. First, different from radio wireless OFDM systems, in acoustic OFDM systems, the signal wave form is compressed/expanded in time domain. Second, Doppler causes frequency offset and results in ICI (inter-carrier-interference) since orthogonality among sub-carriers is lost. The second impact also can be considered through point of view of time varying channel. For example, if the channel impulse response h_0, h_1, h_2 changes within an OFDM symbol, then, Fourier transform of $[h]$ will not be a diagonal matrix.

2.3.1 Time Compression/Expansion Caused by Doppler

First, we consider impact of Doppler effect in time domain. In acoustic communication, many papers assumes that all delay paths has a common/dominated Doppler rate caused by moving between transmitters and receivers. Under this assumption, the received signal is written as

$$R(t) = \sum_{i=1}^{L} A_i S\Big((1+\Delta+\delta_i)(t-\tau_i)\Big) \tag{2.21}$$

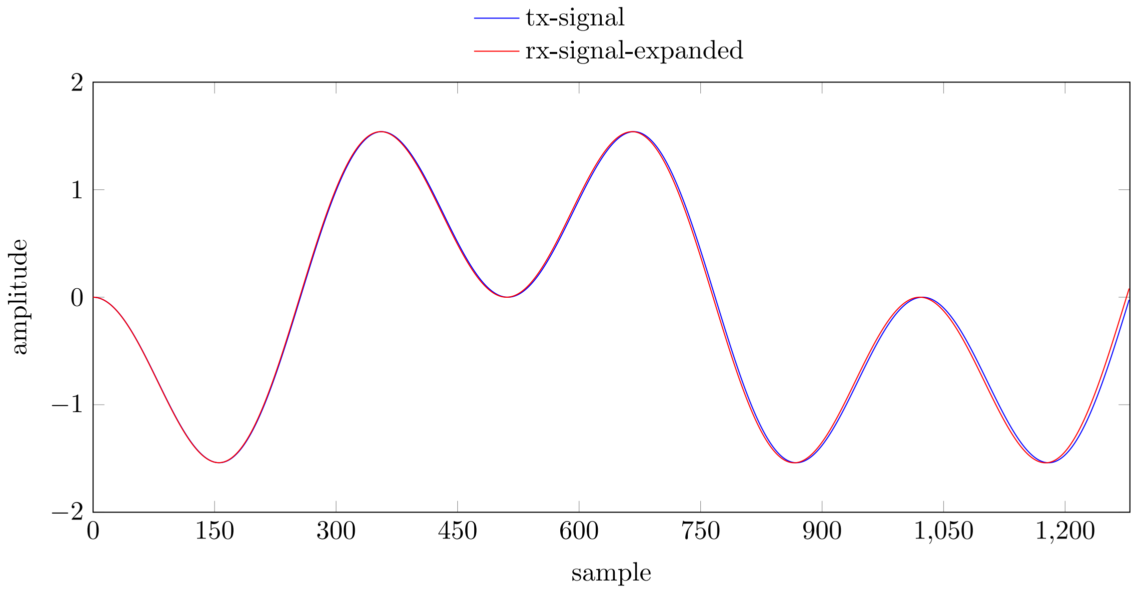

FIGURE 2.9: expanded received signal due to Doppler

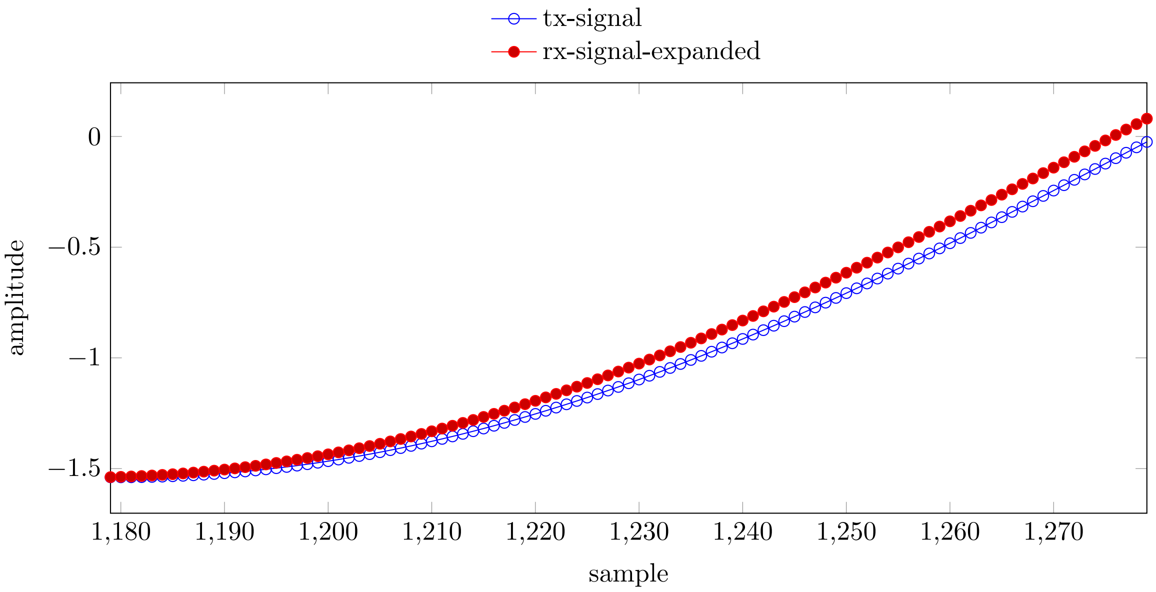

FIGURE 2.10: tail of an OFDM symbol, expanded received signal due to Doppler

$$\Delta = \frac{v}{C}, C \approx 1500m/s \tag{2.22}$$

Here, A_i, τ_i and $(\Delta + \delta_i)$ is attenuation, delay and Doppler rate of path i^{th}. There are L paths, and Doppler rate of each path has a variation of $\delta << \Delta$, and v is relative speed between a transmitter and a receiver. At the receiver side, signal is sampled at a speed of F_s such as 96kHz in our system.

$$R(n) = \sum_{i=1}^{L} A_i S\Big((1 + \Delta + \delta_i)(nT_s - \tau_i)\Big) \tag{2.23}$$

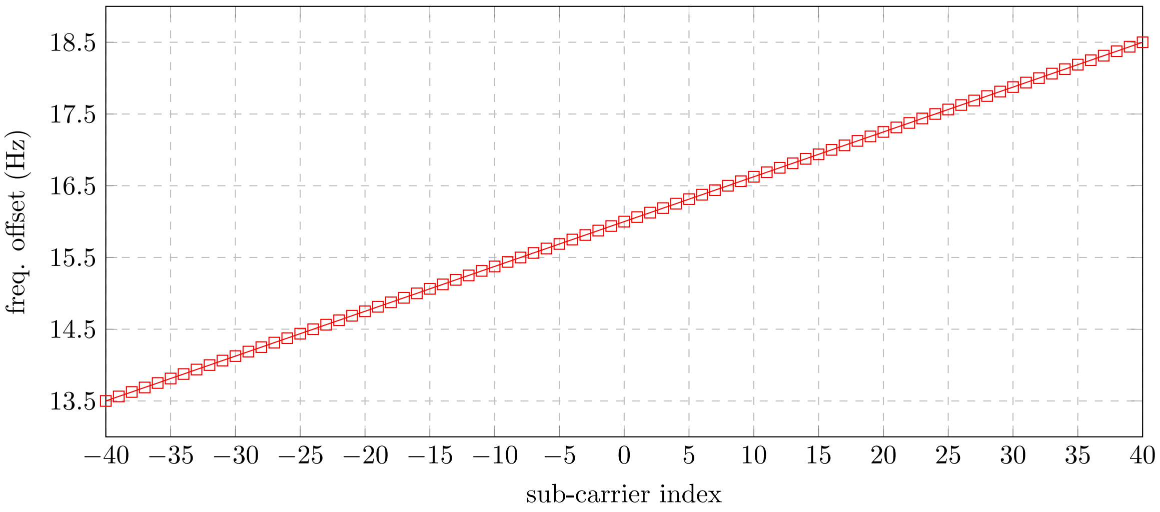

FIGURE 2.11: non-uniform Doppler shift, $N_c = 81, f_0 = 93.75Hz, f_c = 24kHz$

When $\Delta > 0$, the waveform signal is compressed, and when $\Delta < 0$ the signal is compressed. This phenomenon is equivalent to a sampling clock offset as

$$F_s' = \frac{F_s}{(1 + \Delta)} \tag{2.24}$$

Figure 2.8 gives an example signal in case of expansion. As shown in figure 2.9 and figure 2.10 due to the expansion, the head and the tail of an OFDM symbol (cyclic prefix and its copied portion) are mismatched. The second impact is the drift of FFT window over OFDM symbols. Finally, some samples will be lost, or some unwanted samples will be added to an OFDM symbol due to compression/expansion.

2.3.2 Non-uniform Doppler shift Caused by Doppler

In frequency domain, Doppler causes frequency offset. Since system bandwidth is close to carrier frequency, OFDM systems are considered as wideband systems, and each subcarrier experiences a different amount of frequecy offset as shown in figure 2.11. This is called non-uniform Doppler in [2, 11, 12, 17, 18, 19]. When frequency offset happens, orthogonality among sub-carriers lost, and ICI appears. We denotes $R(t)$ is the received signal in time domain. Channel consists of L paths, each path has an attenuation of A_i, and all paths has a Doppler rate of Δ. $D(k)$ and $Y(k)$ are transmitted and received data at sub-carrier k, respectively.

$$R(t) = \sum_{i=1}^{L} \sum_{k=0}^{N-1} A_i D(k) e^{j2\pi(f_c + kf_0)(1+\Delta)(t-\tau_i)} \tag{2.25}$$

Provided that all paths has the same Doppler rate Δ, after down-conversion we can re-write the above equation as

$$R_B(t) = \sum_{i=1}^{L} \sum_{k=0}^{N-1} A_i D(k) e^{j2\pi\left(kf_0+(f_c+kf_0)\Delta\right)t} e^{-j2\pi(fc+kf_0)(1+\Delta)\tau_i} \tag{2.26}$$

We denote

$$H(k) = \sum_{i=1}^{L} A_i e^{-j2\pi(f_c+kf_0)(1+\Delta)\tau_i} \tag{2.27}$$

Finally, we get

$$R_B(t) = \sum_{k=0}^{N-1} H(k)D(k) \underbrace{e^{j2\pi\left(kf_0+(f_c+kf_0)\Delta\right)t}}_{non-Dopp} \tag{2.28}$$

After FFT,

$$Y(k) = H(k)D(k) \underbrace{\frac{1}{N} \sum_{n=0}^{N-1} e^{-j2\pi(\frac{fc}{f0}\Delta+k\Delta)\frac{n}{N}}}_{phase-rotation} + \underbrace{\frac{1}{N} \sum_{\substack{l=0 \\ l\neq k}}^{N-1} \sum_{n=0}^{N-1} H(l)D(l)e^{-j2\pi(l-k+\frac{fc}{f0}\Delta+l\Delta)\frac{n}{N}}}_{ICI} \tag{2.29}$$

Here, $D(k)$ and $Y(k)$ are transmitted and received symbol at sub-carrier k, respectively. $H(k)$ is the channel transfer function, and Δ is the Doppler rate. N is the number of FFT points. The common frequency offset of $\frac{fc}{f0}\Delta$ is the same for all sub-carrier. The non-uniform frequency offset ($l\Delta$) depends on the sub-carrier index. According to equation (2.31), received symbol $Y(k)$ has two effects such as phase-rotation and inter-carrier interference (ICI).

Chapter 3

The Proposed Transceiver Architecture

3.1 Overview

OFDM communication systems have been developed over decades and became popular today such as ISDB-T, DVB-T, 4G-LTE, and so on. To enable those systems working reliably, engineers have put great effort on developing transceiver architectures. Those transceiver architectures are great

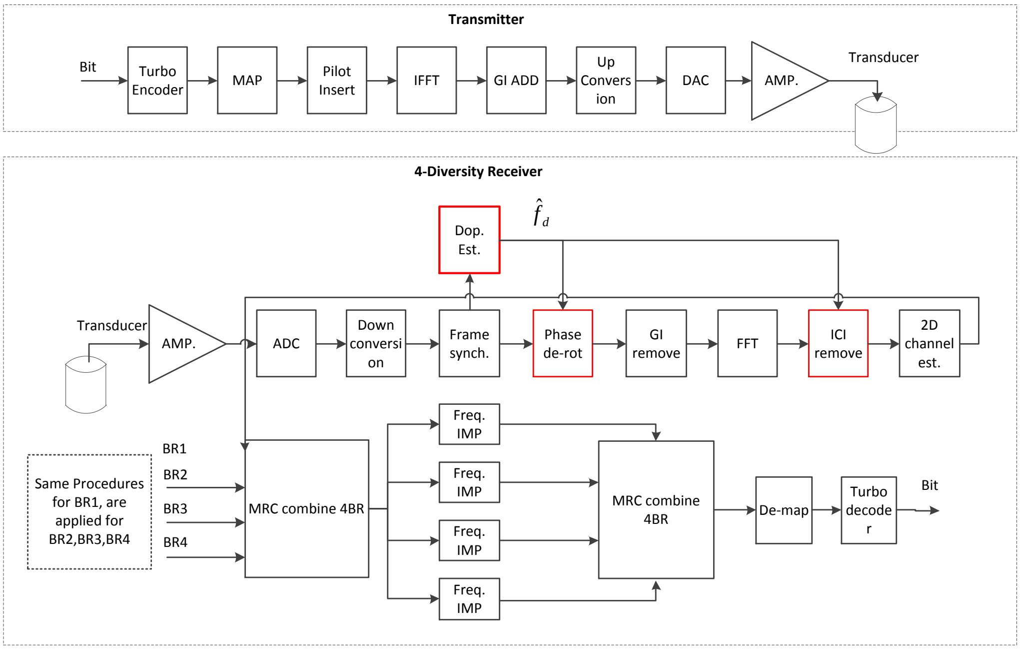

FIGURE 3.1: Proposed Transceiver Architecture

references for us when designing an acoustic OFDM for underwater environment. We consider state-of-the-art algorithms in radio wireless communication for acoustic communication, and also propose new algorithms to solve new challenges posed by the underwater environment.

When designing system parameters and singal processing methods, several factors are taken into account. We try to balance performance in term of bit error rate, data speed with computational complexity and hardware cost. Also, through doing experiments we find optimal parameters for our target application. For example, the length of guard interval, or the threshold for clipping impulsive noise in time domain [27, 28].

First, time and frequency synchronization is challenging for underwater acoustic communication (UAC) since the Doppler effect cause severe frequency offset in frequency domain, and time compression/expansion in time domain. In addition, high ambient noise and impulsive noise also make synchronization become more difficult. Therefore, we consider several techniques for synchronization. Second, the highlights of this thesis are methods to deal with Doppler effect that is one of the greatest challenge in UAC. We have put a lot of effort in algorithms to estimate time varying Doppler rate and compensate its impacts. Third, estimation of channel under severe ICI caused by Doppler and impulsive noise is very challenged. We consider the state-of-the-art channel estimation that utilized in 4G-LTE, and further propose robust channel estimation combined ICI cancellation. Third, we also investigate applying Turbo decoding with different code rate, and different modulation level, QPSK, 16QAM and 64QAM.

The following sections will present transmitter and receiver architecture of our system.

3.2 Transmitter

3.2.1 Data Frame Structure

The transmitter architecture is shown in figure 3.1, and the details are described in the following. In [9, 29, 30, 31, 32, 33], Linear Frequency Modulation (LFM) Chirp is attached to the beginning and the end of a data frame as shown in figure 3.2. The Chirp signal has two functions, the first one is to detect the beginning of a data frame and the second function is to measure an average Doppler rate over the data frame. Details about frame detection and Doppler rate estimation using the Chirp will be presented in next sections. Second, our data frame is shown in figure 3.2. Rather than using Chirp signal, we employ a preamble as shown in figure 3.2 (the below frame structure). The preamble consist of two three OFDM symbols and supports frame detection and estimation of Doppler shift and/or Doppler rate which is equivalent to few times of sub-carrier space.

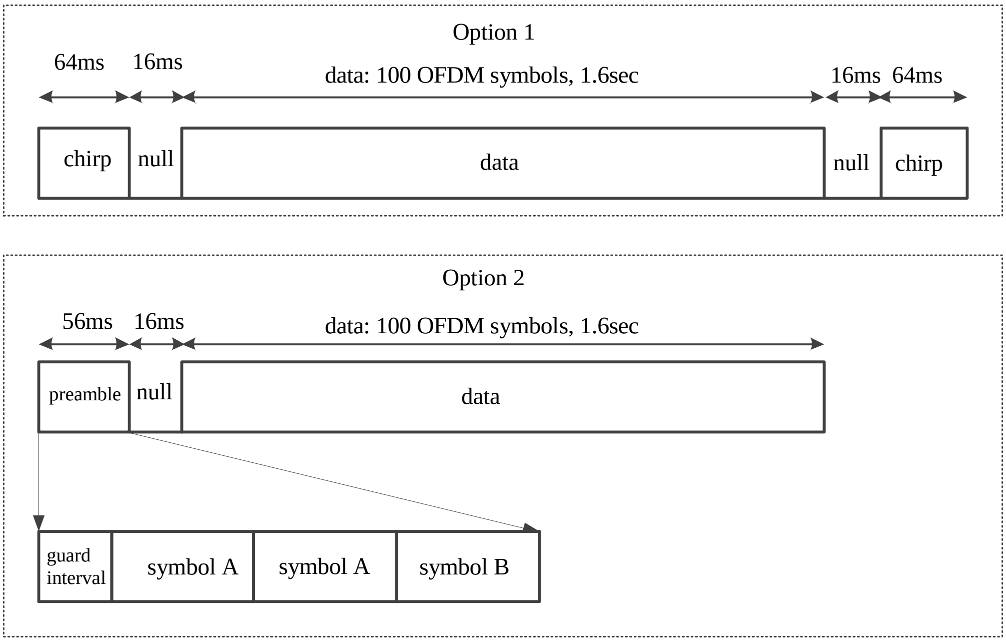

FIGURE 3.2: Data Frame Structure

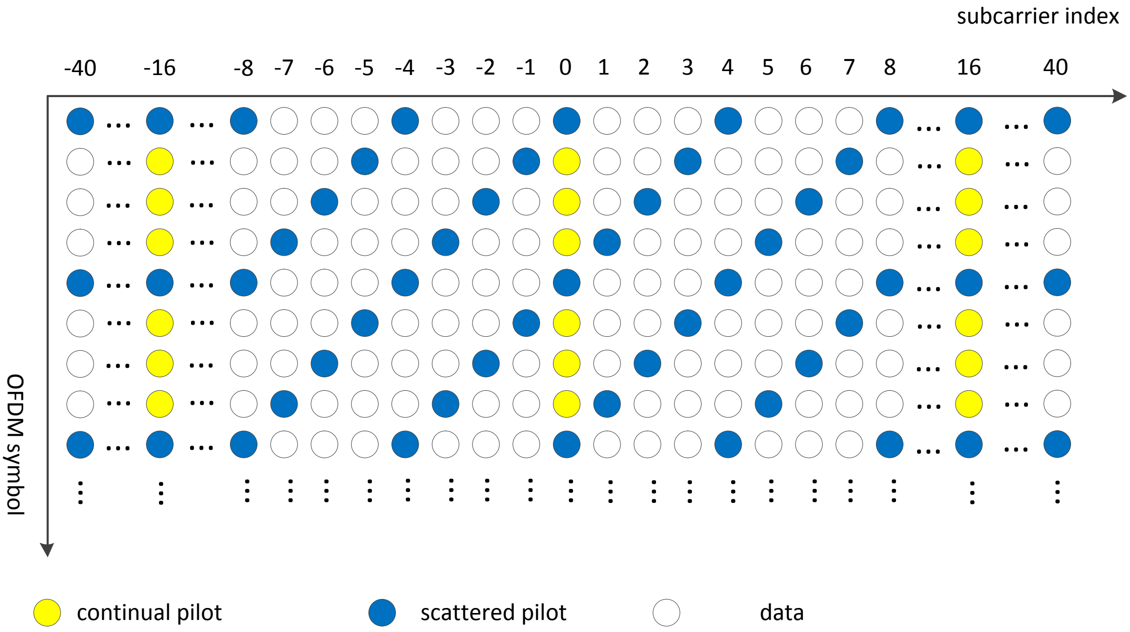

FIGURE 3.3: Pilot Pattern

3.2.2 Pilot Structure

It depends on several factors to choose an optimal pilot structure. Two parameters are considered such as the maximum Doppler shift and delay spread. According to principle of Nyquist sampling, the distance between two pilots should small enough to measure time varying channel caused by Doppler and frequency selective fading caused by delay spread. Assuming that the distance between two pilots

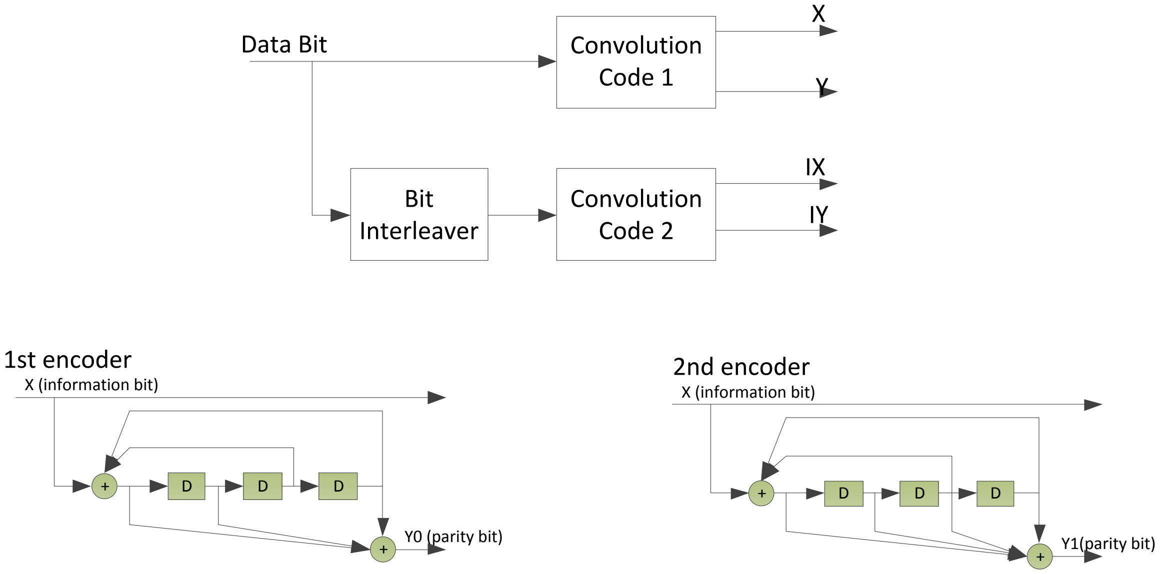

Figure 3.4: Turbo Encoder

in frequency domain, and time domain are pf_0 and qT_{sb}, respectively. Then, the maximum Doppler shift and maximum delay spread can be estimated are

$$f_{dmax} = \frac{1}{2qT_{sb}} \tag{3.1}$$

$$\tau_{max} = \frac{1}{2pf_0} \tag{3.2}$$

Here, f_0 and T_{sb} are the sub-carrier space, and OFDM symbol length included guard interval, respectively. Due to severe Doppler, continual pilots which mean $q = 1$ is employed in our system. Then, we consider a pilot patterns are shown in figure 3.3. The scattered pilot makes a trade-off between sampling channel in time and frequency domain. This pattern is robust to time varying channel.

3.2.3 Turbo Encoder

The strongest forward error correction method currently are Turbo and LDPC (low-density parity-check). We prefer Turbo because several reasons. First, the bit errors in our systems is random since it is caused by ICI, ambient noise and impulsive noise. Second, due to flexibility of Turbo code that allow setting different code rate easily through puncture. Third, Turbo decoding also can be done without matrix inversion while LDPC requires matrix related computation. The adopted Turbo encoder is shown in figure 3.4.

3.3 Receiver Architecture

The overall receiver architecture is depicted in figure 3.1. The highlights are (1) robust time/frequency synchronization enabling frame detection and tracking of time varying Doppler rate over OFDM symbols. (2) Methods for compensating impacts of Doppler effect, and Chanel estimation under severe ICI and impulsive noise. (3) Impulsive noise cancellation in both time and frequency domain also are Impulsive. Finally (4) 4-Diversity receiver provides significant performance gain.

3.3.1 Time and Frequency Synchronization

The purpose of time synchronization is detecting the beginning of a data frame. We consider two methods, the first one is using the Chirp signal that is very resilient to Doppler, and the second one is using two identical OFDM symbols as the preamble of a data frame. To detect the beginning of a data frame, the received signal is correlated with the pre-known Chirp stored at the receiver side. The peak of the correction function indicates the beginning of the data frame. The merits of this method are resilient to Doppler, and easy to implement. The disadvantage is the peak of the correction function degrades when SNR (Signal to Noise Ratio) decrease. Also, this method does not support estimation of frequency at the beginning of a data frame. To estimate an average Doppler rate over the entire frame, Chirp signal must be attached to the beginning and the end of a data frame as shown in figure 3.2.

Another way to do time synchronization is using repeating pattern such as two identical OFDM symbols. Two windows are utilized to compute the self-correlation at the receiver side. The peak of the self-correlation also indicates the beginning of the data frame. This method requires more computation costs, but can work under low SNR region. Frequency offset caused by Doppler or equipment also can be detected at the beginning of a data frame. As shown in figure 3.2, to estimate frequency offset which is few times of a sub-carrier space, symbol B is inserted. Special structure of symbol A and B enables estimating very high frequency offset. The first step is fractional frequency estimation using Cyclic Prefix as shown in [10, 34, 35] and the second step is integer frequency offset estimation using special structure of A and B as presented in [41].

3.3.2 Review of Doppler Shift/Rate Estimation

It is noted that using only one Chirp is able to detect the begining of a data frame and not able to track the time varying Doppler over OFDM symbols. Also, the preamble formed by three OFDM symbols only can estimates frequency offset at the begining of a data frame. To track the time varying Doppler changing over OFDM symbols, we must consider further techniques. In radio wireless communication, conventional methods are using Cyclic Prefix [10, 35, 34] or using continual pilots [35, 36] to estimate

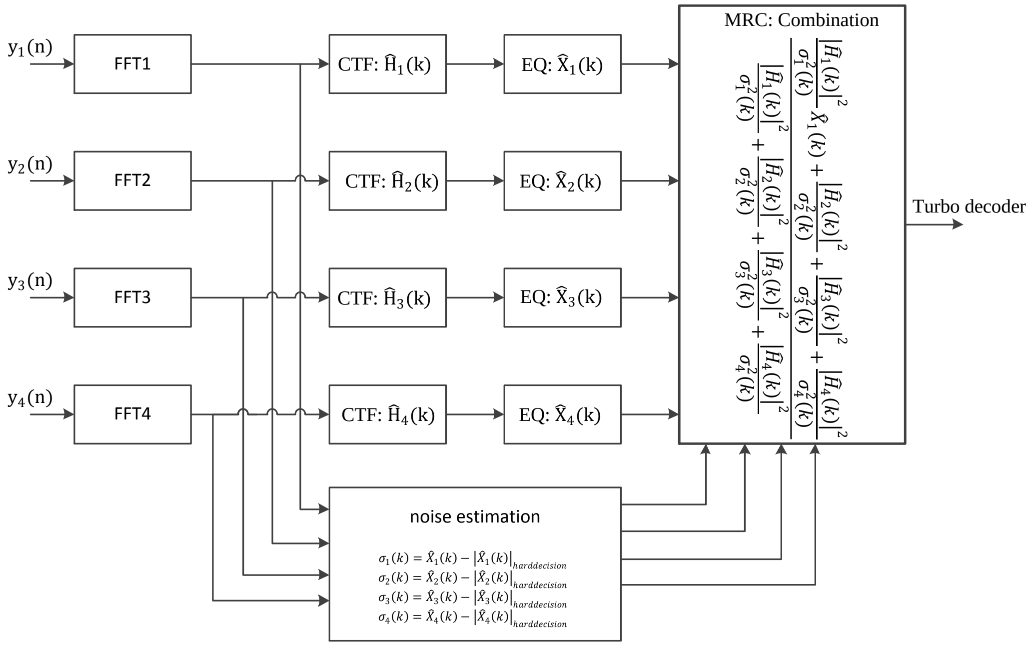

Figure 3.5: 4-Diversity Receiver

frequency offset symbol-by-symbol. However, the maximum frequency offset can be estimated are limited by $f_0/2$. In the next chapter, we will propose a robust method for tracking the time varying Doppler by using continual pilots in conjunction with monitoring the drift of Power Delay Profile (PDF).

3.3.3 Diversity Receiver

MIMO-OFDM, diversity receiver are very powerful technique and widely applied in state-of-the-art systems such as 4G-LTE, OFDM mobile receivers. Multipath channel also happens in UAC, therefore we apply 4-Diversity Receiver with post-FFT processing, MRC combination to enhance the SNR (Signal to Noise Ratio).

In short, four transducers are separated about 10(cm) which is greater than the wavelength of 6.25(cm) (carrier frequency of 24kHz). So, each transducer experiences a different (uncorrelated) channel transfer function. Considering the same sub-carrier k, the channel transfer function $H(k)_{transducer}$ at different transducer is different. $H(k)_{transducer1}$ suffers deep fade (high attenuated) while $H(k)_{transducer2}$ is not. Therefore, by combining signal from different transducers after FFT demodulation in a proper manner will improve SNR. MRC (maximal ratio combining) is utilized to combine signal from 4 transducers after FFT as follows.

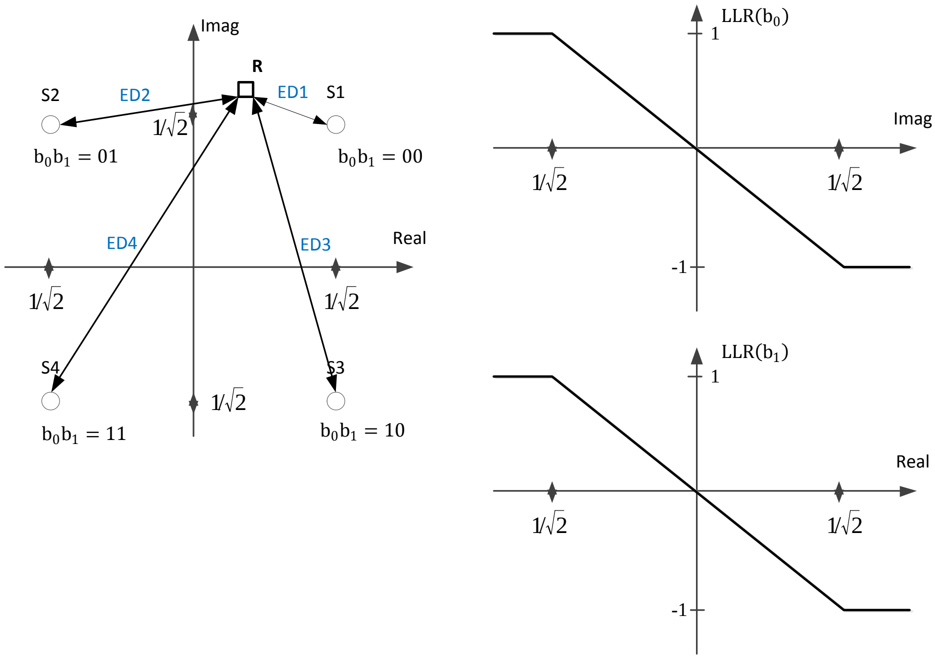

Figure 3.6: QPSK soft-demaping

3.3.4 Impulsive Noise Cancellation

Through our experiments, and also mentioned in sea in Shizuoka, and Okinawa, impulsive noise appears in the shallow sea more than in deep sea [18, 27, 28, 37]. In time domain, a simple method in [27, 28, 38] is clipping the noise signal which is greater than a pre-defined threshold. An optimal threshold can be determined through experiments. More complicated methods in frequency are proposed in [1-10]. These methods usually are iterative methods and require hard-decision data (after QAM demodulation). In our system, hard-decision after 4-Diversity receiver provide a reliable input for frequency IMP noise cancellation methods.

3.3.5 Turbo Decoder

Algorithms for Turbo decoding have been presented through literatures, such as can be found in [39]. We will summary interesting ideas on Turbo code in an intuitive manner. First, Turbo decoding needs information from soft-demapping. In cases of QPSK, 16QAM, 64QAM soft-demapping is a little different from BPSK cases. For example, considering QPSK as shown in figure 3.6. We denote R is received QPSK symbol as shown in the constellation. $P(b_0 = 1|R)$ is the probably bit $b_0 = 1$ given the received symbol R. Likewise, $P(b_0 = 0|R)$ is the probably bit $b_0 = 0$ given the received symbol R. $|R - S_i|^2$ is the Euclidean distance, and σ^2 is random noise power. Then the LLR (Log Likelihood Ratio) for a bit can be computed as

$$
\begin{aligned}
LLR(b_0) &= \log \frac{P(b_0 = 1|R)}{P(b_0 = 0|R)} \\
&= \log \left(\frac{P(S = S_3|R) + P(S = S_4|R)}{P(S = S_1|R) + P(S = S_2|R)} \right) \\
&= \log \left(\frac{exp(\frac{-1}{2\sigma^2}|R - S_3|^2) + exp(\frac{-1}{2\sigma^2}|R - S_4|^2)}{exp(\frac{-1}{2\sigma^2}|R - S_1|^2) + exp(\frac{-1}{2\sigma^2}|R - S_2|^2)} \right) \\
&\approx \log \frac{\max \left(exp(\frac{-1}{2\sigma^2}|R - S_1|^2), exp(\frac{-1}{2\sigma^2}|R - S_2|^2) \right)}{\max \left(exp(\frac{-1}{2\sigma^2}|R - S_1|^2), exp(\frac{-1}{2\sigma^2}|R - S_2|^2) \right)} \\
&= \frac{-1}{2\sigma^2} \left(|R - S_3|^2 - |R - S_2|^2 \right)
\end{aligned}
\tag{3.3}
$$

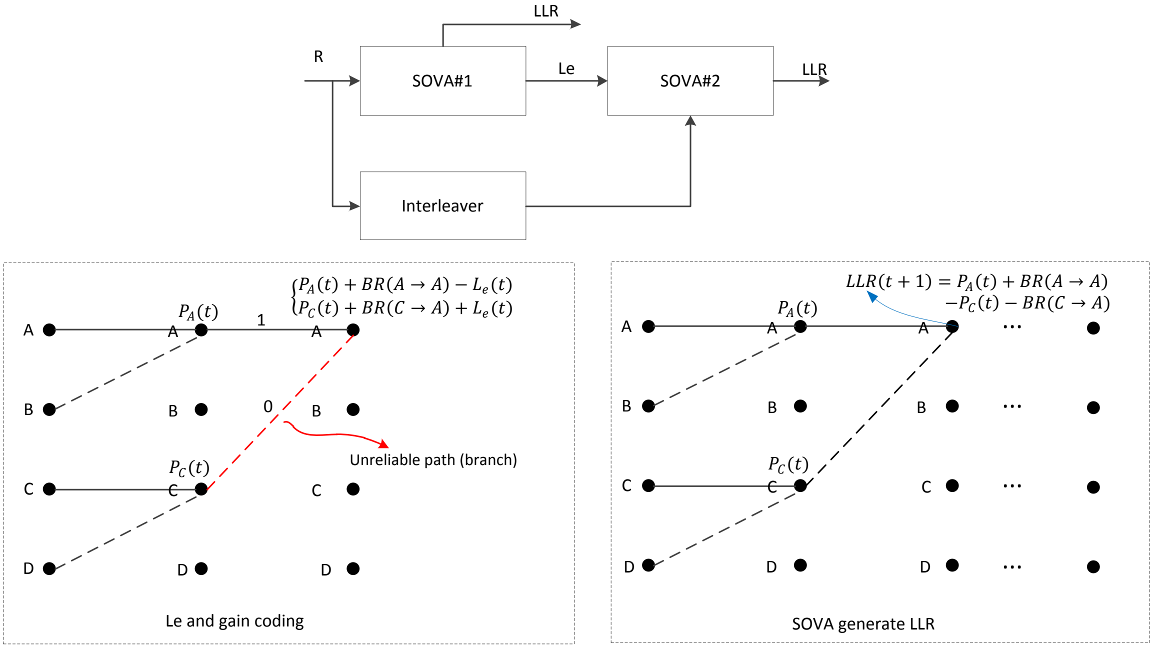

Figure 3.7: Turbo Decoding

For more details, please refer to [39]. The LLR also can be computed through a simple approximation as shown in figure 3.6. Similarly, LLR for 16QAM and 64QAM also can be computed. Second, we review generating LLR when using SOVA (Soft Output Viterbi Algorithm). As illustrated in figure 3.7. the difference between two path metrics going to node A at instant time t indicates the reliability, LLR of bit $b(t)$

$$
LLR(b_0(t)) = P_A(t-1) + BR(A \to A) - P_C(t-1) - BR(C \to A) \tag{3.4}
$$

Finally, Turbo code achieves coding gain through using L_e which is generated from SOVA. As shown in figure 3.7. SOVA1 generates LLR_{out} and Le for every decoded bit. Le is utilized to force/modify the branch metric when computing the branch metric at SOVA2. For example, after SOVA1 if$Le(b(k))$

indicates that bit $b(k) =' 1'$ reliably, then the branch matrix at SOVA2 when computing at the instant time k should be modified as follow

$$\begin{cases} BR_{forced}(A \to A) = BR(A \to A) - \Delta, \Delta \approx Le \\ BR_{forced}(B \to A) = BR(B \to A) + \Delta, \Delta \approx Le \end{cases} \tag{3.5}$$

Chapter 4

Doppler Rate Estimation and Non-Uniform Doppler Compensation

4.1 Introduction

The highlight of this thesis is estimation and compensation impacts of Doppler that is one of the most difficult part in acoustic OFDM systems. In radio OFDM wireless systems such as ISDB-T, 4G-LTE, Doppler causes frequency offset, and time compression/expansion is eligible. However, in acoustic OFDM time compression/expansion caused by Doppler is significant compared to radio wireless OFDM. For example, LTE-4G operating around $2(GHz)$ supports receivers moving at $500(km/h)$. This moving speed causes a Doppler shift of $950(Hz)$ which is about 6.33% of a typical sub-carrier space of $15000(Hz)$. State-of-the-art algorithms for time varying channel is able to deal with a Doppler spread of 10% of sub-carrier.

On the other hand, a velocity of only $1(m/s)$ causes a frequency offset of $16Hz$ which is 33.33% of a sub-carrier (f_0=48Hz) in our acoustic system. The time compression/expansion is around 2 samples over an OFDM symbol of 3072 samples. Therefore, convetional methods in radio wireless are not powerful enough for acoustic communication. Next, acoustic OFDM systems usually are wideband systems when system bandwidth is comparable to carrier frequency. For example, our system bandwidth is around $8kHz$ which is 1/3 of carrier frequency $24kHz$. Consequently, each subcarrier experiences a different amount of frequency offset depending the subcarrier index, and this phenomemon is called non-uniform Doppler. Finally, when multipath and severe Doppler rate/shift happens simultanesouly, it is very challenged to estimate channel. Although assuming that all delay paths has a simliar Doppler rate as in [9, 11, 12, 31, 33, 40], and the channel is sparse consisting of only few path, channel estimation is still very difficult since all pilots already corrupted by severe ICI.

In the following, we will present methods for estimating Doppler shift and Doppler rate. We consider both time and frequency based methods for compensating impacts of Doppler. In addition, methods to estimate channel under severe ICI and noise are proposed.

4.2 Estimation of Doppler Rate/Doppler Shift

In this section, we explain two impacts of Doppler in time and frequency domain. Considering a vertical link communication such as a transmitter at the sea bottom and receivers near the sea surface, the channel consists of two path, a light of sigh path and a surface reflection path. Since Doppler mainly caused by the moving of the transmitter, Doppler rate/shift of two paths are similar. Therefore, we can consider a common Doppler rate as follow.

$$R(t) = \sum_{i=1}^{L} A_i S\Big((t-\tau_i)(1+\Delta+\delta_i)\Big), \delta_i << \Delta = v/C \tag{4.1}$$

Methods for estimating the common/dominant Doppler rate can be classified in two groups. First, in radio wireless cyclic prefix or continual pilots is utilized to estimate the frequency offset caused by Doppler. Second, in acoustic communication the Chirp (LFM) is attached to the begining and the tail of a data frame to estimate an average Doppler rate over an entire data frame as in [12, 29, 31, 32, 33].

4.2.1 Existing Methods for Estimating Doppler

4.2.1.1 Using Cyclic Prefix

According to [34, 35, 41] it is possible to use cyclic prefix to estimate frequency offset. We define $r(n)$ is received signal in time domain. Assuming that delay spread is much smaller than guard interval, and an offset ϵ happen. Then, the frequency offset ϵ can be estimated as follows.

$$\epsilon = \min_{\epsilon} \sum_{n=0}^{N_{GI}-1} |r(n)e^{j2\pi\epsilon} - r(n+N)|^2, \qquad \epsilon = f_d T_0 \tag{4.2}$$

$$\epsilon = \frac{1}{2\pi}\angle\Bigg(\sum_{n=0}^{N_{GI-1}} \frac{r^*(n)r(n+N)}{|r(n)||r(n+N)|}\Bigg) \tag{4.3}$$

The maxim frequency offset can be estimated is $f_0/2$ since $-\pi \leq \angle \leq \pi$. However, under multipath condition, the Cyclic Prefix is contaminated by ISI (inter-symbol interference), so accuracy of the

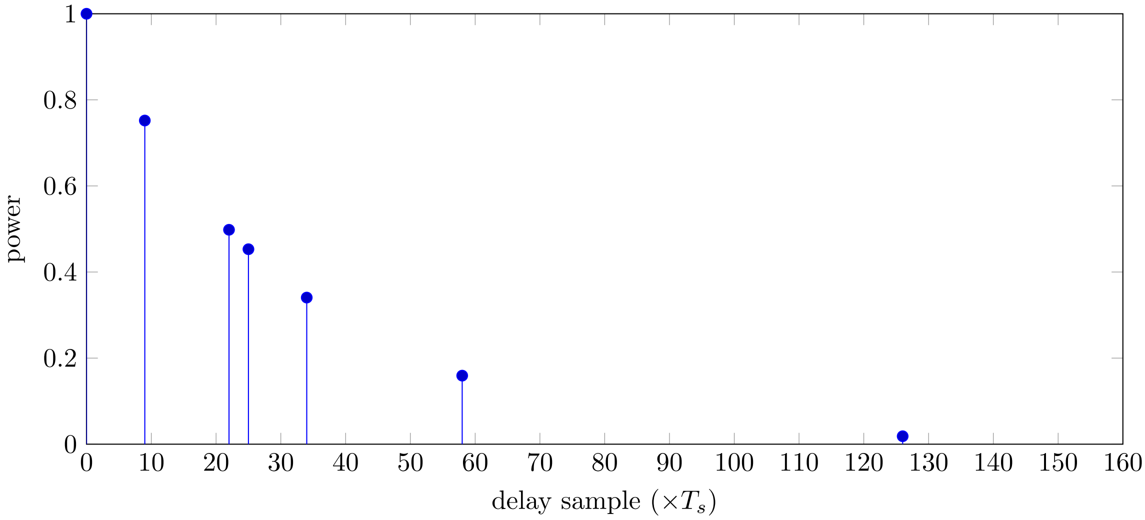

FIGURE 4.1: Power Delay Profile of TU Extended Model [10]

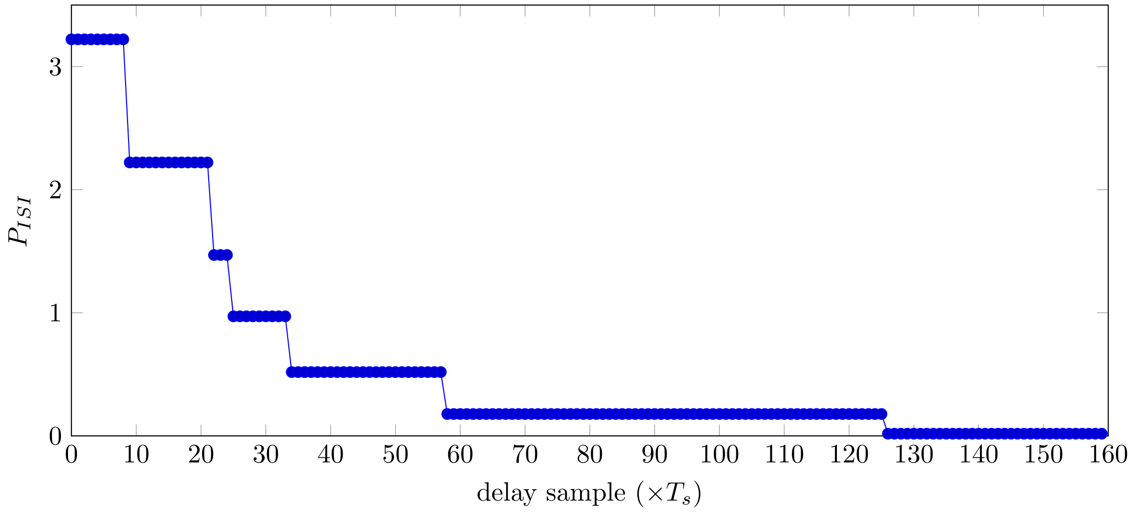

FIGURE 4.2: ISI Power Over Samples of Guard Interval = 160 samples Ts

method is degraded by multipath channel. Given the power delay profile, it is possible to improve the accuracy of the estimation through computing ISI (inter-symbol interference) over delay samples.

$$P_{ISI}(i) = \sum_{\tau > iT_s} P(\tau) \tag{4.4}$$

Here $P(\tau)$ is the given power delay profile, and $T_s = 1/F_s$ is sampling period. Then the estimation of ϵ is modified as

$$\hat{\epsilon} = \frac{\epsilon(i)/P_{ISI}(i)}{\sum_{i=0}^{N_{GI}-1} 1/P_{ISI}(i)} \tag{4.5}$$

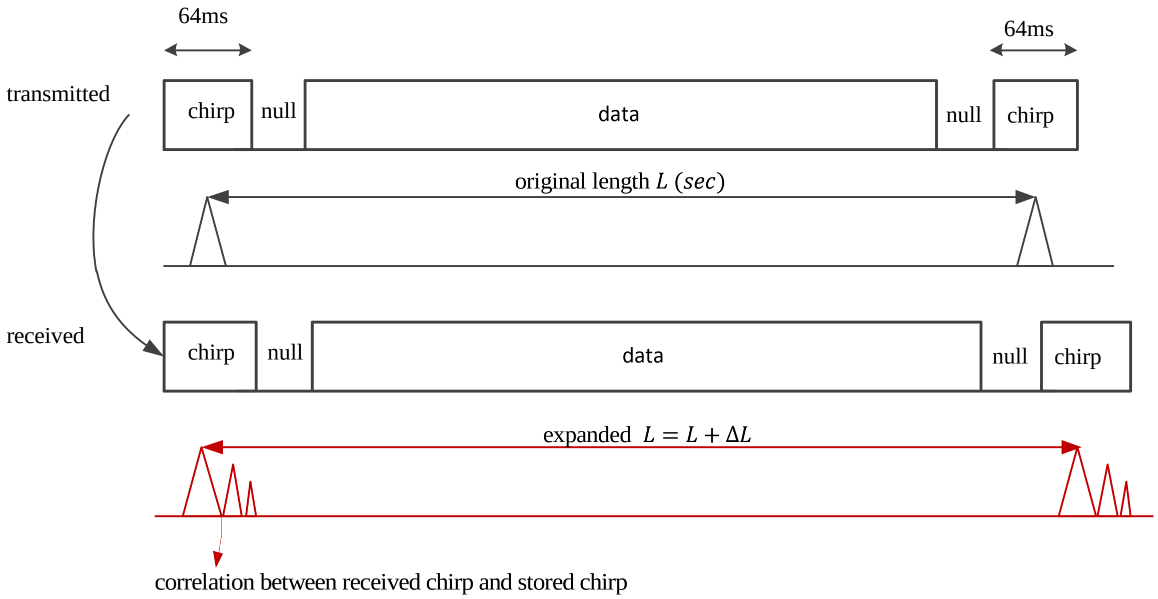

FIGURE 4.3: Doppler rate estimation using Chirp pre/postample

4.2.1.2 Linear Frequency Modulation (Chirp) Signal

The linear frequency modulation or so-called chirp signal which is resilient to Doppler is attached to the beginning and the end of a data frame to detect the beginning of a frame, and measure an average Doppler rate over the entire frame. The chirp signal at baseband $C_{BB}(t)$ is written as

$$C_{BB}(t) = e^{j\pi Bt^2/T_0} \tag{4.6}$$

The chirp signal at passband $C_{PB}(t)$ is written as

$$C_{PB}(t) = real\left(e^{j\pi(Bt^2/T_0+f_ct)}\right) \tag{4.7}$$

The product BT_0 is recommended should be not less than 100. For example, we choose $B = 2000(Hz), T_0 = 64ms$ so $BT_0 = 128$. At the receiver side, received signal is correlated with pre-known Chirp pre/postamble. The first peak of the correlation detects the beginning of a data frame. Assuming that the received signal is expanded due to Doppler, the distance between two peaks is extend to L'. An average Doppler rate is estimated as

$$\Delta = \frac{L' - L}{L} \tag{4.8}$$

In the low SNR (signal to noise ratio) region it is difficult to ensure the accuracy of this method. In addition, the chirp does not support tracking the time varying Doppler over OFDM symbols.

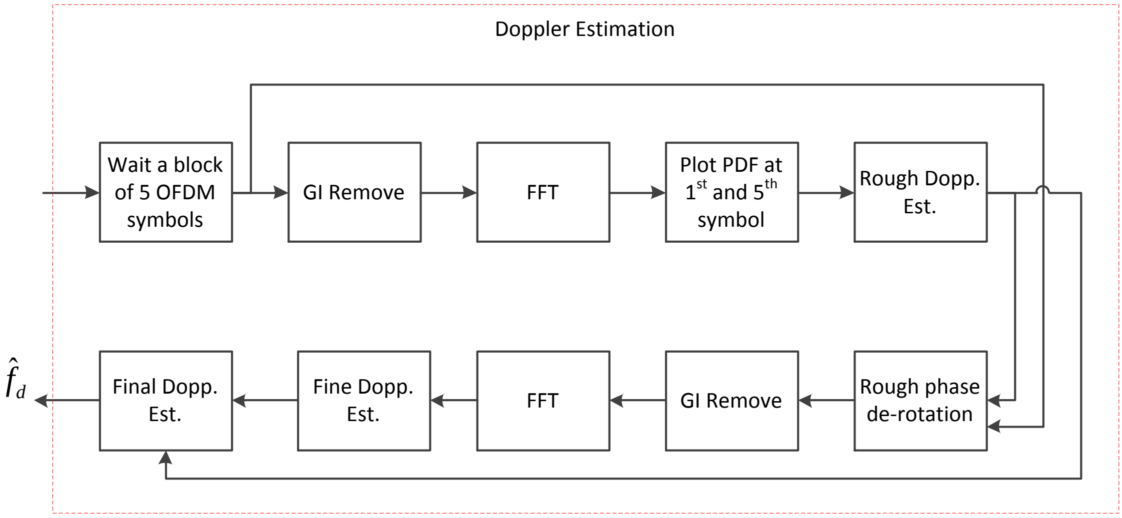

FIGURE 4.4: Proposed Doppler Estimation

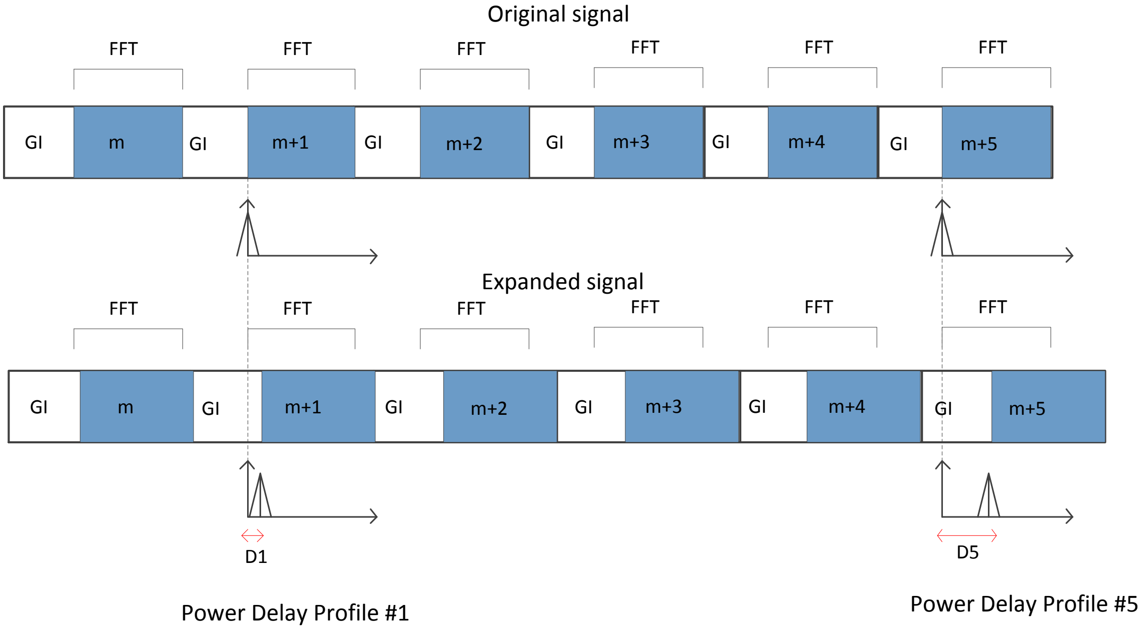

FIGURE 4.5: Drift of Power Delay Profile over ofdm symbols

4.2.2 Proposed Method for Estimating Doppler

4.2.2.1 Rough Estimation by Monitoring the drift of Power Delay Profile

In this section we present a time varying Doppler shift estimation by monitoring the drift of Power Delay Profile (PDP) in conjunction with using continual pilots. To boost the estimation range, we propose a rough Doppler estimation through monitoring the drift of PDF due to Doppler-induced expansion/compression. The signal processing of Doppler estimation is shown in figure 4.5. Doppler causes expansion/compression of signal wave form in the time domain. In turn, when the position of FFT window is fixed at the receiver side, we will observe the drift of PDF over OFDM symbols. This phenomenon is described in figure 4.5 in case of the received signal is expanded. At the receiver side, PDF can be obtained from channel transfer function measured at pilot positions. PDF is obtained at symbol (m+1),(m+5),(m+9) and so on since those symbols have more pilots than others. As shown in figure 4.5 when the signal is expanded, the peak of PDF will be drifted to the right side, and the amount $(D_5 - D_1)T_s$ indicates how much signal is expanded. Here, D_1 and D_5 are the drift amount of PDF measured at OFDM symbol (m+1) and (m+5) in scale of sample period, respectively. As mentioned above in (4) Doppler rate of Δ causes an expansion/compression of $\Delta N_s T_s$, therefore, when the expansion/compression is $(D_5 - D_1)T_s$, the Doppler rate should be

$$\hat{\Delta}_R = \frac{D_5 - D_2}{4T_{sb}} \tag{4.9}$$

Δ_R denotes the rough estimate Doppler rate. The rough estimation Δ_R is fed into a phase-rotation to alleviate impact of Doppler. Then, the residual Doppler rate/shift is estimated by using continual pilots in the next section.

4.2.2.2 Fine Estimation by using Continual Pilots

The accuracy of the rough estimation depends on the sampling speed. The smallest expansion/-compression over 4 OFDM symbols can be detected is a sample period T_s, and the corresponding smallest frequency offset can be detected is $f_c/(4N_s)$. Therefore, we need a fine estimation of Doppler shift following the rough estimation. After the rough estimation, Doppler is alleviated by a phase de-rotation using the estimated $\hat{\Delta}_R$ using continual pilots. Structure of scattered and continual pilot is shown figure 3.3. C_p is the sub-carrier indexes of continual pilots in a OFDM symbol. Frequency offset caused by imperfection of equipment, or in the case all delay paths has a common Doppler shift, using continual pilots is able to estimate the frequency offset. Considering the residual Δ_R, the received at basedband of ofdm symbol m is written as

$$r(m,t) = \left\{ \sum_{k=0}^{N-1} H(k,m)D(k,m)e^{j2\pi k f_0 (t+(m-1)T_{sb})} \right\} e^{j2\pi\Delta_R (t+(m-1)T_{sb})} \tag{4.10}$$

After IFFT processing,

$$Y(k,m) = \int_0^{T_0} r(m,t)e^{-j2\pi k f_0 t} dt \tag{4.11}$$

$$Y(k,m) \approx H(k)D(k,m)e^{j2\pi\Delta_R (m-1)T_{sb}} \int_0^{T_0} e^{j2\pi\Delta_R t} \tag{4.12}$$

$$Y(k,m+1) \approx H(k)D(k,m+1)e^{j2\pi\Delta_R (m)T_{sb}} \int_0^{T_0} e^{j2\pi\Delta_R t} \tag{4.13}$$

Here, $0 \leq t \leq T_0$, and T_0 the ofdm symbol length excluded guard interval. T_{sb} is ofdm symbol length included guard interval. $H(k,m)$ is channel transfer function caused by multipath channel at sub-carrier k of symbol m. At continual pilots, we can obtain

$$\hat{H}(k,m) = \frac{Y(k,m)}{D(k,m)}, k \in CP \tag{4.14}$$

$$\hat{H}(k,m+1) = \frac{Y(k,m+1)}{D(k,m+1)}, k \in CP \tag{4.15}$$

If there is no frequency offset or time varying channel, $H(k,m)$ and $H(k,m+1)$ are the same. Frequency offset causes a phase rotation on every sub-carriers k, and the phase rotation over from symbol m to $(m+1)$ indicates frequency offset as

$$\hat{\Delta}_f = \frac{1}{2\pi T_{sb}} \angle \left\{ (\hat{H}^*(k,m)\hat{H}(k,m+1)) \right\} \tag{4.16}$$

We denote Δ_f is fine estimation which is residual Doppler after estimation and compensation Doppler from the rough estimation stage. The total estimate Doppler rate is

$$\hat{\Delta} = \hat{\Delta}_R + \hat{\Delta}_f \tag{4.17}$$

The corresponding frequency offset is

$$\hat{\epsilon}(k) = \hat{\Delta}(f_c + kf_0) \tag{4.18}$$

Here, $\hat{\epsilon}(k)$ is non-uniform Doppler shift which depends on position (index k) of a sub-carrier.

4.2.2.3 Multi-Resampler

So far using only cyclic prefix or continual pilot can estimate a maximum Doppler shift of $f_0/2$. The proposed method monitoring the drift of PDF in conjunction with using continual pilot is able to estimate a Doppler shift greater than $f_0/2$. However, this method is post-FFT processing, which mean estimation of PDF from ICI-contaminated pilots are very noisy. Since Doppler shift is high, such as close to f_0, the estimated PDF from pilots is not reliable. Therefore, we further propose pre-FFT estimation using CP for high Doppler rate case. For example, a relative velocity of $5(m/s)$ causes a compression/expansion of 4.27 samples over an OFDM symbol of 1280 samples in our system. The equivalent frequency offset is 80Hz $f_0 = 96.375Hz$, so the above methods are not sufficient. Therefore, we propose a multi-resampler consisting of branches to estimate the time compression/expansion. The muti-resampler can estimate severe time varying Doppler such as a frequency much greater than $f_0/2$ and changes over OFDM symbols.

There are two impacts of Doppler on the cyclic prefix, one is phase rotation, and another is time compression/expansion. Therefore, each branch of the multi-resampler consists of a phase rotator, a resampler and a metric calculator. The branch which generates the largest metric indicates the time compression/expansion. Due to the Doppler effect, the received signal is compressed or expanded depending the direction of velocity. When a transmitter approaching a receiver, the arrival signal is compressed in time domain as observed from receiver side. Likewise, when a transmitter moving away from a receiver, from the receiver side, we observe that the arrival signal is expanded. We assume that there are L delay path, each delay path has an attenuation of A_i, and all paths has a similar Doppler rate of $(\Delta+\delta_i)$ with a variation $\delta_i << \Delta$. This assumption is widely accepted for underwater acoustic communication such as in [11, 12, 32, 33].

$$\Delta = \frac{v}{C}, C = 1500m/s \tag{4.19}$$

Here, v is the relative velocity between a transmitter and a receiver, and C is propagation speed of acoustic signal in the water. We also assume that Δ is a constant within an OFDM symbol, but changes over OFDM symbol. Then, the received signal is written as.

$$R(t) = \sum_{i=1}^{L} A_i S\Big((t-\tau_i)(1+\Delta+\delta_i)\Big) \tag{4.20}$$

After sampling, and down-conversion the sampled signal is written as

$$x(n) = \underbrace{\left(\sum_{k=0}^{N_{FFT}-1} H(k)D(k)e^{j2\pi k f_0(1+\Delta+\delta_i)nT_s}\right)}_{compression/expansion} \underbrace{e^{j2\pi f_c(\Delta+\delta_i)nT_s}}_{phaserotation} \tag{4.21}$$

$$H(k) = \sum_{i=1}^{L} A_i e^{-j2\pi(f_c+kf_0)(1+\Delta+\delta_i)(nT_s-\tau_i)} \tag{4.22}$$

T_s is sampling period. $H(k)$ is the complex gain representing frequency selective fading caused by delay τ_i. The Doppler effect causes two impacts. The first impact is a common phase rotation of $e^{j2\pi(\Delta+\delta_i)f_c nT_s}$. The second impact is time compression/expansion that means each sample is compressed/expanded $(\Delta+\delta_i)T_s(sec)$.

As shown in figure 4.6, each branch consists of a phase rotator for de-rotating the common phase rotation in (4), a resampler for compensating the compression/expansion, and finally a metric calculator. The branch with $\alpha(m)$ which is closest to the actual Doppler rate Δ generates the largest metric. Two important parameters of the multi-resampler are $\pm\Delta_{max}$ which is the biggest time compression/expansion can be estimated, and $\pm\Delta_{min}$ which is the smallest compression/expansion can be estimated. Then, the number of branches needed is

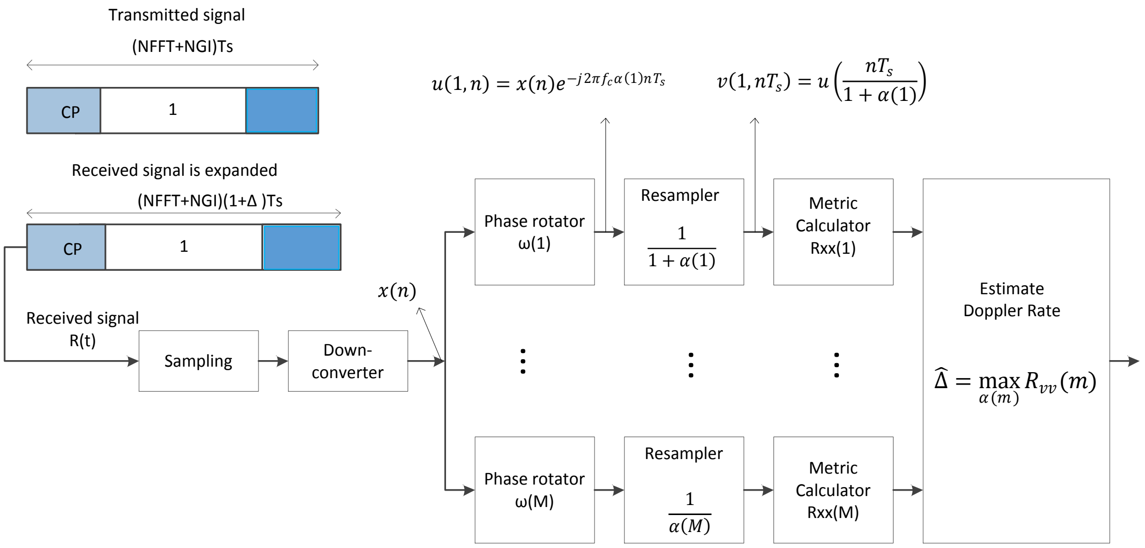

Figure 4.6: Proposed Multi-Resampler

$$M = 2\frac{\Delta_{max}}{\Delta_{min}} + 1 \tag{4.23}$$

The pre-defined phase rotation of branch m, and the pre-defined sampling rate are computed as following

$$\alpha(m) = \left(m - \frac{M+1}{2}\right)\Delta_{min} \tag{4.24}$$

At branch m, a phase rotation is applied as

$$u(m,n) = x(n)e^{-j2\pi f_c \alpha(m) nT_s} \tag{4.25}$$

After the phase rotation, signal at branch m is re-sampled as

$$v(m,nT_s) = u\left(m, \frac{nT_s}{(1+\alpha(m))}\right) \tag{4.26}$$

If $\alpha(m) \approx \Delta$, after phase rotation and re-sampling, the head and the tail of cyclic prefix should be the same. Therefore, the similarity between the head and the tail is considered as a metric, and is computed as

$$R_{vv}(m) = \left\{ \sum_{n=1}^{N_{GI}} |v(m,n) - v(m,n+N_{FFT})|^2 \right\}^{-1} \tag{4.27}$$

Finally, the Doppler rate is estimated

$$\hat{\Delta} = max_{\alpha(m)} R_{vv}(m) \tag{4.28}$$

The Cyclic Prefix (CP) is distorted by inter-symbol-interference (ISI) due to multipath channel. Therefore, we only use a portion of the CP for estimating the Doppler, and equation 4.27 is re-written as

$$R_{vv}(m) = \left\{ \sum_{n=1+\gamma}^{N_{GI}} |v(m,n) - v(m,n+N_{FFT})|^2 \right\}^{-1} \tag{4.29}$$

The optimum of γ depends on the power delay profile. We simply choose $\gamma = N_{GI}/2$, with N_{GI} is the number samples of CP.

4.3 Compensation Impacts of Doppler

4.3.1 Existing Methods for Compensating Doppler

There are two types of method for compensating Doppler rate, resampling in time domain, and non-uniform Doppler shift compensation in frequency domain. We will review the resampling methods in [9, 12, 29, 32, 33, 40] and how to perform the resampling in a low complexity manner. Also, we review a simple non-uniform phase rotation method which proposed in [2]. Finally, we show our proposal method that is a non-uniform ICI matrix representing impacts of non-uniform Doppler shift in frequency domain.

4.3.1.1 Re-sampling in Time Domain

A straightforward way to compensate the compressed/expanded wave form is re-sampling in time domain. After the time scale (Doppler rate) is estimated by using the Chirp or multi-resampler, re-sampling can be performed before down-conversion or after down-conversion. When re-sampling is performed before down-conversion, the re-sampled is written as

$$\bar{R}(nT_s') = R\Big(n\frac{T_s}{1+\hat{\Delta}}\Big) \tag{4.30}$$

$$\bar{R}(nT_s') = \sum_{i=1}^{L} A_i S\Big((nT_s - \tau_i)\Big(\frac{1+\Delta+\delta_i}{1+\hat{\Delta}}\Big)\Big) \tag{4.31}$$

Here, R and $barR$ is the received signal before and after re-sampling. S denotes transmitted ofdm signal in time domain. The residual Doppler will be compensated by ICI cancellation.

$$\frac{1+\Delta+\delta_i}{1+\hat{\Delta}} = 1 + \gamma_i, \gamma_i << \Delta \tag{4.32}$$

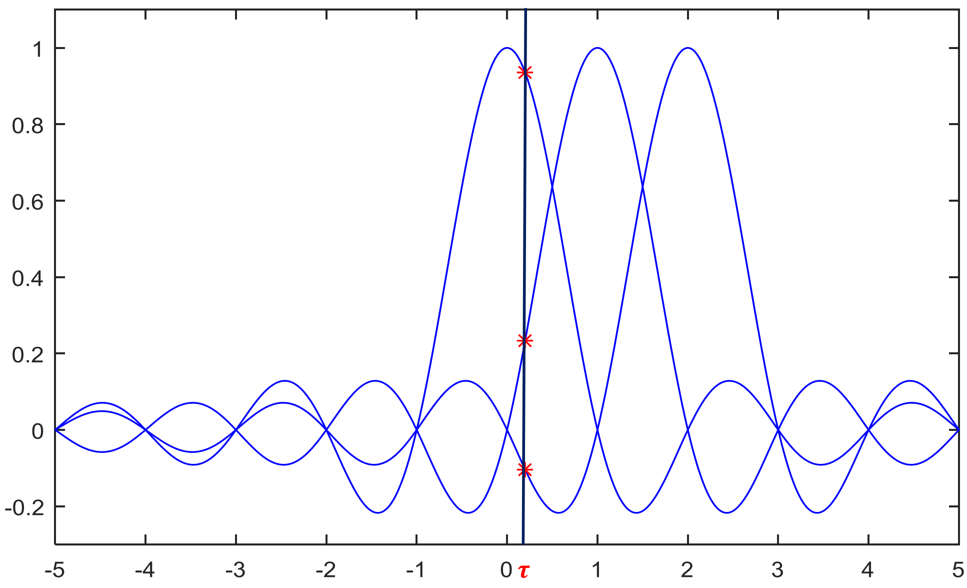

FIGURE 4.7: sinc interpolation for arbitrary rate re-sampling

When re-sampling is performed after down-conversion, we need to add a phase rotation following the re-sampler block.

$$\bar{x}(n) = \underbrace{\sum_{k=0}^{N_{FFT}-1} H(k)D(k)e^{j2\pi k f_0 (\frac{1+\Delta+\delta_i}{1+\hat{\Delta}})nT_s} e^{j2\pi f_c (\frac{\Delta+\delta_i}{1+\hat{\Delta}})nT_s}}_{baseband-sampled} \underbrace{e^{-j2\pi f_c \frac{\hat{\Delta}}{1+\hat{\Delta} nT_s}}}_{phaserotator} \tag{4.33}$$

As illustrated in figure 4.7, to perform an arbitrary re-sampling rate, we need to find $S(nT_s + \tau)$, with τ is an arbitrary value within $0T_s \leq \tau < T_s$. T_s is the sampling period.

$$S(n+\tau) = \sum_{i=-Q+1}^{Q} sinc(\Delta + i)S(n+i) \tag{4.34}$$

$$sinc(x) = \frac{sin(\pi x)}{\pi x} \tag{4.35}$$

For example, $n = 8$ and $Q = 7$ so we have

$$S(8+\tau) = \sum_{i=-6}^{7} sinc(\Delta + i)S(8+i) \tag{4.36}$$

In the left side of $S(8+\tau)$ 7 samples from $2 \rightarrow 8$, and in the right-side 7 samples from $9 \rightarrow 15$ are utilized for interpolation. Generally, $2Q$ neighbors of $S(n+\tau)$ are taken into account. For example, we choose $Q = 7$. To implement the arbitrary rate re-sampling in a low complexity manner, we first

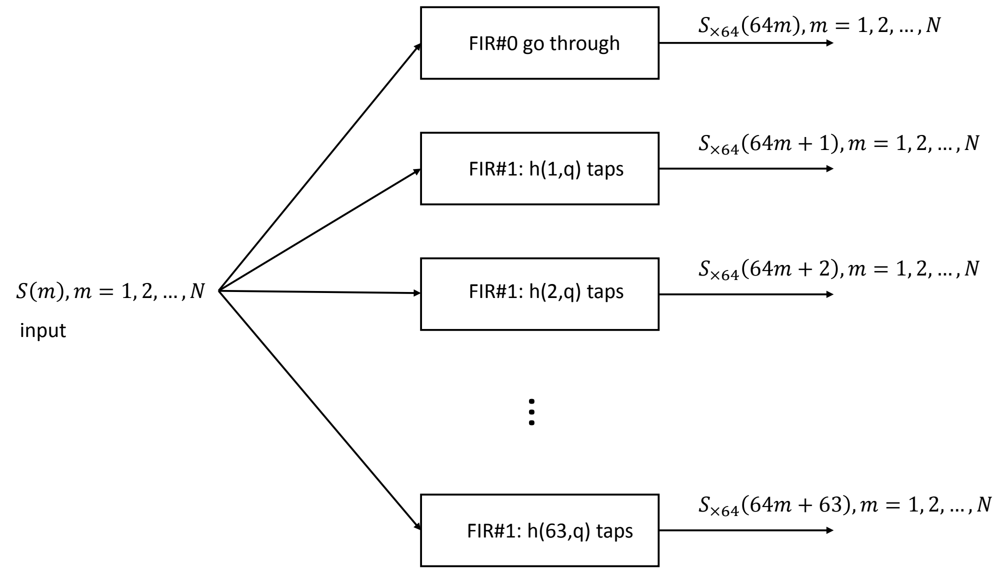

FIGURE 4.8: a bank of 64 FIR filters

up-sample ×64 times of $S(n)$, then apply hold-sample when down-sampling. The hold-sample means

$$S(n+\tau) = S_{\times 64}\Big(64 * n + round(\tau \times 64)/T_s)\Big), \tag{4.37}$$

Up-sampling ×64 times of $S(n)$ can be performed by using a bank of 64 FIR filters as in figure 4.8. The taps of each filter are computed as follow

$$\begin{aligned} h(n,q) &= sinc(q \times T_s/64 + n) \\ n &= 1, 2, \ldots, 63 \\ q &= -Q+1, -Q+2, \ldots, Q \end{aligned} \tag{4.38}$$

Here, n is index of FIR, and q is index of filter tap. There are several techniques to do the re-sampling such as polynomial interpolation, sinc function interpolation, or up-and-down sampling. The below figure shows result of re-sampling by those techniques.

4.3.1.2 A Simple Non-Uniform Phase Rotation

The paper [2] proposed a simple method for compensating the impacts of Doppler rate in frequency domain. In short, since each sub-carrier experiences a difference frequency offset, it applies a simple non-uniform phase rotation which means each sub-carrier will be de-rotated a different phase. We define $R(t)$ is the received signal in time domain. Channel consists of L paths, each path has an attenuation of A_i, and all paths has a Doppler rate of Δ. $D(k)$ and $Y(k)$ are transmitted and received data at sub-carrier k, respectively.

$$R(t) = \sum_{i=1}^{L} \sum_{k=0}^{N-1} A_i D(k) e^{j2\pi(f_c+kf_0)(1+\Delta)(t-\tau_i)} \tag{4.39}$$

Provided that all paths has the same Doppler rate Δ, after down-conversion we can re-write the above equation as

$$R(t) = \sum_{i=1}^{L} \sum_{k=0}^{N-1} A_i D(k) e^{j2\pi(kf_0+\epsilon(k))t} e^{-j2\pi(fc+kf_0)(1+\Delta)\tau_i} \tag{4.40}$$

We denote

$$H(k) = \sum_{i=1}^{L} A_i e^{-j2\pi(f_c+kf_0)(1+\Delta)\tau_i} \tag{4.41}$$

$$\epsilon(k) = (f_c + kf_0)\Delta \tag{4.42}$$

Finally, we get

$$R_B(t) = \sum_{k=0}^{N-1} \underbrace{H(k)}_{multipath} D(k) \underbrace{e^{j2\pi(kf_0+\epsilon(k))t}}_{non-Dopp} \tag{4.43}$$

The paper [2] considered ICI as random noise, and utilizes a simple non-uniform phase rotation to compensate the non-uniform Doppler shift. After FFT demodulation the signal at sub-carrier k can be written as

$$Y(k) \approx H(k)D(k)e^{j2\pi\epsilon(k)} sinc(\pi(l-k+\epsilon(k))) + \underbrace{I(k)}_{ICI} + W(k) \tag{4.44}$$

The estimation of Doppler rate/shift is obtained from previous sections $\hat{\Delta}$. So an estimation $\hat{\epsilon}$ also is determined.

$$\hat{\epsilon} = (f_c + kf_0)\hat{\Delta} \tag{4.45}$$

After FFT, $Y(k)$ is fed into a non-uniform phase-rotation in which each sub-carrier is multiplied by a phase rotation as

$$\bar{Y}(k) = Y(k)e^{-j2\pi\hat{\epsilon}(k)} \tag{4.46}$$

The rest impacts of channel is only channel transfer function caused by multipath, so $\bar{Y}(k)$ is fed into channel estimation and 1-tap equalizer following. However, for high modulation order such as 64QAM, the impact of ICI in equation (1) can not be negligible, and we take the ICI into account in the next section.

4.3.2 Proposed non-uniform ICI cancellation

Go further from [2] we take the ICI into account. Under an assumption that all delay paths has a similar Doppler shift/rate, we are able to separate impacts of Doppler from multipath, and remove ICI before channel estimation. After FFT demodulation, we re-write equation (4.44) as follow. With the estimate Doppler from previous sections (Doppler estimation), the non-uniform ICI matrix also is computed. Then impact of Doppler is removed from the received signal as

$$\begin{bmatrix} Y(1) \\ Y(2) \\ \vdots \\ Y(N-1) \\ Y(N) \end{bmatrix} = \begin{bmatrix} I(1,1) & I(1,2)\dots & I(1,N-1) & I(1,N) \\ I(1,2) & I(2,2)\dots & I(2,N-1) & I(1,N) \\ \vdots & \vdots\ddots & \vdots & \vdots \\ I(1,N-1) & I(2,N)\dots & I(N-1,N-1) & I(N-1,N) \\ I(1,N) & I(2,N)\dots & I(N-2,N) & I(N-1,N) \end{bmatrix} \times \begin{bmatrix} H(1)\times D(1) \\ H(2)\times D(2) \\ \vdots \\ H(N-1)\times D(3) \\ H(N)\times D(N) \end{bmatrix} \tag{4.47}$$

$$I(k,l) = \begin{cases} e^{j\pi\hat{\Delta}k} sinc(\hat{\Delta}k) & \text{if } k \equiv l \\ sinc(\pi(l-k+\hat{\Delta}l))e^{j\pi(l-k+\hat{\Delta}l)} & \text{if } k \neq l \end{cases} \tag{4.48}$$

The estimation of Δ is found from previous sections. After ICI already is removed, the impact of channel is only frequency selective fading caused by mulipath, and can be easily equalized by a simple 1-Tap equation.

$$[\bar{Y}] = [\hat{I}]^{-1}[Y] \tag{4.49}$$

$$[\bar{Y}] \approx [H][D] \tag{4.50}$$

After channel estimation,

$$[\hat{D}] = \frac{[\bar{Y}]}{[\hat{H}]} \tag{4.51}$$

Chapter 5

Time Varying Channel Estimation and ICI Cancellation

5.1 Analysis of Time Varying Channel in OFDM

As mentioned in literature [25, 42, 23, 43, 44, 45, 46, 47, 48] doubly selective channel (both Doppler shift and mulipath happens) is one of the most challenging topics in OFDM systems. In this section, we try to distill impacts of time varying channels on OFDM system. First, we describe time varying

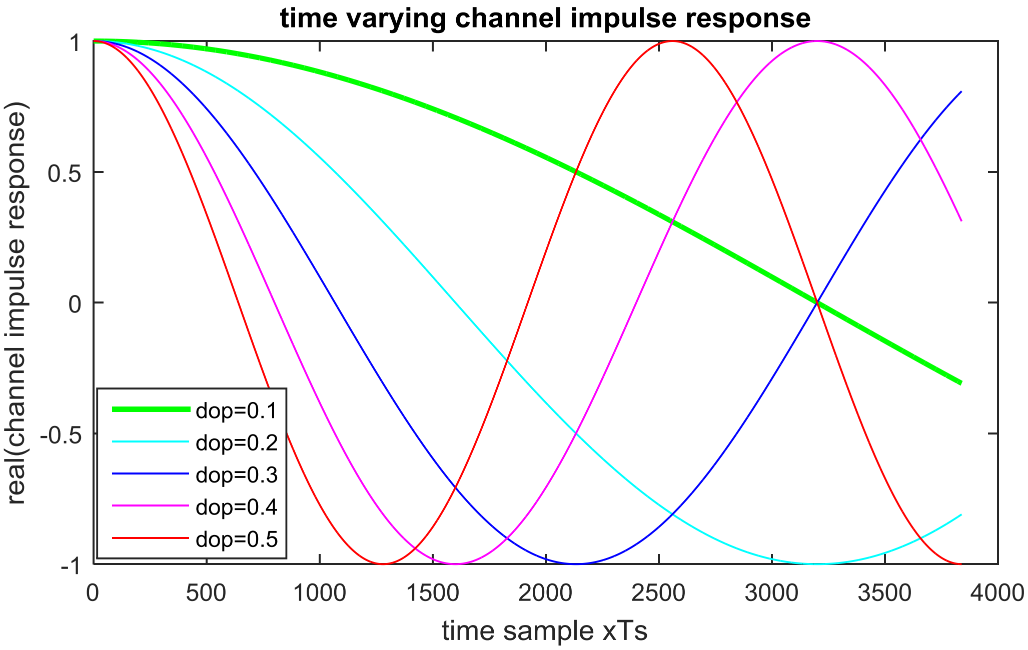

FIGURE 5.1: time varying channel impulse response of 1^{st} tap, $f_d = dop \times f_0$, 1280 samples/an OFDM symbol

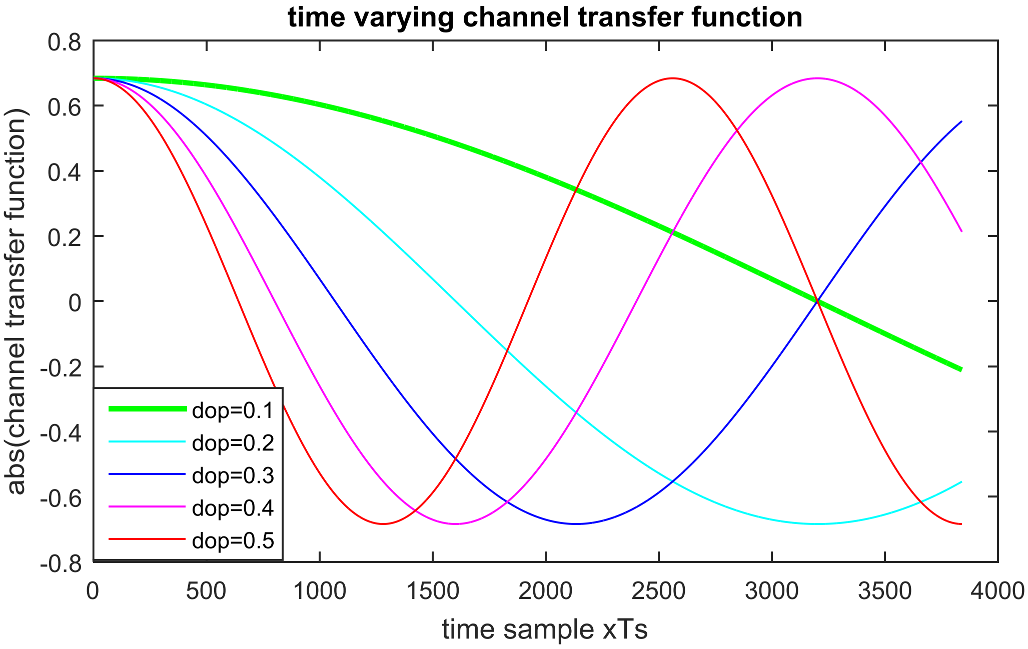

FIGURE 5.2: time varying channel transfer function of 10^{th} sub-carrier, $f_d = dop \times f_0$, two paths has same dop, 1280 samples/an OFDM symbol

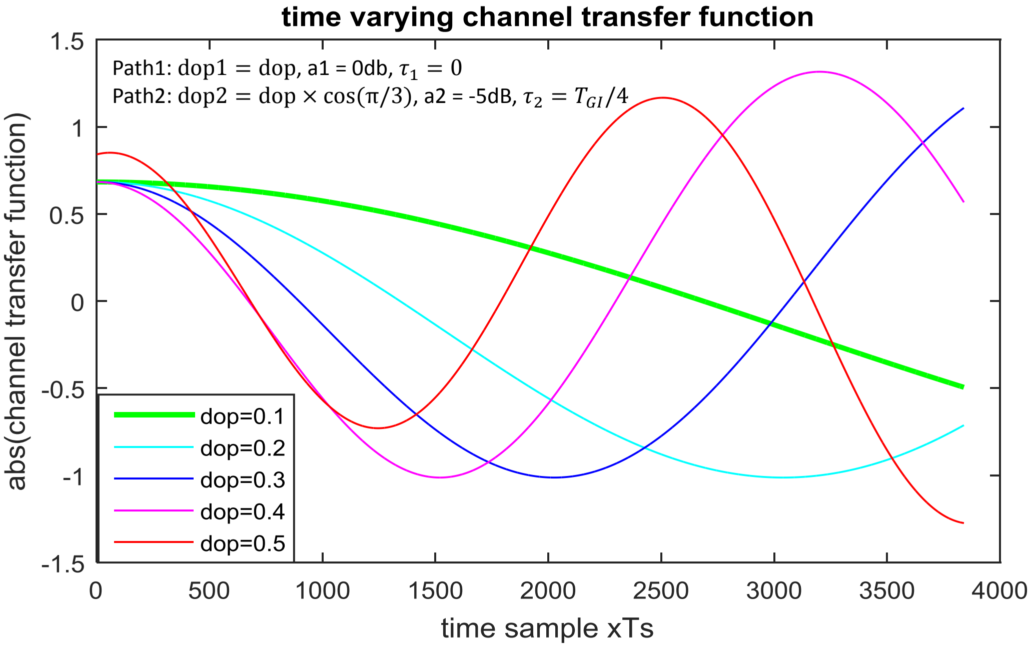

FIGURE 5.3: time varying channel transfer function of 10^{th} sub-carrier, $dop1 = dop, dop2 = dop \times cos(\pi/3)$, 1280 samples/an OFDM symbol

by Taylor series. Next, we consider the effectiveness of linear approximation using two first elements of Taylor series. Then, we explain relation between δh and ΔH. Finally, we show how to estimate channel and parameters needed for ICI cancellation. Generally, the time varying channel impulse response can be describe by Taylor series as

$$h_i(t) = h_i(t_0) + \frac{h'(t_0)}{1!}(t - t_0) + \frac{h''(t_0)}{2!}(t - t_0)^2 + R_2(t) \tag{5.1}$$

Here, $R_2(t)$ is the remainder of Taylor series expansion. As shown in figure 5.1, 5.2, 5.3, when Doppler shift is not greater than $0.1f_0$ CIR and CTF changes linearly within an OFDM symbol (1280 samples). Therefore, it is effective to approximate the channel by two first elements of Taylor series as

$$h_i(n) = \bar{h_i} + \delta_i n, \quad \frac{-N}{2} \leq n \leq \frac{N}{2} \tag{5.2}$$

Here, $h_i(n)$ is time varying path i, and slope δ_i quantifies how fast the path changes in time. We further separate the slope $[\delta]$ and time index $[n]$ as

$$
\begin{bmatrix}
h_0(-3.5) & 0 & 0 & 0 & 0 & 0 & h_2(-3.5) & h_1(-3.5) \\
h_1(-2.5) & h_0(-2.5) & 0 & 0 & 0 & 0 & 0 & h_2(-2.5) \\
h_2(-1.5) & h_(-1.5)1 & h_0(-1.5) & 0 & 0 & 0 & 0 & 0 \\
0 & h_2(-0.5) & h_1(-0.5) & h_0(-0.5) & 0 & 0 & 0 & 0 \\
0 & 0 & h_2(0.5) & h_1(0.5) & h_0(0.5) & 0 & 0 & 0 \\
0 & 0 & 0 & h_2(1.5) & h_1(1.5) & h_0(1.5) & 0 & 0 \\
0 & 0 & 0 & 0 & h_2(2.5) & h_1(0) & h_0(2.5) & 0 \\
0 & 0 & 0 & 0 & 0 & h_2(3.5) & h_1(3.5) & h_0(3.5)
\end{bmatrix}
=
\underbrace{\begin{bmatrix}
\bar{h}_0 & 0 & 0 & 0 & 0 & 0 & \bar{h}_2 & \bar{h}_1 \\
\bar{h}_1 & \bar{h}_0 & 0 & 0 & 0 & 0 & 0 & \bar{h}_2 \\
\bar{h}_2 & \bar{h}_1 & \bar{h}_0 & 0 & 0 & 0 & 0 & 0 \\
0 & \bar{h}_2 & \bar{h}_1 & \bar{h}_0 & 0 & 0 & 0 & 0 \\
0 & 0 & \bar{h}_2 & \bar{h}_1 & \bar{h}_0 & 0 & 0 & 0 \\
0 & 0 & 0 & \bar{h}_2 & \bar{h}_1 & \bar{h}_0 & 0 & 0 \\
0 & 0 & 0 & 0 & \bar{h}_2 & \bar{h}_1 & \bar{h}_0 & 0 \\
0 & 0 & 0 & 0 & 0 & \bar{h}_2 & \bar{h}_1 & \bar{h}_0
\end{bmatrix}}_{\bar{h}-circularmatrix}
+
\underbrace{\begin{bmatrix}
\delta_0 & 0 & 0 & 0 & 0 & 0 & \delta_2 & \delta_1 \\
\delta_1 & \delta_0 & 0 & 0 & 0 & 0 & 0 & \delta_2 \\
\delta_2 & \delta_1 & \delta_0 & 0 & 0 & 0 & 0 & 0 \\
0 & \delta_2 & \delta_1 & \delta_0 & 0 & 0 & 0 & 0 \\
0 & 0 & \delta_2 & \delta_1 & \delta_0 & 0 & 0 & 0 \\
0 & 0 & 0 & \delta_2 & \delta_1 & \delta_0 & 0 & 0 \\
0 & 0 & 0 & 0 & \delta_2 & \delta_1 & \delta_0 & 0 \\
0 & 0 & 0 & 0 & 0 & \delta_2 & \delta_1 & \delta_0
\end{bmatrix}}_{circular-matrix}
\times
\underbrace{\begin{bmatrix}
-3.5 & 0 & 0 & 0 & 0 & 0 & 0 & 0 \\
0 & -2.5 & 0 & 0 & 0 & 0 & 0 & 0 \\
0 & 0 & -1.5 & 0 & 0 & 0 & 0 & 0 \\
0 & 0 & 0 & -0.5 & 0 & 0 & 0 & 0 \\
0 & 0 & 0 & 0 & 0.5 & 0 & 0 & 0 \\
0 & 0 & 0 & 0 & 0 & 1.5 & 0 & 0 \\
0 & 0 & 0 & 0 & 0 & 0 & 2.5 & 0 \\
0 & 0 & 0 & 0 & 0 & 0 & 0 & 3.5
\end{bmatrix}}_{diagonal-matrix}
\tag{5.3}
$$

In the frequency domain,

$$
[F][h][F]^{-1} = \underbrace{[F][\bar{h}][F]^{-1}}_{[\bar{H}]-diagonal} + \underbrace{[F][\delta][F]^{-1}}_{[\Delta]-diagoal} \times \underbrace{\Big([F][t][F]^{-1}\Big)}_{[T]-cicular} \tag{5.4}
$$

Total of channel transfer function and ICI

$$
[I] = [\bar{H}] + [T][\Delta] \tag{5.5}
$$

Now we consider the relationship between δh the slope of channel taps in time domain and ΔH the slope of channel transfer function. We denote the time varying channel transfer function is function of time samples $H(k,n)$. At instant time n samples $nT_s(sec)$, the channel transfer function $H(k,n)$ is computed via FFT of channel impulse response $h(l,n)$ as

$$\begin{aligned}
[H(n)]_{N\times 1} &= [F]_{N\times N}[h]_{N\times 1} \\
[H(n)] &= [F]_{N\times N}\Big([\bar{h}]_{N\times 1} + [\delta]_{N\times N}[n]_{N\times 1}\Big) \\
[H(n)] &= [F]_{N\times N}[\bar{h}]_{N\times 1} + [F]_{N\times N}[\delta]_{N\times N}[n]_{N\times 1} \\
[H(n)] &= [\bar{H}] + \underbrace{\Big([F][\delta][F]^{-1}\Big)}_{\Delta-diagonal}[F][n] \\
[H(n)] &= [\bar{H}] + [\Delta](N\times n)
\end{aligned} \tag{5.6}$$

Therefore, when the channel impulse response changes in time with the slope $[\delta]$, the channel transfer function also changes in time with a slope Δ and

$$[\Delta] = [F][\delta][F]^{-1} \tag{5.7}$$

Conclusion, the $[\delta]$ and $[\Delta]$ can be interchangeable in term of constructing the ICI. In following sections, we show that working with $[\Delta]$ is more convenient.

5.2 Conventional Channel Estimation

In OFDM based systems such as DVB-T, ISDB-T, and 4G-LTE, channel estimation usually is performend in frequency domain and consits of two steps. The first step is estimating channel transfer function at pilot poisitions by least square, and the scond step is interpolating the channel transfer function for all subcarrier as presented in [23, 35, 47, 49]. First, channel transfer function is computed at pilots as

$$\hat{H}(k) = \frac{Y(k)}{X(k)}, \qquad k \in Pilot \tag{5.8}$$

Next, the estimate channel transfer function at pilots are fed into two interpolation, one is in frequency direction, and the other is in time direction. The interpolation is implemented by using raised cosine filter. Interpolation factors of two interpolates in this case is ×2.

5.2.1 Interpolation using FIR Filter

There are two parameters are considered to compute the taps of raised cosine filter for interpolation. The first on is the cut-off frequency and the other is roll-off factor. For interpolation in frequency domain, the cut-off frequency of raised-cosine filter depends on how fast the channel transfer function

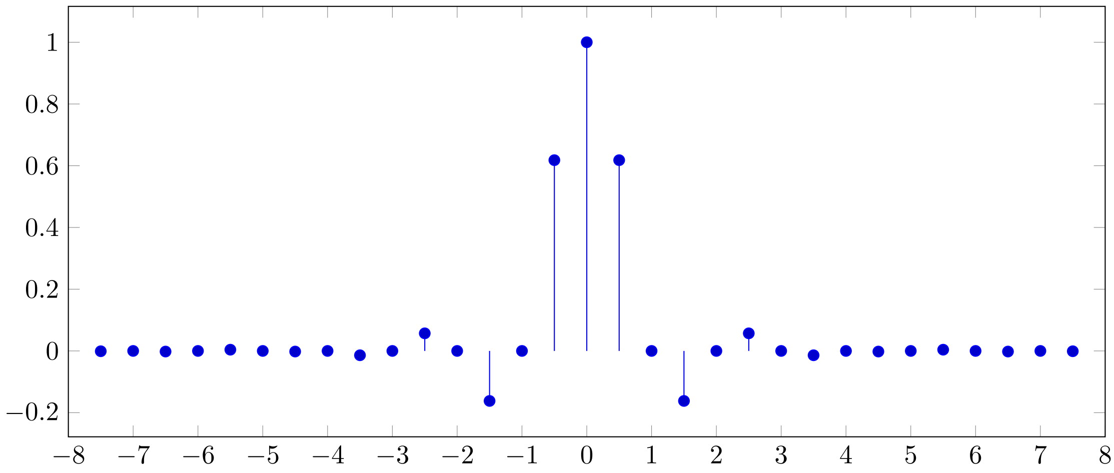

Figure 5.4: raised cosine taps $f_{cut} = 0.5, \beta = 0.35$

changes across sub-carriers, or how large the delay spread is. With the pattern pilots shown in our pilot pattern, the distance between two pilots in frequency domain is $4f_0$, so the maximum delay spread can be measured without aliasing is $T_0/8$. Assuming that delay spread is small than $T_0/8$, the cut-off frequency of raised-cosine filter can be choose $1/2$. $(2N+1)$ taps of the raised-cosine filter for interpolation in frequency direction is below. The roll-off factor β is chosen around 0.3 so that the interpolated channel transfer function is smoothed.

$$h(n) = \frac{sin(\pi n/2)}{\pi n/2} \times \frac{cos(\pi \beta n/2)}{1-(\beta n)^2}, \qquad n = -N:1:N, f_{cut} = 0.5, \beta \approx 0.35 \tag{5.9}$$

Here, β is the roll-off factor. The taps and channel transfer function of raised-cosine filter for frequency interpolation is shown in figure 5.4 and figure 5.5. Similarly, for the interpolation in time direction, the cut-off frequency of raised-cosine filter depends on how fast the channel changes in time domain, or how large the Doppler spread. Assuming that the Doppler spread is smaller than $1/(8T_{sb})$ which is $f_0/12$ since GI is $T_0/2$. A cut-off frequency of 0.33 can be chosen, and $(2N+1)$ taps of the raised-cosine filter for interpolation in time domain is

$$h(n) = \frac{sin(\pi n/3)}{\pi n/3} \times \frac{cos(\pi \beta n/3)}{1-(\beta n/1.5)^2}, \qquad n = -N:1:N, f_{cut} = 0.33, \beta \approx 0.3 \tag{5.10}$$

Here, β is the roll-off factor. The taps and channel transfer function of raised-cosine filter for frequency interpolation are computed in the same way.

FIR-based interpolation is low complexity, however, this method is not optimal when delay spread and Doppler spread may change. Interpolated values of edge sub-carriers and edge symbols are not accurate due to the Gibbs phenomenon [1-10]. In the next section, we will review an LMMSE base interpolation, in which, delay spread and Doppler spread is taken into account when determining the interpolation through auto-correlation functions.

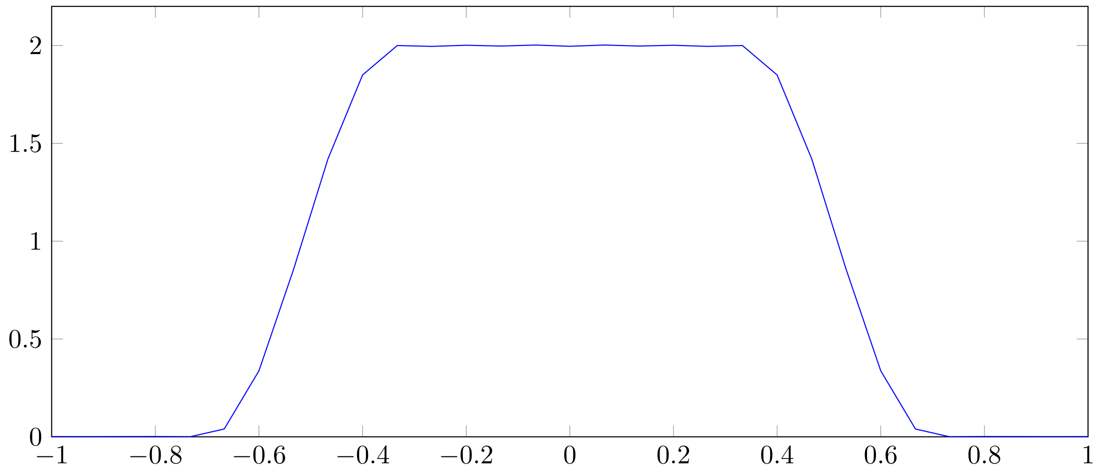

FIGURE 5.5: transfer function of rs $f_{cut} = 0.5, \beta = 0.35$

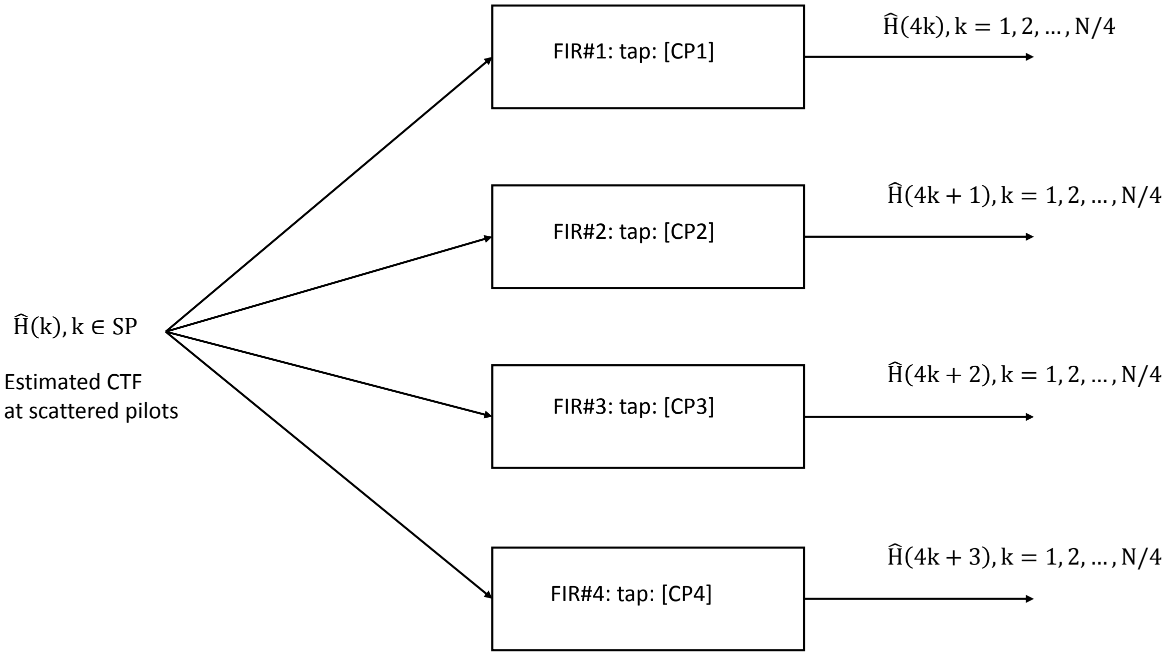

FIGURE 5.6: LMMSE channel interpolation

5.2.2 LMMSE Based Interpolation

From the estimate channel transfer function at pilots, the whole channel transfer function can be estimated by LMMSE based interpolation. The LMMSE based interpolation can be implemented in a simple manner using FIR filters as shown in figure 5.6. The filter taps are computed as follow

$$R_{HH}(k) = \frac{1}{N} \sum_{n=0}^{N} H(n+k)H^*(n) \tag{5.11}$$

$$\begin{bmatrix} [R_{HH}] = R_{HH}(1) & R^*_{HH}(5) & R^*_{HH}(9) & R^*_{HH}(11) & R^*_{HH}(17) & R^*_{HH}(21) \\ R_{HH}(5) & R_{HH}(1) & R^*_{HH}(5) & R^*_{HH}(9) & R^*_{HH}(11) & R^*_{HH}(17) \\ R_{HH}(9) & R_{HH}(5) & R_{HH}(1) & R^*_{HH}(5) & R^*_{HH}(9) & R^*_{HH}(11) \\ R_{HH}(13) & R_{HH}(9) & R_{HH}(5) & R_{HH}(1) & R^*_{HH}(5) & R^*_{HH}(9) \\ R_{HH}(17) & R_{HH}(13) & R_{HH}(9) & R_{HH}(5) & R_{HH}(1) & R^*_{HH}(5) \\ R_{HH}(21) & R_{HH}(17) & R_{HH}(13) & R_{HH}(9) & R_{HH}(5) & R_{HH}(1) \end{bmatrix} \tag{5.12}$$

$$\begin{aligned} [CP_1] &= [R_{HH}(9) \quad R_{HH}(5) \quad R_{HH}(1) \quad R^*_{HH}(5) \quad R^*_{HH}(9) \quad R^*_{HH}(13)]/[R_{HH}] \\ [CP_2] &= [R_{HH}(10) \quad R_{HH}(6) \quad R_{HH}(2) \quad R^*_{HH}(4) \quad R^*_{HH}(8) \quad R^*_{HH}(12)]/[R_{HH}] \\ [CP_3] &= [R_{HH}(11) \quad R_{HH}(7) \quad R_{HH}(3) \quad R^*_{HH}(3) \quad R^*_{HH}(7) \quad R^*_{HH}(11)]/[R_{HH}] \\ [CP_4] &= [R_{HH}(12) \quad R_{HH}(8) \quad R_{HH}(4) \quad R^*_{HH}(2) \quad R^*_{HH}(6) \quad R^*_{HH}(10)]/[R_{HH}] \end{aligned} \tag{5.13}$$

Here, $R_{HH}(k)$ is the auto-correlation function, and $[R_{HH}]$ is the auto-correlation matrix. Taps/-coefficients of FIR filters are $[CP_1], [CP_2], [CP_3], [CP_4]$. This method requires information about the channel through the auto-correlation functions which describes how fast the channel varies over sub-carriers in frequency domains, and over OFDM symbols in time domain. However, the channel transfer functions are available only at pilots. To solve this problem, we can initialize $R_{HH}(k, 1)$ of the first OFDM symbol with assumption that all sub-carriers is pilot in the first OFDM symbol. When OFDM symbol $m > 1$ arrives, $R_{HH}(k, m-1)$ is utilized for channel estimation, and equalization. Channel at all sub-carrier index can be estimated through using hard-decision of equalized data

$$\hat{H}(k, m) = \frac{Y(k, m)}{X(k, m)_{harddecision}} \tag{5.14}$$

$R^I_{HH}(k, m)$ can be computed from $\hat{H}(k, m)$ using equation (4.31). Then $R_{HH}(k, m)$ at symbol m is updated as

$$R_{HH}(k, m) = \beta R_{HH}(k, m-1) + (1-\beta) R^I_{HH}(k, m), \qquad 0 \leq \beta \leq 1 \tag{5.15}$$

Here, β is memory factor, and depends on how fast the channel changes in time domain. We can choose β around 0.8 for Doppler shift around 10% of a sub-carrier space.

5.3 Proposed Channel Estimation and ICI Cancellation

Since ICI happens due to mobility of OFDM receiver, and/or time varying channel, pilots (freq. domain) already experience ICI. Therefore, estimating channel from ICI-corrupted pilots is very challenged. In addition, performance of ICI cancellation and channel equalization depends on the accuracy of channel estimation. In this section, we propose methods for channel estimation under ICI, and ICI cancellation as well. Overall, we consider three methods. The first one is iterative channel estimation and ICI cancellation. The key idea is removing ICI from pilots and re-estimating

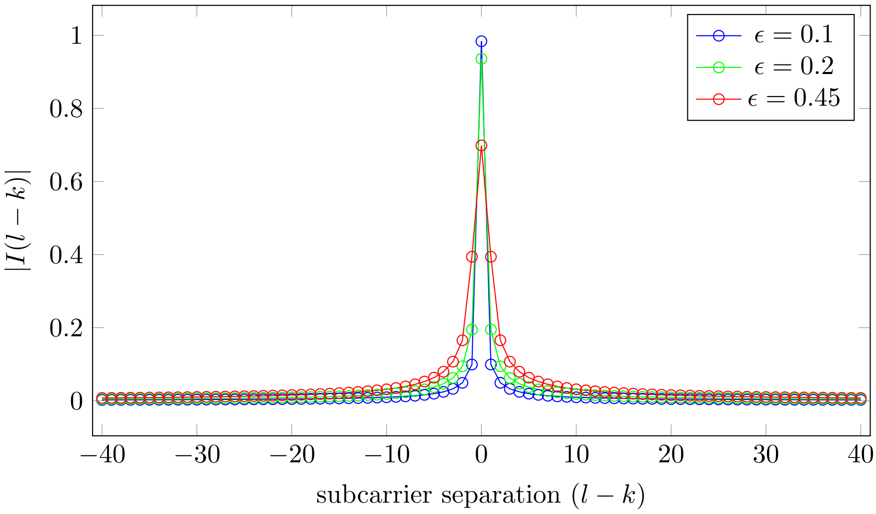

FIGURE 5.7: $|I(k \leftarrow l)|$

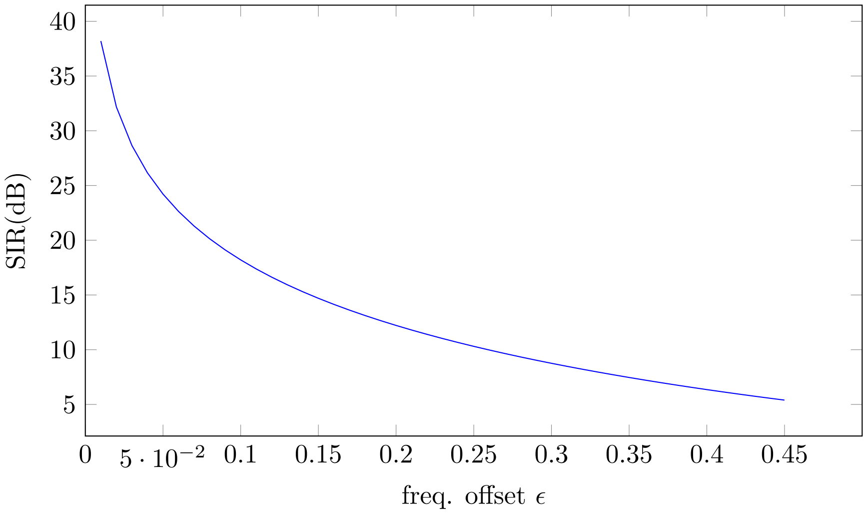

FIGURE 5.8: CNR due to ICI $10log(\frac{P_{sub}}{P_{ICI}})$

channel at the second iteration. Since the re-estimated channel is more accurate, better performance can be achieved. The second method consider a strong de-noising method called SALAS. We apply SALAS to improve then accuracy of channel estimation under ICI (noise)figure 5.7 and figure 5.8. Finally, we consider a parametric channel estimation which searching for attenuation, delay, Doppler shift of each path. Since the channel consist of a few paths, this method is robust to noise (ICI), and promise to provides a good performance.

ICI degrades the accuracy of channel estimation. After FFT-demodulation, the signal at subcarrier k under ICI and random noise is written as

$$Y(k) = H(k,k)D(K) + \underbrace{\sum_{l=1, l\neq k}^{N} H(l,k)D(l)}_{ICI} + \underbrace{W(k)}_{AWGN} \tag{5.16}$$

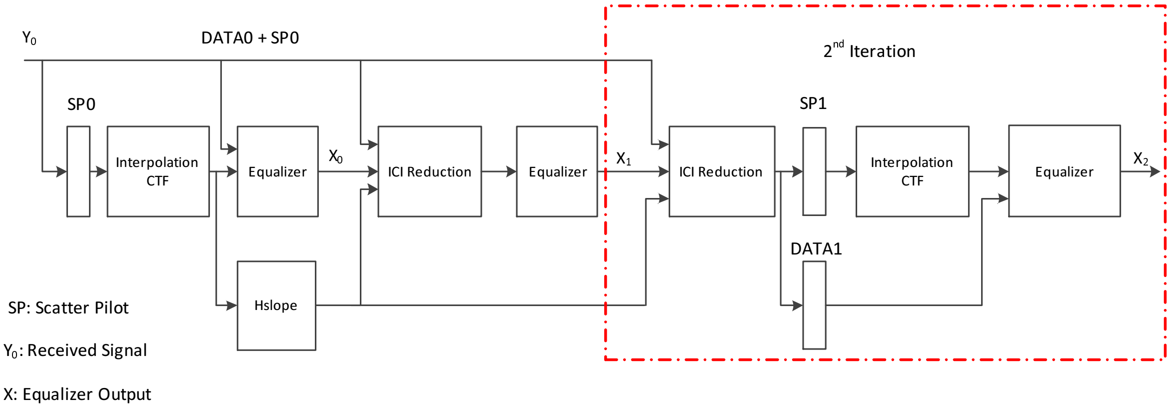

FIGURE 5.9: iterative channel estimation and ici cancellation

$$[\mathbf{Y}] = [\mathbf{H}][\mathbf{D}] + [\mathbf{W}] \tag{5.17}$$

$Y(k)$ and $D(k)$ are received and transmitted data at subcarrier k, respectively. $H(k,l)$ is ICI from subcarrier l to subcarrier k and $W(k)$ is AWGN noise. The channel transfer function (CTF) at pilots are computed from (1) using Least Square as

$$\hat{H}(k,k) = H(k,k) + \frac{ICI(k)}{D(k)} + \frac{W(k)}{D(k)}, k \in SP, pilot - position \tag{5.18}$$

Clearly, $\hat{H}(k,k)$ is corrupted by ICI, and then the estimated CTF is noisy though the LMMSE is applied in [20, 47] for interpolating the CTF at all subcarrier positions. In addition, the estimated $H(\hat{k},k)$ is the most important part of ICI cancellation since $H(\hat{k},k)$ is the main diagonal of ICI matrix, and it is used to find the slope of time varying channel transfer function. In conclusion, ICI cancellation performance strongly depends on the accuracy of $H(\hat{k},k)$

5.3.1 Iterative Channel Estimation and ICI Cancellation

Since estimated CTF is already contaminated by ICI, we propose an iterative channel estimation and ICI cancellation. The idea is removing ICI from pilots and re-estimating $H(k,k)$ at the second iteration. Figure 5.9 shows this scheme. Details about the method can be found in [1-10].

5.3.2 SALSA De-noising Channel Estimation

Conventional methods for denoising can be classified in two methods. The first one figure 5.10.b . is using a threshold as proposed in [48] and the second figure 5.10.c. is using a filter proposed in [50, 51]. Performance of these methods is limited by two reasons. The first one is Gibbs phenomenon. When a threshold is applied and some taps are suddenly cut-off, this suddenly changes cause distortion as

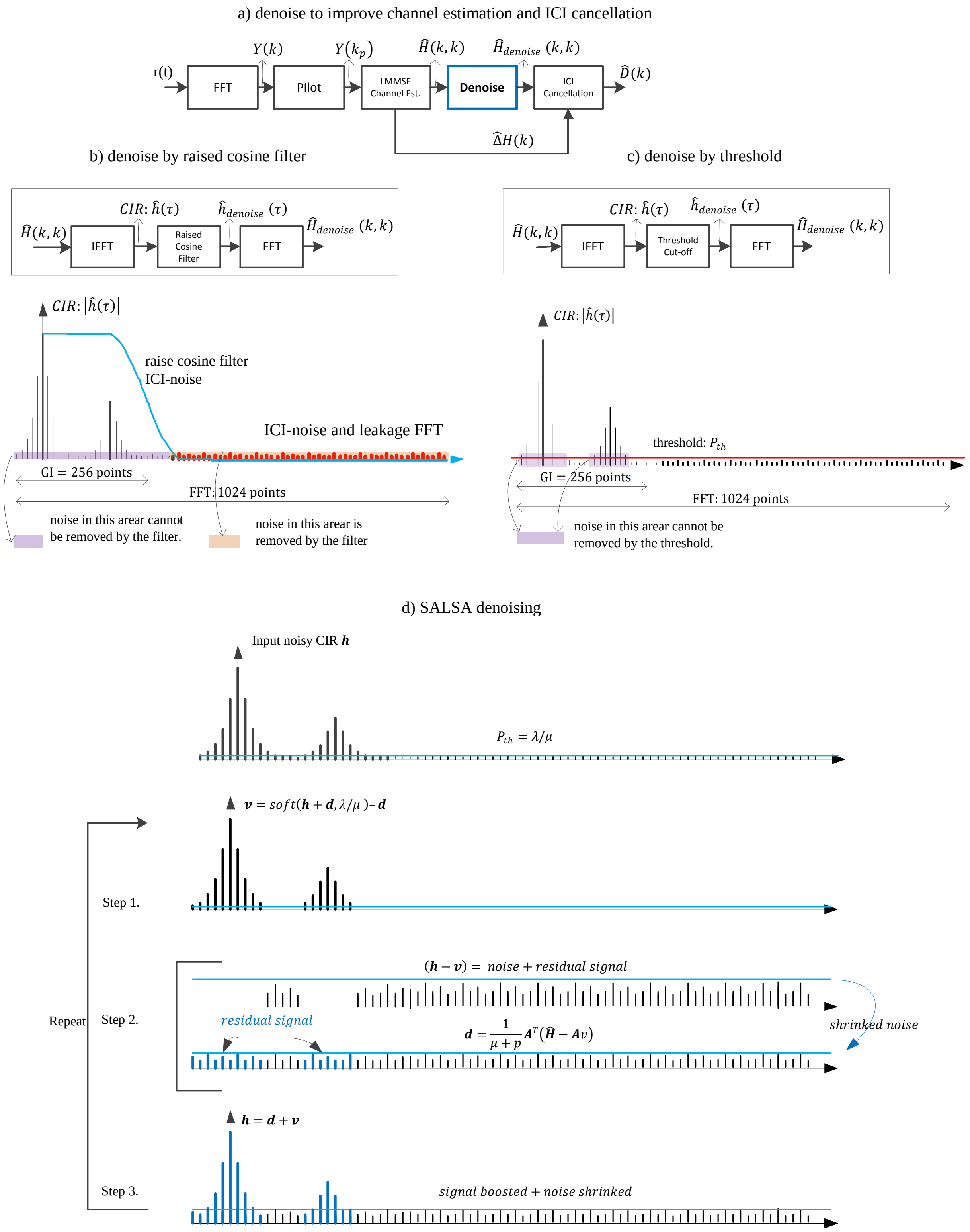

FIGURE 5.10: improved channel estimation by de-noising

described in Gibbs phenomenon. Secondly, either a threshold or a filter is not able to removed noise attached to strong taps (CIR).

Recently, an efficient algorithm in sparse signal processing called SALAS in figure 5.10.d). has been proposed in [42, 52]. This algorithm is low complexity, free-matrix operations, and globally convergent as presented in [53]. Most importantly, this algorithm correct the leakage problem of FFT, and does not cause Gibbs phenomenon. Therefore, we investigate applying this algorithm for de-noising the estimated channel in OFDM systems and compare with conventional methods. Simulation results show the SALSA clearly outperform conventional noise reduction methods, and so improve significantly channel estimation and ICI cancellation. Now we present SALSA and apply it for de-noising in channel estimation. In compressing/sparse signal processing, de-noising the CIR can be considered as below

$$h^{opt} = \arg\min_{h} \frac{1}{2}||\hat{H} - Ah||_2^2 + \lambda||h||_1 \tag{5.19}$$

Here, $\hat{H}$ is the noisy CTF estimated from the previous section, and A is FFT matrix. The optimal estimation of CIR can be found by solving (6). Solving optimization (6) includes a energy constraint $||\hat{H} - Ah||_2^2$, or so-called l_2 norm, and sparsity constraint $\lambda||h||_1$ or so-called l_1 norm. SALSA solving (6) is summarized as

Algorithm 1 SALSA for basic pursuit denoising

```
initialize: $\mu > 0$, $\mathbf{d}$
repeat
.    $\mathbf{v} \leftarrow \text{soft}\ (\mathbf{h} + \mathbf{d}, \lambda/\mu) - \mathbf{d}$
.    $\mathbf{d} \leftarrow \frac{1}{\mu+p}\mathbf{A}^{\mathbf{T}}(\hat{\mathbf{H}} - \mathbf{A}\mathbf{v})$
.    $\mathbf{h} \leftarrow \mathbf{d} + \mathbf{v}$
end
```

$\mathbf{A}^T$ is IFFT matrix. Therefore, this algorithm does not require matrix inversion. In addition, $\mathbf{A}$ and $\mathbf{A}^T$ are FFT and IFFT matrix, so the computational cost is low. For details about the SALSA, please refer to [42, 52, 53]. We explain the SALSA in an intuitive way as shown in figure 5.10.d).

5.3.3 Path-Searching Channel Estimation

In this section, we aim to handle higher Doppler shift, from 10% to 20% of a subcarrier space. Such a high Doppler shift happens in underwater acoustic communication, or wireless systems with very high speed receivers such as bullet trains, or wireless systems operating at high frequency (above 2(GHz)) . In those cases, the channel is sparse consisting of few distinctive paths, but has long delay spread, and each path has a severe Doppler shift. Under such a severe Doppler shift, the raw estimation of channel transfer function at pilots are already corrupted by ICI(inter-carrier interference). Consequently, interpolating the whole channel transfer function from corrupted pilots yield a poor performance.

Our ideas are separating ICI caused by Doppler and channel transfer function caused by delays and removing ICI from received signal before estimating the channel transfer function or the diagonal of an ICI matrix as shown later. Therefore, our method can estimate channel more accurately under severe Doppler shift. Similar to principle of Matching Pursuit algorithm, we estimate the first path, then subtract the first path from the received signal, and continue to search for the second path. We utilize scattered and continual pilots in two successive OFDM symbol to estimate Delay and Doppler shift of each path and then the attenuation of each path also is estimated. After parameters of paths are determined, we consider three ICI cancellation solutions. The first solution called **I-ICI** (Inverse-ICI) directly solves the ICI matrix equation by finding an inverse matrix of the ICI matrix, or finding N inverse of sub-matrix. The second solution is **J-ICI** (Jacobi-ICI) which apply Jacobi iteration method for solving the ICI matrix equation without finding an inverse matrix. Finally, the third solution is **S-ICI** (Slope-ICI) which uses a linear approximation model for channel transfer function and Jacobi iteration method rather than matrix inversion. We also consider iterative ICI cancellation and re-estimating channel after ICI is removed from pilots.

The base-band OFDM signal of OFDM symbol m is written as follow

$$S(t) = \sum_{k=0}^{N-1} D(k) e^{j2\pi k f_0 t} \qquad 0 \leq t \leq T_0 \tag{5.20}$$

Here, $D(k)$ is symbol at sub-carrier k, f_0 is sub-carrier space, and T_0 is the effective OFDM symbol length. The number of sub-carrier is N. We assume that attenuation, delay and Doppler shift of each path is constant within two successive OFDM symbol, but changes over OFDM symbols. For each path, all sub-carrier experiences a common Doppler shift of $\Delta_i(Hz)$. In addition, the delay spread is assumed smaller than guard interval. Then, the received signal of m^{th} symbol at base band can be written as follow

$$R(t) = \sum_{i=1}^{L} \sum_{k=0}^{N-1} A_i D(k) e^{j2\pi(kf_0+\Delta_i)(t-\tau_i)} \tag{5.21}$$

Here, L is number of delay paths. A_i, τ_i, Δ_i are attenuation, delay, and Doppler shift of i^{th} path. After FFT demodulation, the signal at sub-carrier k of OFDM symbol m is written as follow

$$Y(k) = \sum_{i=1}^{L} \left\{ D(k) A_i B_i(k) sinc(\frac{\pi\Delta_i}{f_0}) e^{\frac{j\pi\Delta_i}{f_0}} + \underbrace{\sum_{\substack{l=0 \\ l\neq k}}^{N-1} D(l) A_i B_i(l) sinc\Big(\pi(l-k+\frac{\Delta_i}{f_0})\Big) e^{j\pi(l-k+\frac{\Delta_i}{f_0})}}_{ICI\ caused\ by\ path\#i} \right\} \tag{5.22}$$

Here, $B_i(k) = e^{-j2\pi(kf_0+\Delta_i)\tau_i}$ represents frequency selective fading caused by delay τ_i. In matrix form,

$$[\mathbf{Y}] = \left\{ \sum_{i=1}^{L} A_i[\mathbf{B_i}][\mathbf{I_i}] \right\} [\mathbf{D}] \tag{5.23}$$

$$[\mathbf{B_i}] = \mathbf{diag}\Big(\mathbf{B_i(k)}\Big) \tag{5.24}$$

$$\mathbf{I_i}(k,k) = sinc\big(\frac{\pi\Delta_i}{f_0}\big)e^{\frac{j\pi\Delta_i}{f_0}} \tag{5.25}$$

$$\mathbf{I_i}(k,l) = sinc\Big(\pi(l-k+\frac{\Delta_i}{f_0})\Big)e^{j\pi(l-k+\frac{\Delta_i}{f_0})} \tag{5.26}$$

$[\mathbf{B_i}]$ is a diagonal matrix which represents frequency selective fading caused by delay τ_i. $\mathbf{I_i}(k,l)$ is amplitude of ICI from sub-carrier l to sub-carrier k. Similar to DVB-T, ISDB-T systems, we utilize a scattered pilot pattern, and continual pilots. For OFDM symbol m, scattered and continual pilots are placed as

$$SP(m) = mod(m-1,4) + 4p + 1, \qquad p = 0,1,2,...40 \tag{5.27}$$

$$CP = 1:16:N, \forall m \qquad N: number-of-subcarrier \tag{5.28}$$

$SP(m)$ and CP indicates positions of scattered pilots and continual pilots in OFDM symbol m, respectively. As principle of Nyquist sampling theorem, the maximum Doppler shift can be estimated by continual pilot is

$$\hat{\Delta}_{max} = \frac{1}{2T_{sb}} = \frac{f_0}{2(1+T_{GI}/T_0)} \tag{5.29}$$

Here, T_{sb} is OFDM symbol length included guard interval T_{GI}. Likewise, the maximum delay can be estimated by scattered pilots from two successive OFDM symbols is

$$\hat{\tau}_{max} = \frac{1}{2f_0} = T_0/2 \tag{5.30}$$

We first search for $(\hat{A_1}, \hat{\tau_1}, \hat{\Delta_1})$ of the first path, then subtract the first path from the received signal, and then continue searching for the 2^{nd} path $(\hat{A_2}, \hat{\tau_2}, \hat{\Delta_2})$. After FFT demodulation, the channel transfer function at pilots are computed as

$$W(k,m) = \frac{Y(k,m)}{D(k,m)}, \qquad k \in SP(m) \cup CP \tag{5.31}$$

$$W(k,m+1) = \frac{Y(k,m+1)}{D(k,m+1)}, \qquad k \in SP(m+1) \cup CP \tag{5.32}$$

First, delay τ_1 is estimated by a cost function as

$$\hat{\tau_1} = \max_{\hat{\tau_1} \in [0:T_s:T_{GI}]} \left| \sum_{k \in S_m} W(k,m) e^{j2\pi k f_0 \hat{\tau_1}} + \sum_{k \in S_{m+1}} W(k,m+1) e^{j2\pi k f_0 \hat{\tau_1}} \right|^2 \tag{5.33}$$

$$\begin{aligned} S_m &= SP(m) \cup CP \\ S_{m+1} &= SP(m+1) \cup CP \end{aligned} \tag{5.34}$$

The delay τ_1 causes a phase rotation $B_1(k) = e^{-j2\pi(kf_0+\Delta_1)\tau_1}$ with a rotation speed of $f_0\tau_1$ across sub-carriers k. Therefore, the cost function de-rotates the phase rotation to find τ_1. After τ_1 is estimated, Δ_1 is estimated using continual pilot as

$$W_\tau(m) = \sum_{k \in CP} \frac{W(k,m)}{|W(k,m)|} e^{j2\pi k f_0 \hat{\tau_1}} \tag{5.35}$$

$$W_\tau(m+1) = \sum_{k \in CP} \frac{W(k,m+1)}{|W(k,m+1)|} e^{j2\pi k f_0 \hat{\tau_1}} \tag{5.36}$$

$$\hat{\Delta_1} = \frac{f_0}{2\pi(1+T_{GI}/T_0)} \angle \left\{ conj(W_\tau(m)) W_\tau(m+1) \right\} \tag{5.37}$$

Considering subcarrier k, the Doppler shift Δ_1 causes a phase rotation from symbol-to-symbol in time domain as $W(k,m+1) = W(k,m)e^{j2\pi\Delta_1(T_0+T_{GI})}$, therefore, the difference in phase between $W(k,m)$ and $W(k,m+1)$ indicates the Doppler shift Δ_1.

Our key idea is removing the ICI from received signal before estimating the attenuation A_1. We re-write (4) for the first path

$$[\mathbf{Y}] = A_1[\mathbf{B_1}][\mathbf{I_1}][\mathbf{D}] + \underbrace{\sum_{i=2}^{L} A_i[\mathbf{B_i}][\mathbf{I_i}][\mathbf{D}]}_{Z_1} \tag{5.38}$$

The residual Z_1 is treated as noise when estimating the first path. After delay $\hat{\tau_1}$ and Doppler shift $\hat{\Delta_1}$ are estimated, the diagonal matrix $[\hat{\mathbf{B_1}}]$ and the ICI matrix $[\hat{\mathbf{I_1}}]$ are determined. Both ICI and impacts of delays are removed

$$[\hat{\mathbf{I_1}}]^{-\mathbf{1}}[\hat{\mathbf{B_1}}]^{-\mathbf{1}}[\mathbf{Y}] = \hat{A_1}[\mathbf{D}] \tag{5.39}$$

To reduce the computational cost, we only keep the diagonal of $[\mathbf{I_1}]$ since $|I(k,l)|$ decays quickly when $|l-k|$ increases. Thus, the attenuation A_1 is averaged as

$$\hat{A}_1 = \frac{1}{N_{SPCP(m)}} \sum_{k \in SP(m) \cup CP} \frac{W(k,m) e^{j2\pi k f_0 \hat{\tau}_i} e^{\frac{-j\pi\hat{\Delta}_1}{f_0}}}{sinc(\frac{\pi\hat{\Delta}_1}{f_0})} \tag{5.40}$$

$N_{SPCP(m)}$ is total number of scattered pilots and continual pilots in OFDM symbol m. The channel transfer function caused by the first path on sub-carrier k is calculated as

$$\hat{H}^{(1)}(k,m) = \hat{A}_1 \hat{B}_1 sinc(\frac{\pi\hat{\Delta}_1}{f_0}) e^{\frac{j\pi\hat{\Delta}_1}{f_0}} \tag{5.41}$$

$$\hat{H}^{(1)}(k,m+1) = \hat{A}_1 \hat{B}_1 sinc(\frac{\pi\hat{\Delta}_1}{f_0}) e^{\frac{j\pi\hat{\Delta}_1}{f_0}} e^{j2\pi(T_0+T_{GI})\hat{\Delta}_1} \tag{5.42}$$

After the first path $(\hat{A}_1, \hat{\tau}_1, \hat{\Delta}_1)$ is estimated, the impacts of the first channel is subtracted from the received signal as follow

$$\hat{H}^{(r)}(k,m) = W(k,m) - \hat{H}^{(1)}(k,m) \tag{5.43}$$

$$\hat{H}^{(r)}(k,m+1) = W(k,m+1) - \hat{H}^{(1)}(k,m+1) \tag{5.44}$$

The residual $\hat{H}^{(r)}(k,m)$ and $\hat{H}^{(r)}(k,m+1)$ are used to search for the 2^{nd} path $(\hat{A}_2, \hat{\tau}_2, \hat{\Delta}_2)$ using the same procedure and cost function as for searching the 1^{st} path. We re-write (4)

$$[\mathbf{Y}] = \left\{ \sum_{i=1}^{L} A_i [\mathbf{B_i}][\mathbf{I_i}] \right\} [\mathbf{D}] \tag{5.45}$$

After $(\hat{A}_i, \hat{\tau}_i, \hat{\Delta}_i)$ are estimated, the total impacts of channel including attenuation, delay, and Doppler shift is determined by a CTF-ICI matrix (channel transfer function-ICI) as

$$[\hat{\mathbf{T}}] = \left\{ \sum_{i=1}^{L} \hat{A}_i [\hat{\mathbf{B}}_\mathbf{i}][\hat{\mathbf{I}}_\mathbf{i}] \right\} \tag{5.46}$$

I-ICI (Inverse-ICI) finds the inverse matrix of matrix $[\hat{\mathbf{T}}]$, then data is recovered as

$$[\hat{\mathbf{D}}] = [\hat{\mathbf{T}}]^{-\mathbf{1}}[\mathbf{Y}] \tag{5.47}$$

The computational cost increases drastically when the size of matrix $[\hat{\mathbf{T}}]$ or equivalently the number of sub-carrier increases. To avoid matrix inversion, we apply Jacobi Iteration method [54] for solving the big matrix equation. The initial $[\hat{\mathbf{D}}]^{(\mathbf{0})}$ is computed as

$$[\hat{\mathbf{D}}]^{(\mathbf{0})} = \frac{[\mathbf{Y}]}{\mathbf{diag}[\hat{\mathbf{T}}]} \tag{5.48}$$

We use the Jacobi iteration method with only 1 iteration, so the data is recovered as

$$[\hat{\mathbf{D}}]^{(\mathbf{1})} = \frac{[\mathbf{Y}] - [\hat{\mathbf{T}}][\hat{\mathbf{D}}]^{(\mathbf{0})}}{\mathbf{diag}[\hat{\mathbf{T}}]} \tag{5.49}$$

It is effective to apply the Jacobi iteration method in this case as the diagonal of $[\mathbf{T}]$ is dominated, and amplitude of off-diagonal elements decay drastically. The interference from sub-carrier l to sub-carrier k is scaled by

$$|I_i(k,l)| = \left| sinc\Big(\pi(l - k + \frac{\Delta_i}{f_0})\Big) \right| \tag{5.50}$$

The scale $|I_i(k,l)|$ decays very quickly when $|l-k|$ increases.

5.3.4 Combination of Path-Searching and Slope-Based ICI Cancellation

The metrit of path-searching is high accuracy under ICI provided that the channel is sparse. However, directly finding an inverst of the ICI matrix in equation 4.17 is high computation cost. Therefore, after channel is estimated by path-searching, we apply the linear approximation model [20, 21, 43, 46, 47, 48, 55, 56] to derive ICI cancellation without any matrix inversion. We re-write (2) as follow

$$R(t) = \sum_{k=0}^{N-1} H(k,t) D_k e^{j2\pi k f_0 t} \tag{5.51}$$

$$H(k,t) = \sum_{i=1}^{L} A_i e^{-j2\pi(kf_0 + \Delta_i)\tau_i} e^{j2\pi\Delta_i t} \tag{5.52}$$

The time varying channel transfer function $H(k,t)$ is approximated by Taylor series as

$$R(t) = \sum_{k=0}^{N-1} \Bigg(\underbrace{H(k)_{mid} + \Delta H(k)(t - \frac{T_0}{2})}_{TaylorSeries} \Bigg) D_k e^{j2\pi k f_0 t} \tag{5.53}$$

After FFT demodulation, the data at sub-carrier k is

$$Y_k = H(k)_{mid} D_k + \sum_{\substack{l=0 \\ l \neq k}}^{N-1} \Omega(l-k) \Delta H(l) D(l) \tag{5.54}$$

$$\Omega(l-k) = \frac{1}{e^{\frac{-j2\pi(l-k)}{N}} - 1} \tag{5.55}$$

$H(k)_{mid}$ and the slope $\Delta H(k)$ is calculated from the estimation of (A_i, τ_i, Δ_i) from Section III

$$\hat{H}(k,m)_{mid} = \sum_{i=1}^{L} \hat{A}_i \hat{B}_i sinc(\frac{\pi\hat{\Delta}_i}{f_0}) e^{\frac{j\pi\hat{\Delta}_i}{f_0}} \tag{5.56}$$

$$\hat{\Delta}H(k) = \frac{\hat{H}(k, m+1)_{mid} - \hat{H}(k, m)_{mid}}{2(1 + T_{GI}/T_0)} \tag{5.57}$$

To solve (32), we apply Jacobi iteration method as follow with an initial $D_k^{(0)}$ is calculated as

$$\hat{D}_k^{(0)} = \frac{Y_k}{\hat{H}_{mid}(k)} \tag{5.58}$$

The data is recovered at the first iteration as follow

$$\hat{D}_k^{(1)} = \left\{ Y_k - \sum_{\substack{l=0 \\ l \neq k}}^{N-1} \Omega(l-k) \hat{\Delta}\hat{H}(l) \hat{D}_l^{(0)} \right\} / \hat{H}_{mid}(k) \tag{5.59}$$

Chapter 6

Simulation and Experimental Results

6.1 Introduction

In the following section we will disclose experimental results taken in Henoko, Oujima Okinawa and in Shizuoka from Oct. 2013 to January 2015. First, experiments in Henoko mainly investigate performance of 4 diversity receiver under impacts of Doppler, impulsive noise and multipath. In addition, the ICI cancellation based on linear approximation of time varying channel also provide gain thought it is slightly due to severe frequency offset and time compression/expansion caused by Doppler. Second, experiments in Oujima investigate performance of Turbo code with code rate 1/2, 1/3 for QPSK, 16QAM and 64QAM. The SOVA based iterative decoding works and reduce bit error rate under low SNR. Most importantly, experiments in Shizuoka consider Doppler effect in detail by moving a transmitter in vertical direction. Methods for estimation and compensation impacts of Doppler in both time and frequency domain are investigated. In addition, by the time of experiments taken in Shizuoka in January 2015, the multi-re-sampler for estimation of Doppler rate, the path-searching channel estimation and the SALAS de-noising for channel estimation under ICI has not developed yet. Therefore, we investigate performance of these algorithms by simulations. The overall system parameters are shown in Table 6.1.

Table 6.1: system parameters

Parameters	Mode	
	2	3
TX-RX Elements	1 TX and 4 RX Transducer	
Sampling Frequency	96000 Hz	
TX Center Frequency	24000 Hz	
FFT Size	1024	2048
OFDM symbol length T	10.667 ms	21.333 ms
GI length	0.5T	
Sub Carrier Spacing	93.75 Hz	46.875 Hz
Number of Sub Carrier	81	161
Modulation	QPSK, 16QAM, 64QAM	
Turbo code	1/2 1/3	

6.2 Simulation Results

6.2.1 Comparison Methods for Synchronization

The metric of using two identical symbols as a preamble are robustness to noise or ability to working in low SNR region. In addition, it is possible to estimate a frequency offset few times of sub-carrier space at the beginning of a data frame. However, this method is affected by ISI (inter-symbol-interference) and time compression/expansion caused by Doppler. On the other hand, the Chirp method is resilient to Doppler but might not work in low SNR region. The threshold for detecting data frame should be adapt to SNR level. In addition, the LFM preamble has to be added to the head and the tail of an OFDM PACKAGE to measure an average Doppller rate over a data frame. Figure 6.1 show simulations of using the Chirp signal, and figure 6.2 is result on air-test using microphone to record acoustic sound transmuted by computers using a speaker. Results in case using of two identical symbols are shown in figure 6.3.

6.2.2 Comparison Methods for Doppler Rate/Shift Estimation

First we investigate estimation of Doppler rate/shift using continual pilots in conjunction with monitoring the drift of PDF. Considering a communication in vertical direction, usually there are a direct path and a surface reflection path. Such as communication is illustrated in figure 6.4. Most importantly, our system aims to mitigate the changing roughly of velocity over time, such as during pulling/pushing the transmitter in our experiment. We create a simulation scenario, in which, the velocity changes over time as shown in figure 6.5 The maximum velocity is 3(m/s) corresponding to a frequency offset of 48(Hz), and the acceleration rate is about 1.7(m/s/s). All Bit Error Rate (BER) is before Turbo decoding. QPSK achieved free error, and 16QAM achieved a stable performance over 10 frames.

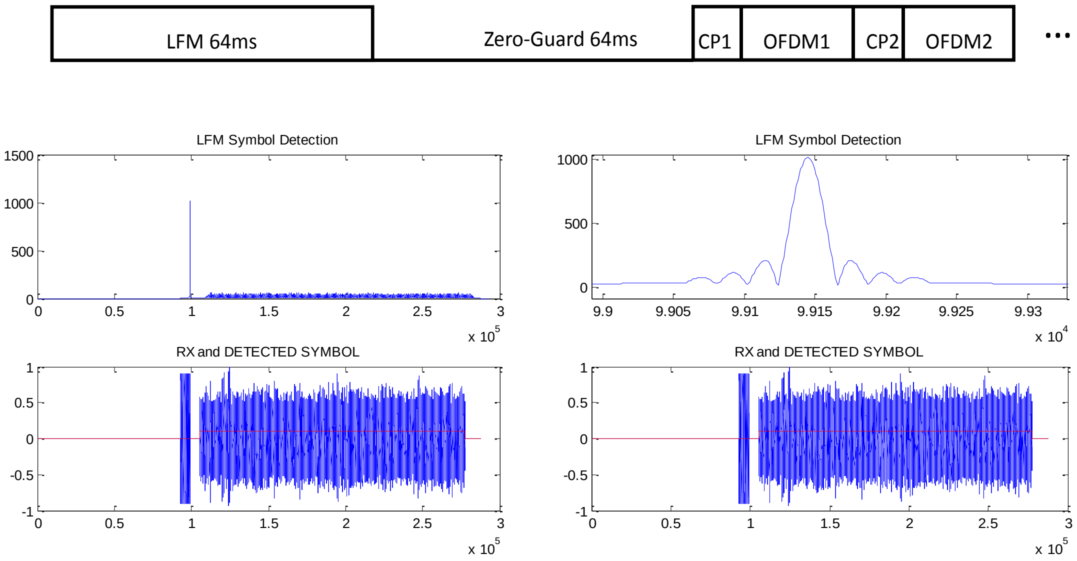

Figure 6.1: LFM simulation

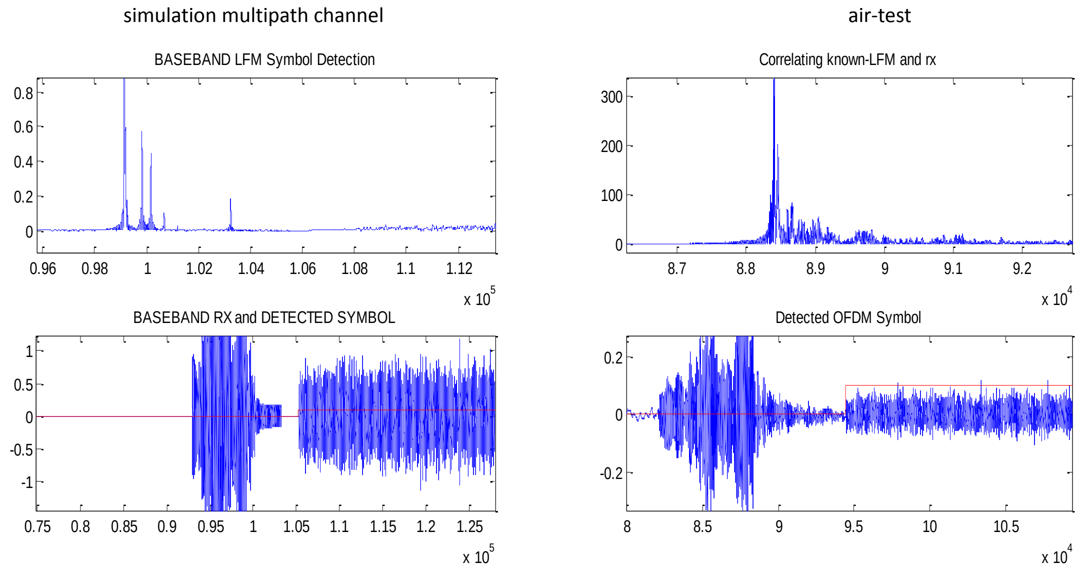

Figure 6.2: LFM airtest

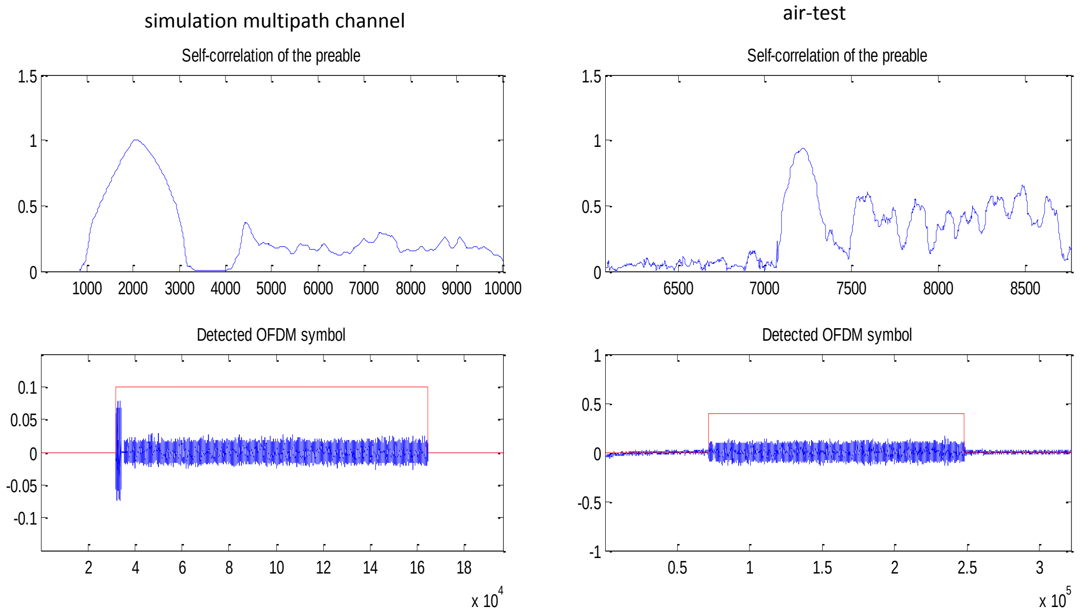

Figure 6.3: two identical symbols airtest

Table 6.2: parameters for multi-resampler

Parameter	Value
Number sub-carrier	N_{sc}=81
FFT size	N_{FFT}=1024
Sampling frequency	96000(Hz)
Sub-carrier space	96.375(Hz)
Symbol length excluded GI	$T_0 = 10.66(ms)$,
Guard interval	$T_{GI} = T_0/4, N_{GI} = 256$
Carrier frequency	$f_c = 24,000Hz$
Δ_{max}	6/1500, $v_{max} = 6(m/s)$
Δ_{min}	0.5/1500,$v_{min} = 0.5(m/s)$
Number of branch	$M = 25$

Second, we investigate performance of the multi-sampler with an acoustic OFDM system shown in Table 6.2. Two delay paths with a delay spread of $T_0/10$, attenuation of two paths are $0dB$ and $-5dB$, respectively. In addition, AWGN noise with $SNR = 25(dB)$ is added. The time varying Doppler rate Δ changes over OFDM symbol as shown in figure 6.5. The Doppler variation of two paths, $\delta_1 = +0.25/1500$, and $\delta = -0.25/1500$ which means the corresponding frequency offset are $f_{\delta 1} = 4Hz$ and $f_{\delta 2} = -4Hz$. With $\Delta_{min} = 0.5/1500$, the residual Doppler scale is $|\Delta_r| \leq \Delta_{min}/2$, and the equivalently residual frequency offset is $|f_{dr}| \leq \Delta_{min} f_c = 8(Hz)$ which is smaller than 10% of the sub-carrier space of $96.375(Hz)$. Therefore, the residual Doppler can be handled by continual pilots, or an ICI canceler. As in figure 6.6 and 6.7 and 6.8 the velocity changes in time with an acceleration rate of $2(m/s/s)$, and the proposal method track the time varying Doppler well. To reduce the computation cost, we only estimate the Doppler after 5 OFDM symbols.

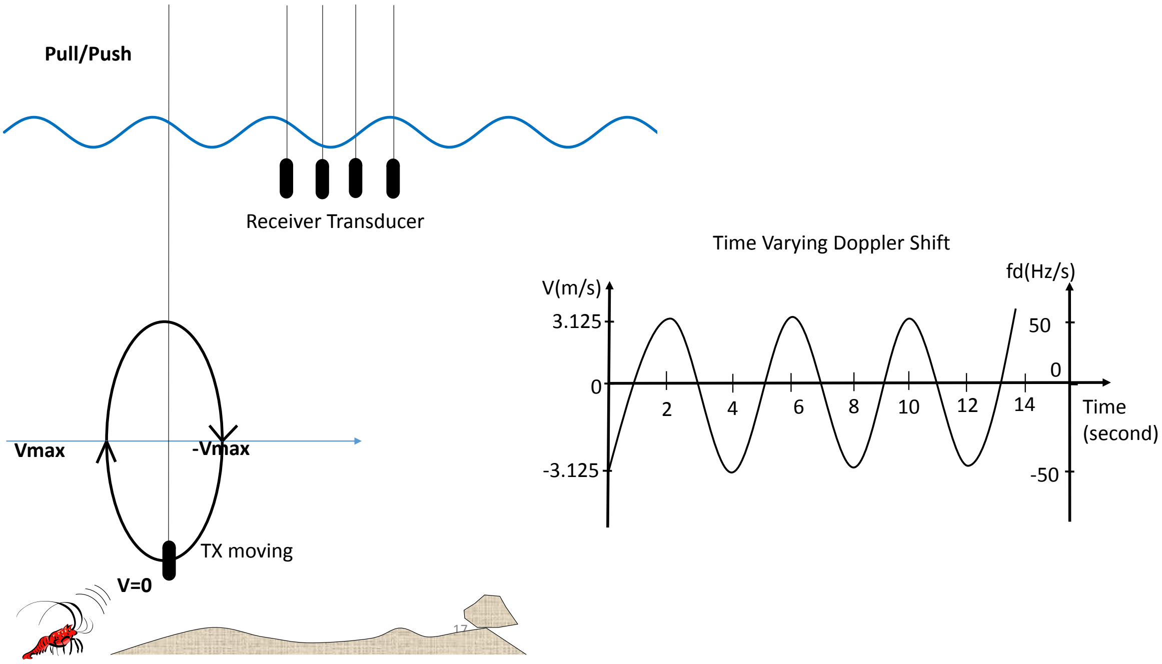

FIGURE 6.4: experiment setting/senario

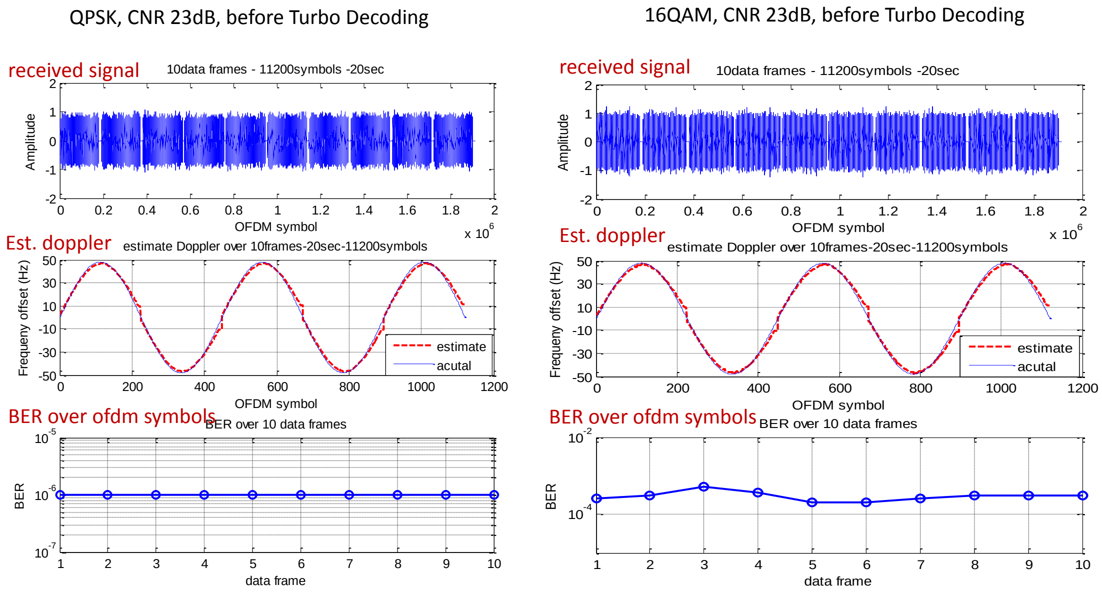

FIGURE 6.5: Doppler estimation (simulation)

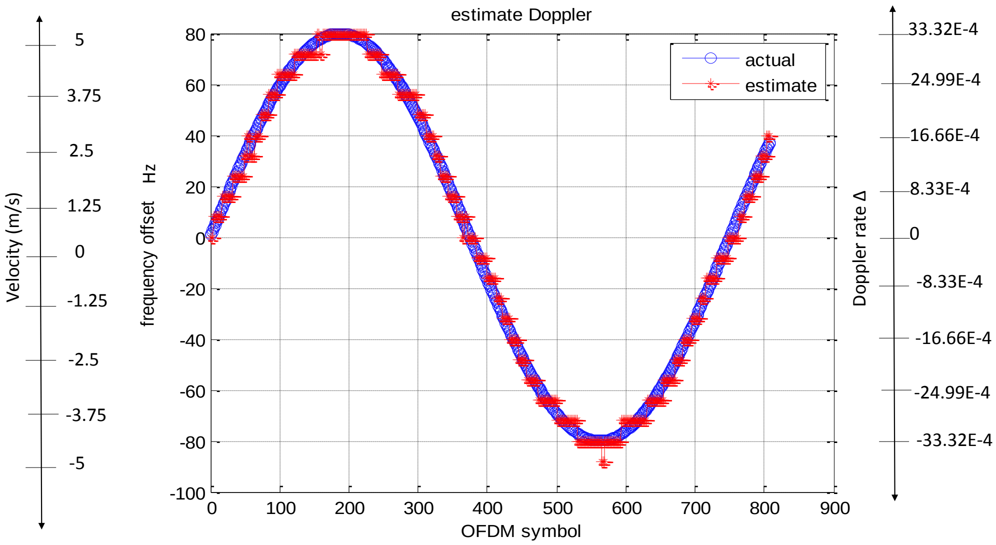

Figure 6.6: multi-resampler simulation

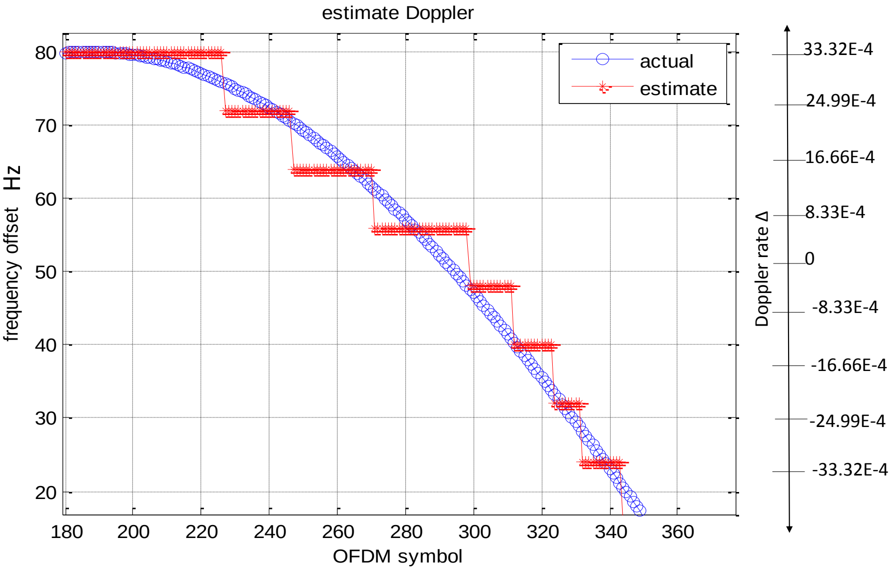

Figure 6.7: multi-resampler simulation zoom in

6.2.3 Comparison Methods for compensation of non-uniform Doppler

First we compare the simple phase rotation method [2] with our method using an ICI metric for compensating the non-uniform Doppler shift. The channel condition is shown in Table. 2, and all paths has a similar Doppler rate Δ. In figure 6.9, wo means without Doppler compensation. wd means Doppler compensating using only the diagonal of the ICI matrix, that is similar to [2] . I-ICI finds the inversion of the ICI matrix, and J-ICI utilizes Jacobi iterative method.

Second, we compare our symbol-by-symbol Doppler compensation two stages in frequency domain with the resampling method in time domain [12]. In short, the re-sampling method re-samples the

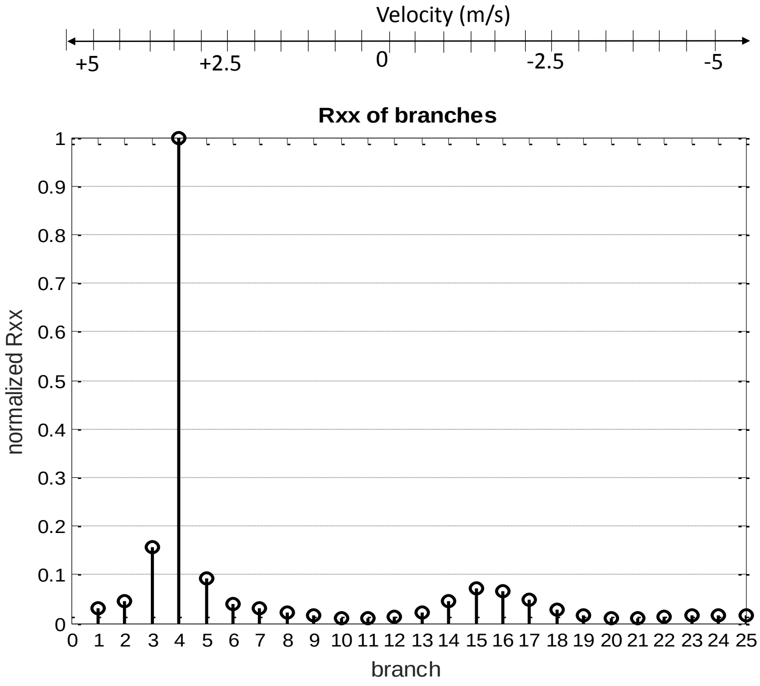

FIGURE 6.8: multi-resampler simulation

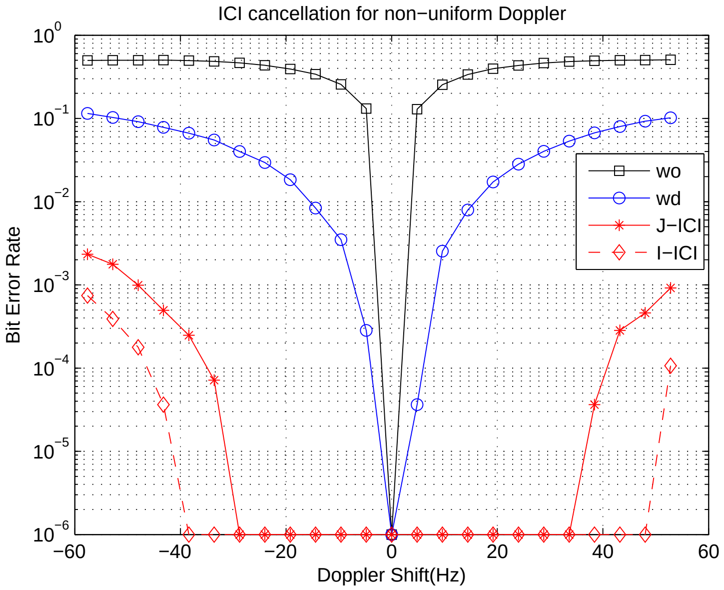

FIGURE 6.9: compare our non-uniform doppler comp. vs. the simple phase rotation [2]

Table 6.3: parameters for channel estimation and ICI cancellation

Parameter	Value
Number Sub-carrier	N=161
FFT Point	NFFT=2048
Sampling Frequency	96000(Hz)
Sub-carrier Space	46.875(Hz)
Guard Interval	$T_{GI} = T_0/4$
Delay	$\tau_1 = 0$, $\tau_2 = T_0/5$
Attenuation	$A_1 = 0dB, A_2 = -5dB$
Doppler shift	$\Delta_1 = -\Delta_2$
Note: OFDM modulation is performed by NFFT, and zeros are inserted in unused sub-carriers	

whole data frame of many OFDM symbols with the same scale, then a phase de-rotation is employed to compensate the residual Doppler. The re-sampling method utilizes LFM (Linear Frequency Modulation) pre/post-ample for Doppler rate estimation, and must store an entire data frame to estimate the Doppler rate. In the first case, the maximum velocity is 2.5(m/s) which causes a Doppler shift of 40(Hz), and changes over time as shown in figure 6.4 for both 16QAM, and 64QAM. The velocity increases from zero to 2.5(m/s) with an acceleration rate around 1(m/s/s) which is reasonable when considering the fluctuation of transmitters due to ocean waves, or pulling/pushing transmitters in our experiments. As shown in figure 6.6, though the maximum Doppler shift as 40(Hz) is greater than $f_0/3$, our tracking method using continual pilots in conjunction with monitoring PDF works well. In 6.5 wo means without Doppler compensation. As mentioned before, re-sampling an entire data frame with a single factor does not fully compensate the time varying Doppler. After re-sampling, the residual position-dependent Doppler still degrades performance. In contrast, our proposal can track and compensate the Doppler shift symbol-by-symbol, provides a stable performance, and outperforms the re-sampling method as shown in 6.5. In detail, with the same acceleration rate of 1(m/s/s), after re-sampling the residual position-dependent Doppler can be negligible for 16QAM, however quite significant for 64QAM. Therefore, symbol-by-symbol Doppler compensation provides gain for 64QAM as in figure 6.5.

6.2.4 Comparison Methods for Channel Estimation and ICI Cancellation

In this section, we compare the LMMSE channel estimation with our path-searching channel estimation. We also investigate performance of ICI cancellation and interative channel estimation and ICI cancelation based on linear approximation of time varying channel [23, 25, 43, 48, 49]. For the LMMSE, we assume that the auto-correlation of channel transfer function, and noise variance are known at receiver side.

System parameters, and two-path channel are shown in Table 6.3. This system is designed for underwater acoustic communication. Our method is still hold for other OFDM systems. In figure 6.10, and 6.11, **LMMSE-ICI** is the LMMSE channel estimation combined the mentioned ICI cancellation.

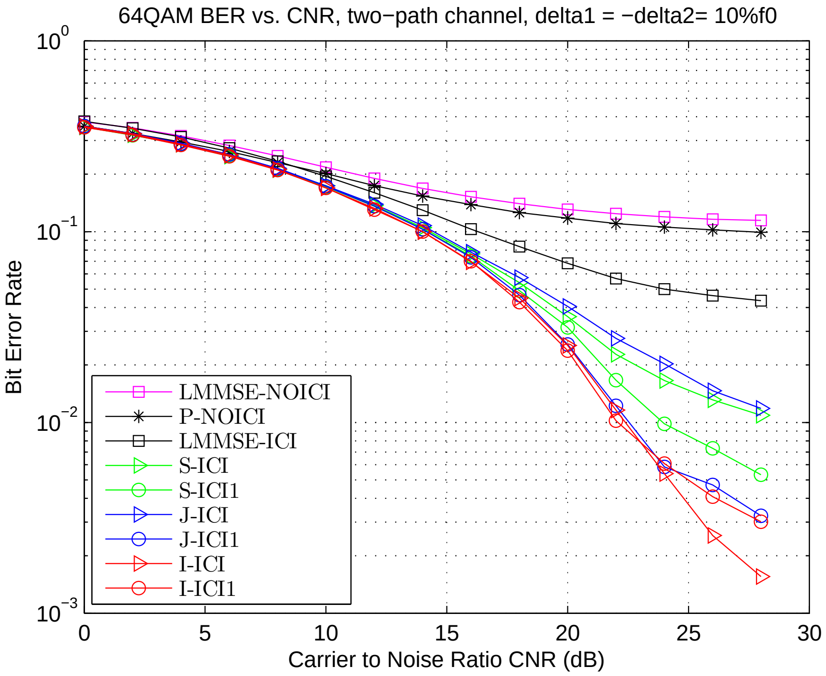

FIGURE 6.10: comparison of channel estimation methods 1

TABLE 6.4: System parameters for SALAS de-noising simulation

Parameter	Value
Number sub-carrier	N_{sc}=161
FFT size	N_{FFT}=2048
Sampling frequency	96000(Hz)
Sub-carrier space	46.875(Hz)
Symbol length excluded GI	$T_0 = 21.33(ms)$,
Guard interval	$T_{GI} = T_0/4, N_{GI} = 256$
Carrier frequency	$f_c = 24,000Hz$
Δ_1 Doppler shift of path 1	$0.06f_0$
Δ_2 Doppler shift of path 2	$-0.06f_0$
Attenuation path 1	$0dB$
Attenuation path 2	$-5dB$
Delay path 1	0
Delay path 2	$T_0/5$
μ	100
λ	7
p	1024
Number of iteration for SALSA	50

P-NOICI means our path searching channel estimation without ICI cancellation. Our channel estimation and ICI cancellation clearly outperforms the **LMMSE-ICI**. The performance gain is due to two reasons. First, our method is able to separate ICI caused by Doppler and channel transfer function caused by delays, and remove ICI before estimating the channel attenuation. Second, continual pilots enable estimating high Doppler shift. In addition, **I-ICI1**, **J-ICI1**, **S-ICI1** are ICI cancellations after re-estimating channel, and they provide performance gain over **I-ICI**, **J-ICI**, **S-ICI**.

We further investigate performance of de-noising by SALSA and compare with conventional de-noising

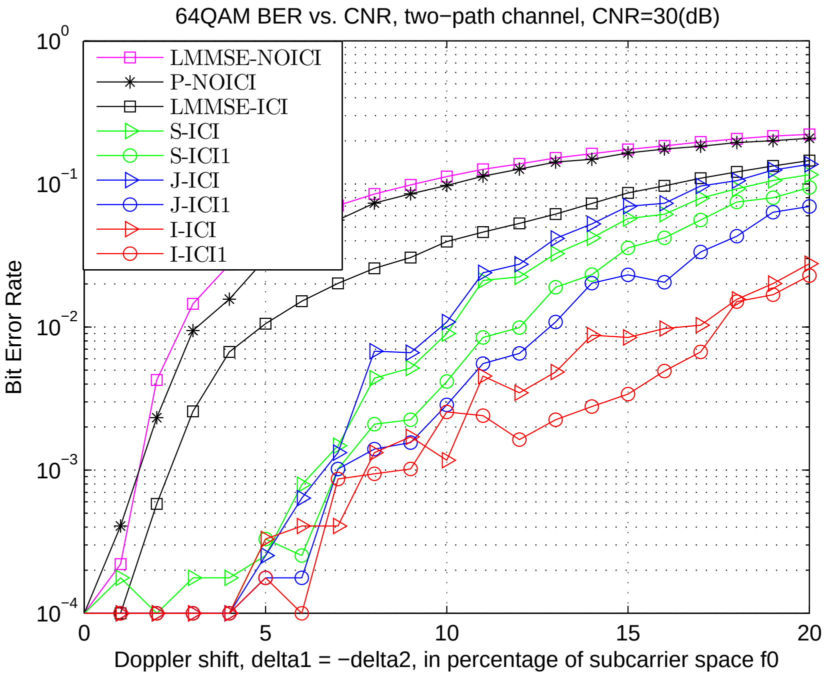

FIGURE 6.11: comparison of channel estimation methods 2

method under mulipath and ICI conditions. System parameters and channel condition are shown in Table 6.4. It is noted that the Doppler shift of $0.06f_0$ is a severe case for existing OFDM-based wireless systems. For instance, with 4G-LTE, the Doppler shift of $0.06f_0$ caused by moving speed of $405(Km/h)$, with center frequency $2.4(GHz)$ and $f_0 = 15(kHz)$. High delay spread of $T_0/5$ which is close to guard interval $T_0/4$ also is considered in our simulation. Simulation for 16QAM and 64QAM in figure 6.12 and figure 6.13 clearly show performance gain of de-noising by SALSA over conventional methods.

6.3 Experiments in Okinawa, Japan

6.3.1 Experiments in Henoko Okinawa

Transceiver architecture for experiments in Henoko is shown in figure 6.14. The experiment site is shown in figure 6.15. The received signal and observed delay profile are shown in figure 6.16 and figure 6.17. Figure 6.20, 6.21, 6.22, 6.23, 6.24, compare bit error rate among 1 single receiver (1BR), 2 diverse receivers (2BR) and four diverse receivers (4BR). The black square marked line means T-IMP (time domain-impulsive cancellation) and Freq-IMP (frequency impulsive noise cancellation)are OFF, and no ICI canceling. The blue triangle marked line means T-IMP and Freq-IMP are OFF, and ICI canceling is applied. Finally, the red line is T-IMP and Freq-IMP are ON, and ICI canceling is applied. In addition, figure 6.24 and 6.23 show Mode 3 when receivers are no moving and moving

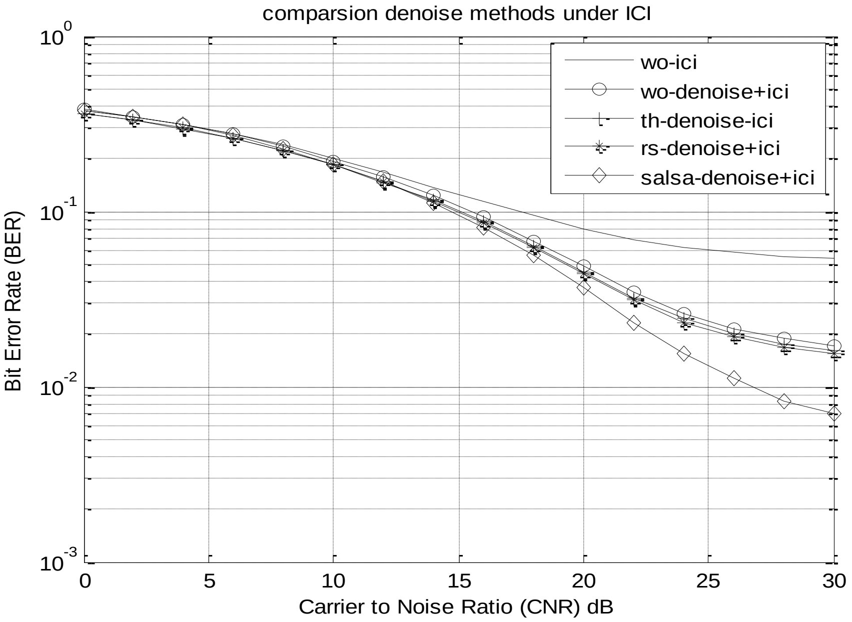

Figure 6.12: SALAS de-noising BER 16QAM

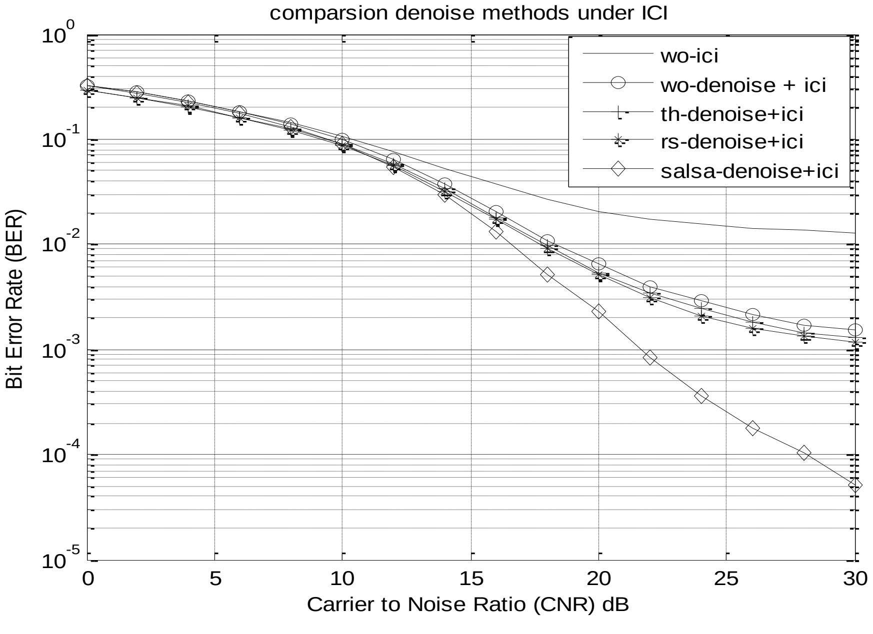

Figure 6.13: SALAS de-noising BER QAM

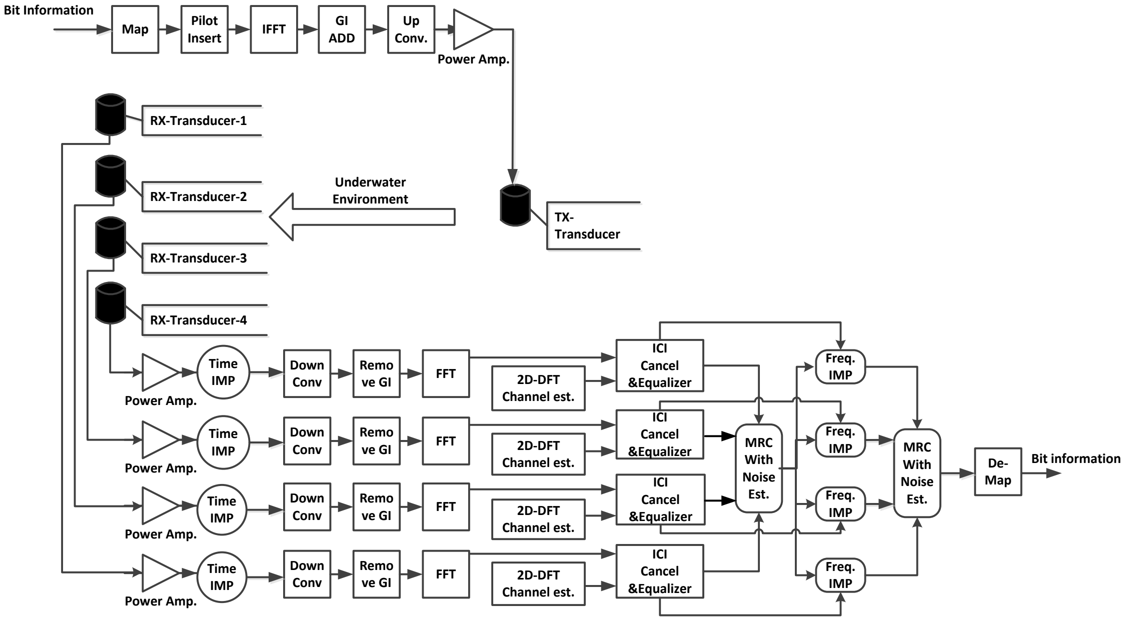

Figure 6.14: transceiver for henoko experiment

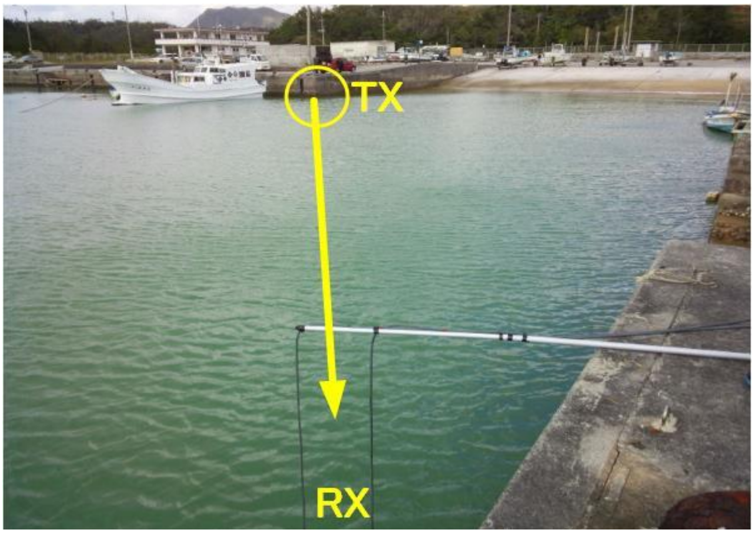

Figure 6.15: henoko experiment site

at 0.6 (m/s), respectively. Similarly, figure 6.22 and figure 6.21 shows Mode 2 when receivers are no moving and moving at 0.9 (m/s), respectively. First, the four diversity improved bit error rate significantly for both no moving and no moving cases. Next, considering moving cases, as shown in figure 6.21 and figure 6.23, constellation figure 6.19 show ICI cancellation improved performance. Overall, the results show that Mode2 is more resilient to time varying channel.

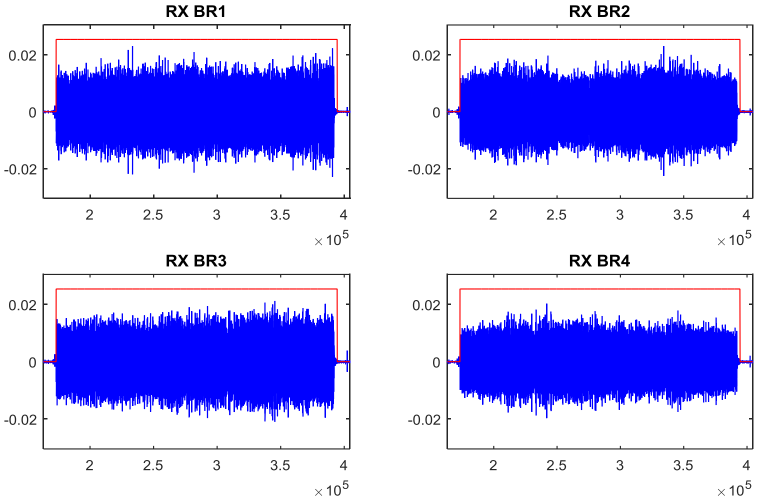

FIGURE 6.16: henoko rx sign

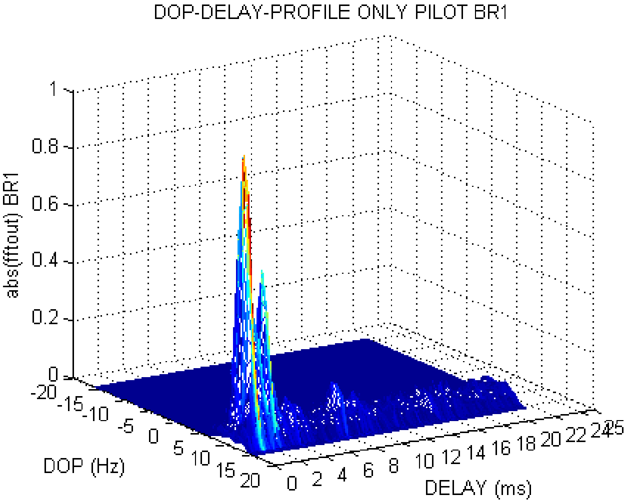

FIGURE 6.17: henoko delay profile

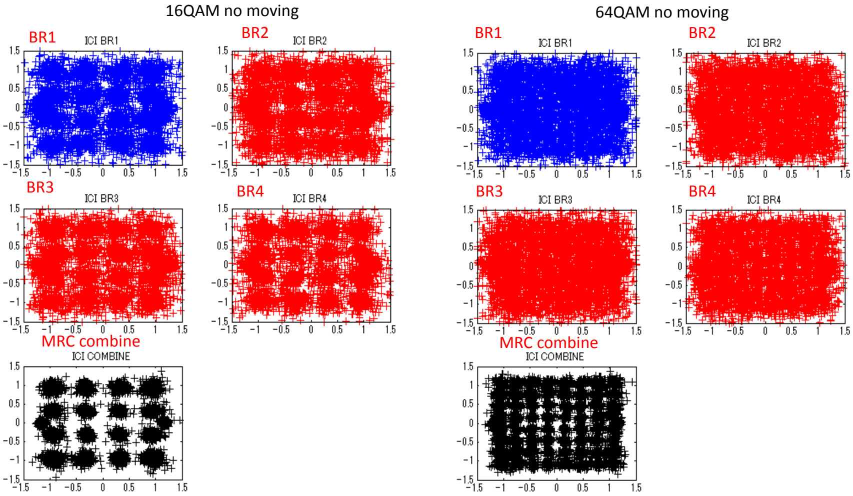

FIGURE 6.18: henoko constellation 1

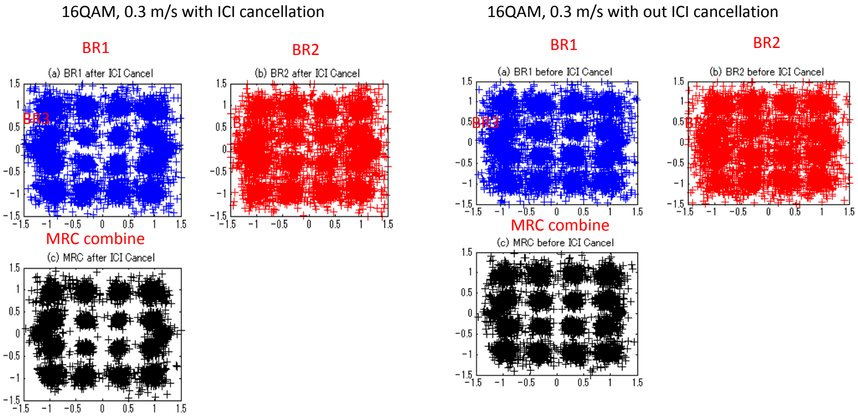

FIGURE 6.19: henoko constellation 2

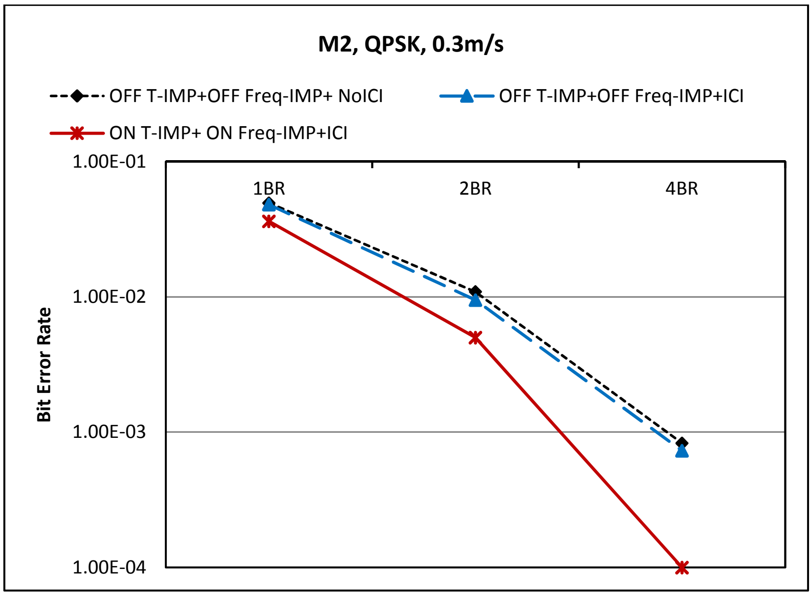

FIGURE 6.20: Henoko Mode2 QPSK move 0.3

6.3.2 Experiments in Oujima Okinawa

In this section experiments are conducted in Oujima Okinawa as shown in figure 6.25 and figure 6.26. The experiments investigate performance of Turbo coding under high ambient noise, impulsive noise, and also impacts of Doppler.

As shown figure 6.27 impulsive noise appeared in the received signal. Delay profile in figure 6.28 has many delay path which is due to the horizontal propagation. The constellation in figure 6.29 of QPSK is quite noisy due to severe doubly selective channel. Though SNR as shown in QPSK constellation is quite low, the Turbo iterative decoding with code rate of 1/2 and 1/3 provides a low bit error rate as shown in figure 6.30 for Mode 2 and Mode 3.

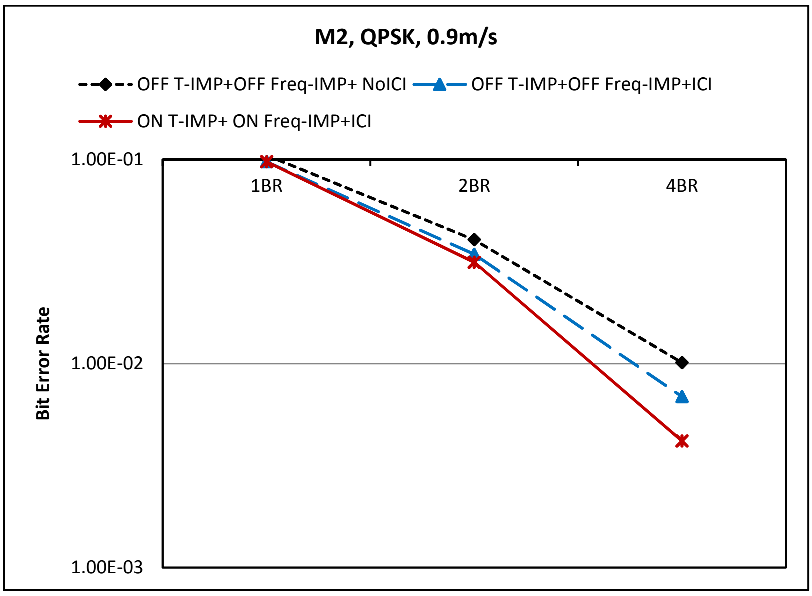

Figure 6.21: Henoko Mode 2 QPSK moving 0.9knot

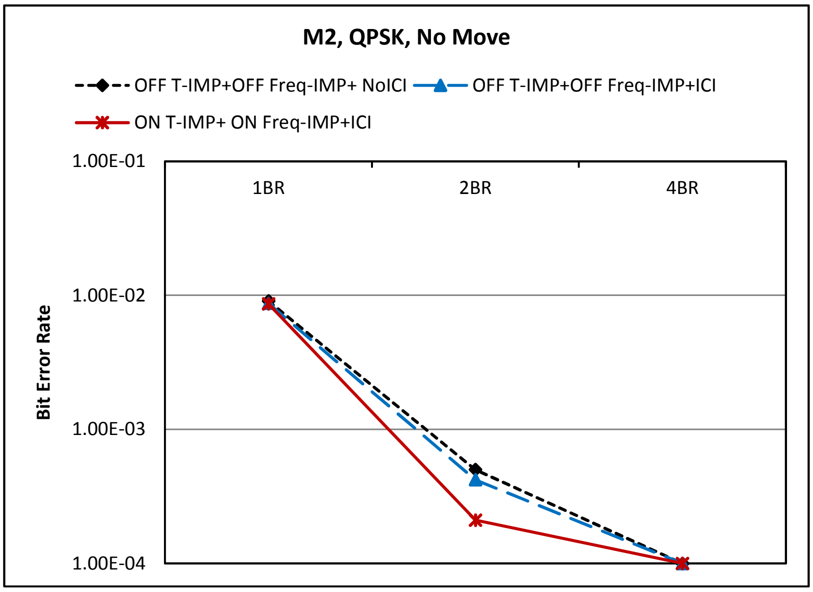

Figure 6.22: Henoko Mode2 QPSK no moving

6.4 Experiments in Shizuoka, Japan

6.4.1 Experiment Site and Setting

Experiments were conducted inside a barrage in figure 6.32 at OKISEATEC company in Shizuoka as shown in figure 6.31 and figure 6.34 in January 2015, in Shizuoka, Japan. There is a moon pool inside the barge as shown in figure 6.35 so that transducers can be dragged down into the water. By a controllable electric motor, a transmitter was periodicity pulled toward the surface, then pushed toward the bottom as in figure 6.35. When the transmitter approaches near the surface, or the

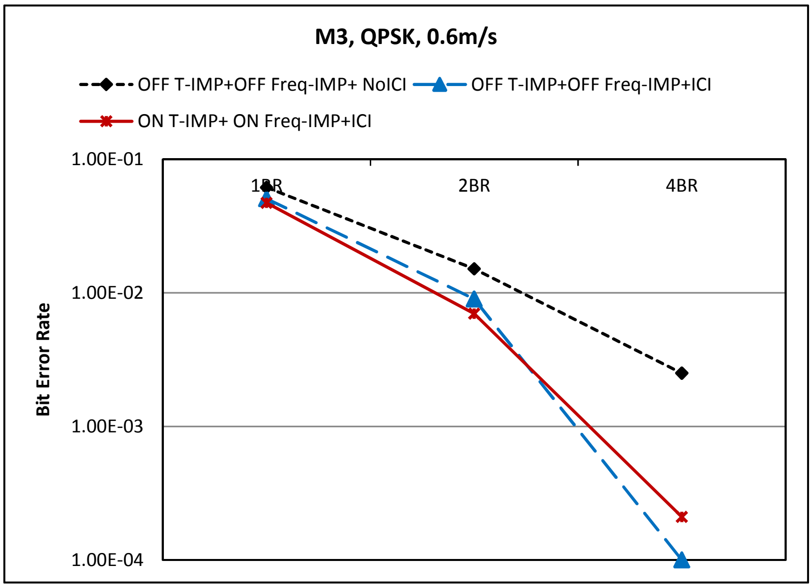

FIGURE 6.23: Henoko Mode3 QPSK moving 0.6knot

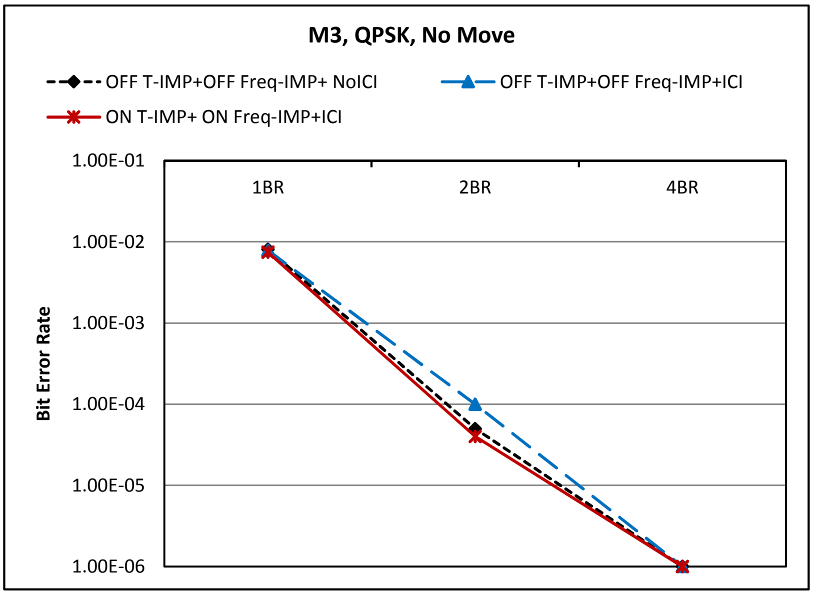

FIGURE 6.24: Henoko Mode3 QPSK no moving

bottom its velocity gradually reduce, then changes direction, increase velocity again. So the Doppler shift changes roughly over OFDM symbols. At the receiver side, four transducers are fixed at 3(m) depth from the surface, and those transducers are spaced equally 10(cm) apart from each other. This space is greater than the wavelength of acoustic signal in our cases, so the received signal at four transducers are uncorrelated and provides diversity gain. System architecture for the experiment is shown in figure 6.36.

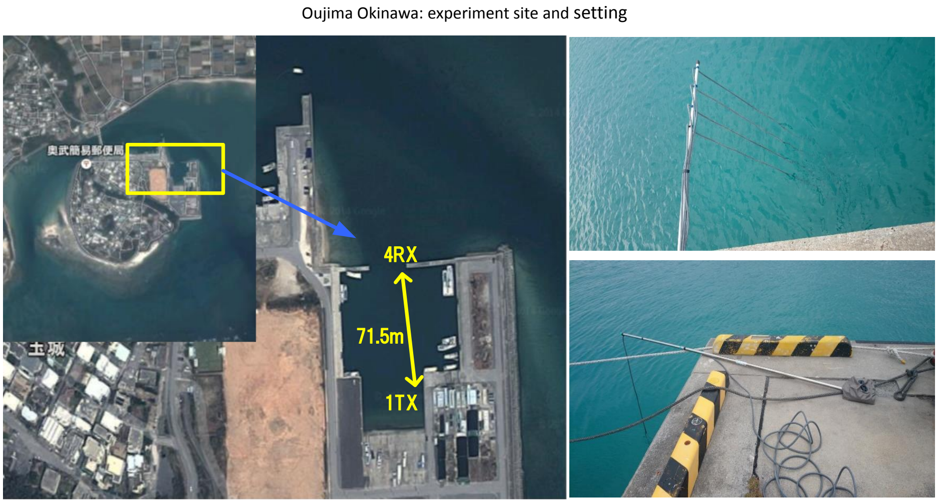

FIGURE 6.25: Oujima experiment site

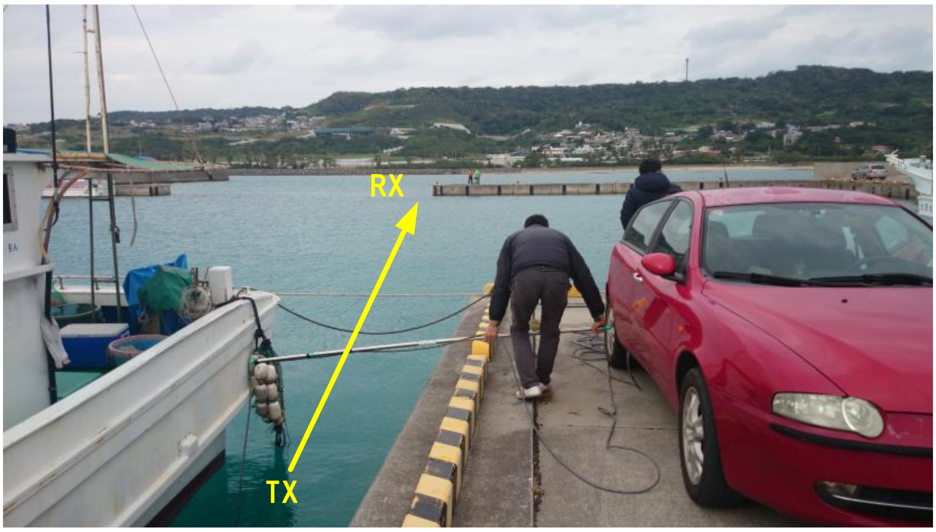

FIGURE 6.26: Oujima experiment site

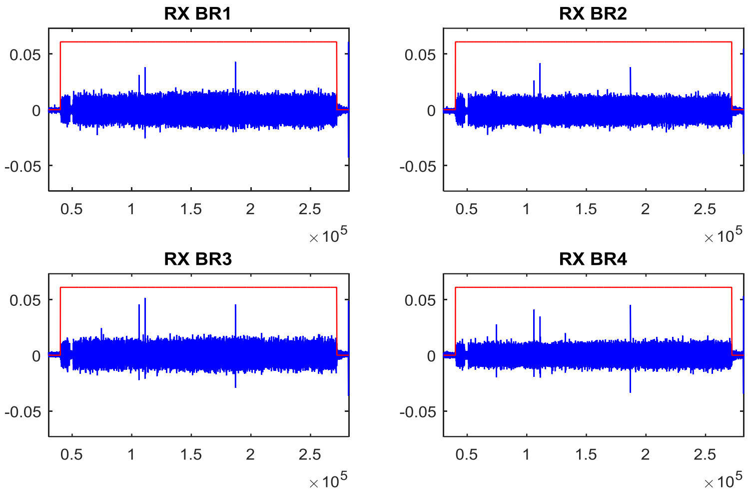

FIGURE 6.27: Oujima rx signal

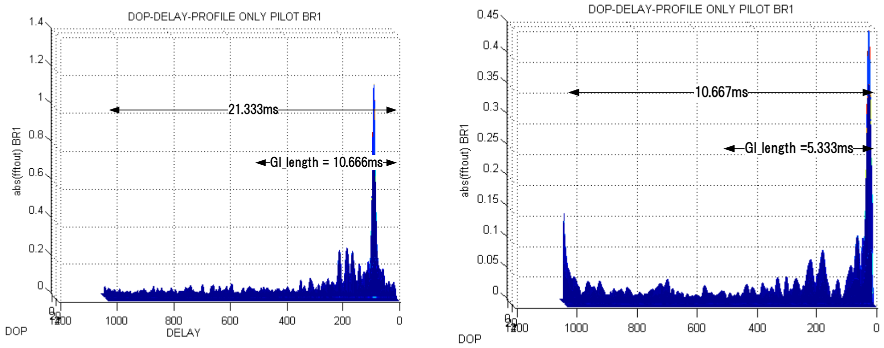

a)Amplitude Delay Profile(Mode3, 0.0m/sec) b)Amplitude Delay Profile(Mode2 0.3m/sec)

FIGURE 6.28: Oujima delay profile

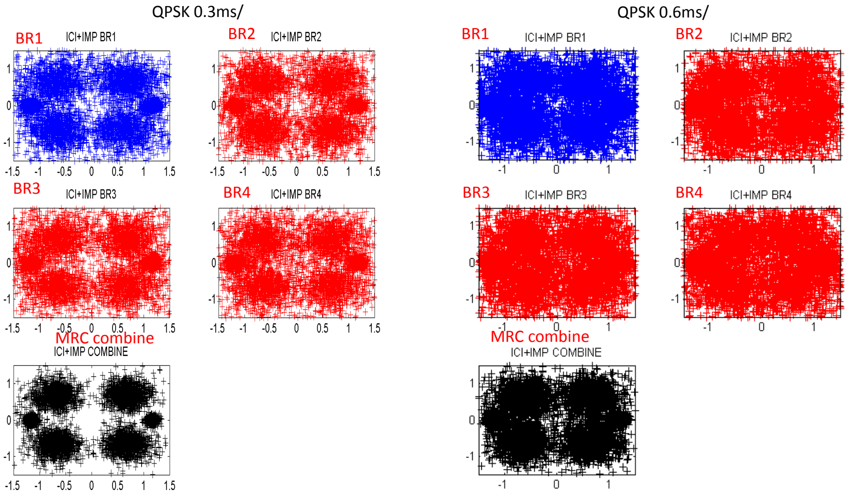

FIGURE 6.29: Oujima constellation

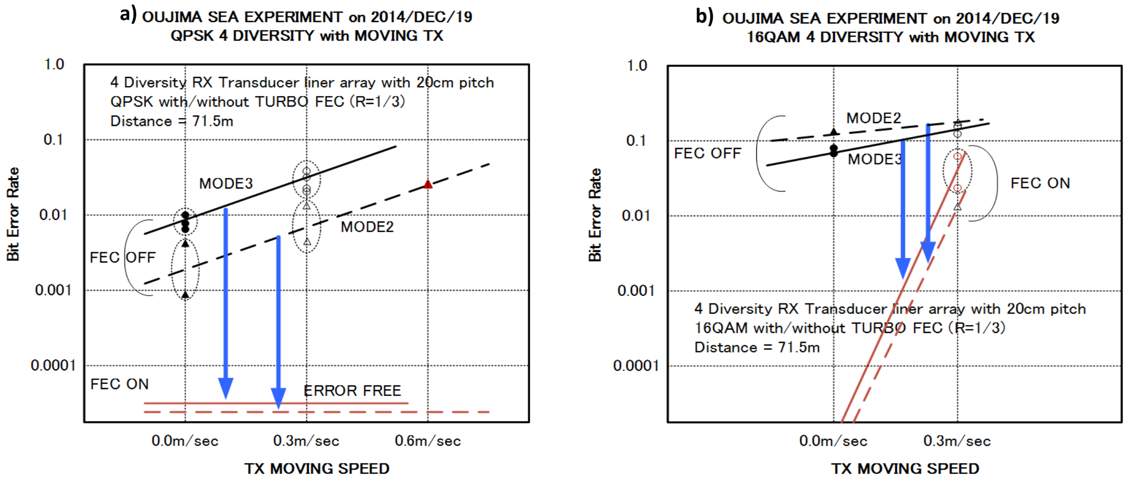

FIGURE 6.30: Oujima BER

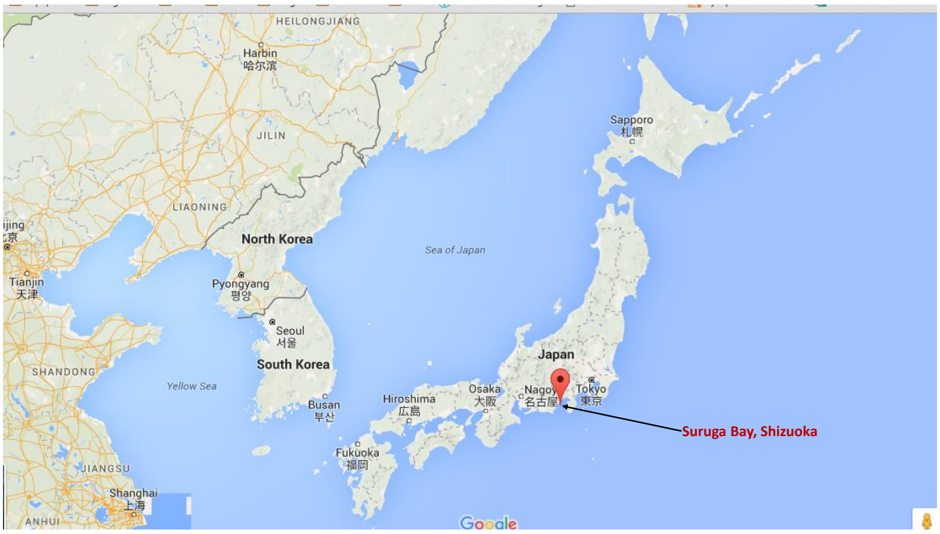

FIGURE 6.31: experiment site

FIGURE 6.32: OKISEATEC Barge

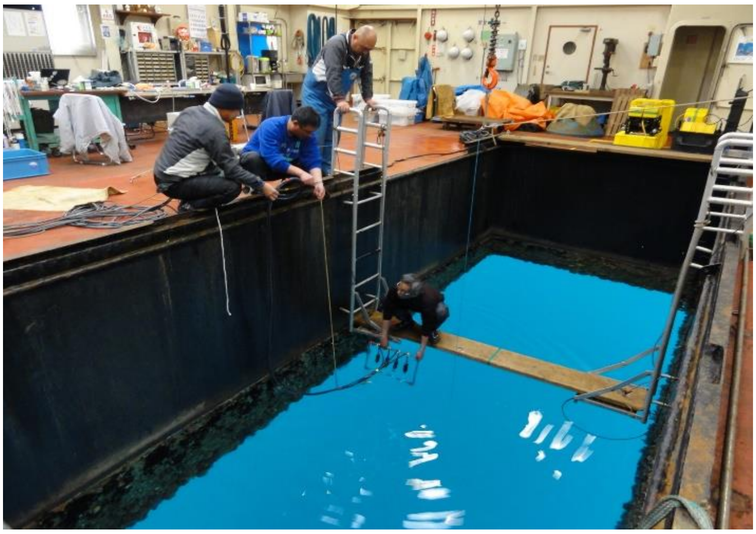

FIGURE 6.33: OKISEATEC moon pool

FIGURE 6.34: performing experiments

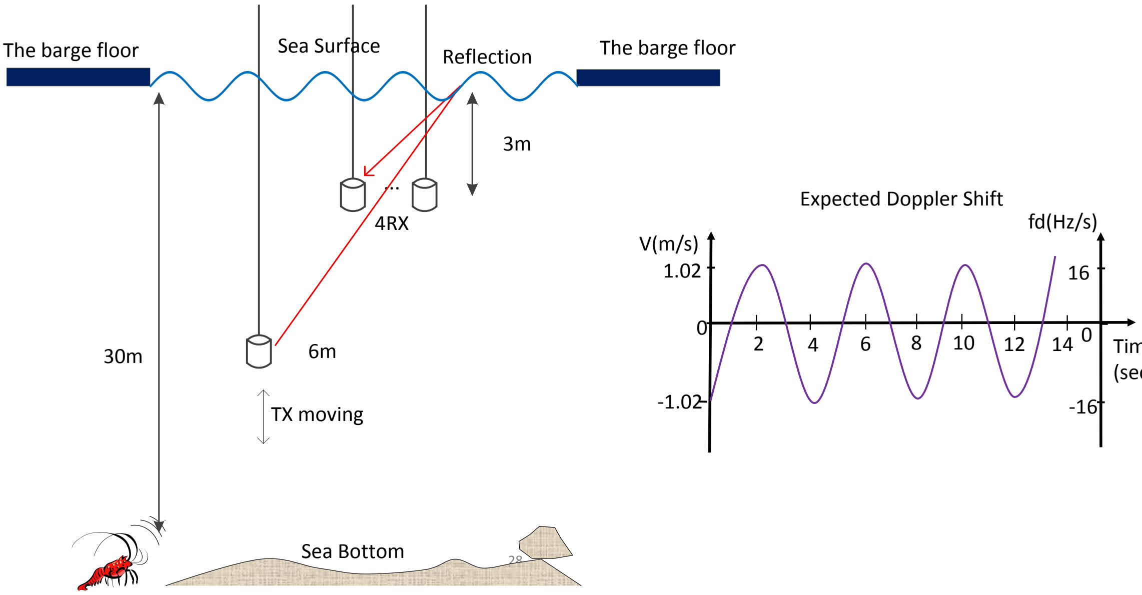

FIGURE 6.35: shizuoka experiment setting

6.4.2 Experimental Results

The estimated Delay Profile in figure 6.37 is consistent with the experiment setting. In the delay profile, there is a direct path, and a surface reflection path, and the distance between them is about 5(ms) which is equivalent to 7.5(m) distance. As the experiment setting, the receivers is in 3(m) depth, and so a reflection path can appear as in figure 6.35.

Figure 6.37 shows the estimation of the time varying Doppler shift over 6 frames, with 4QAM and 16QAM, respectively. The maximum Doppler shift estimated is about 30(Hz) corresponding to the velocity of 2(m/s), that is consistent with the experiment setting. BER (Bit Error Rate) over frames

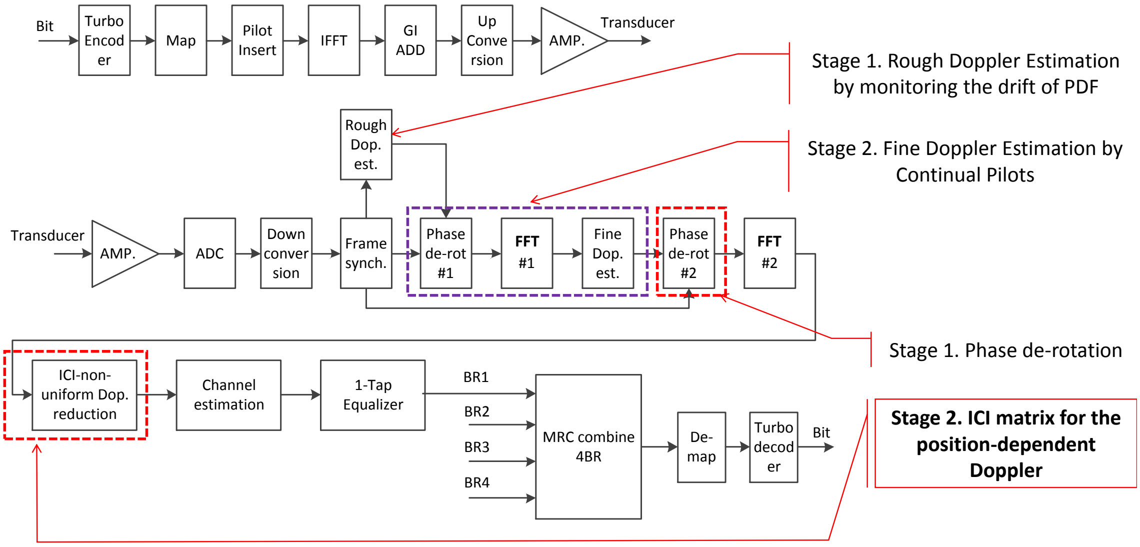

FIGURE 6.36: transceiver architecture for experiments in Shizuoka

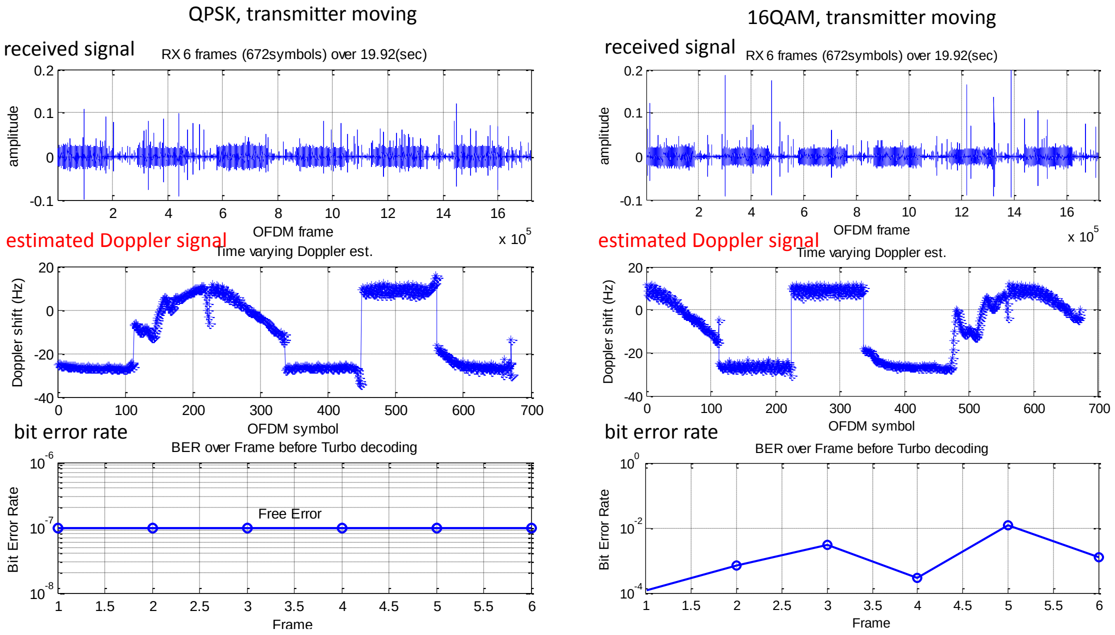

FIGURE 6.37: Shizuoka Doppler estimation

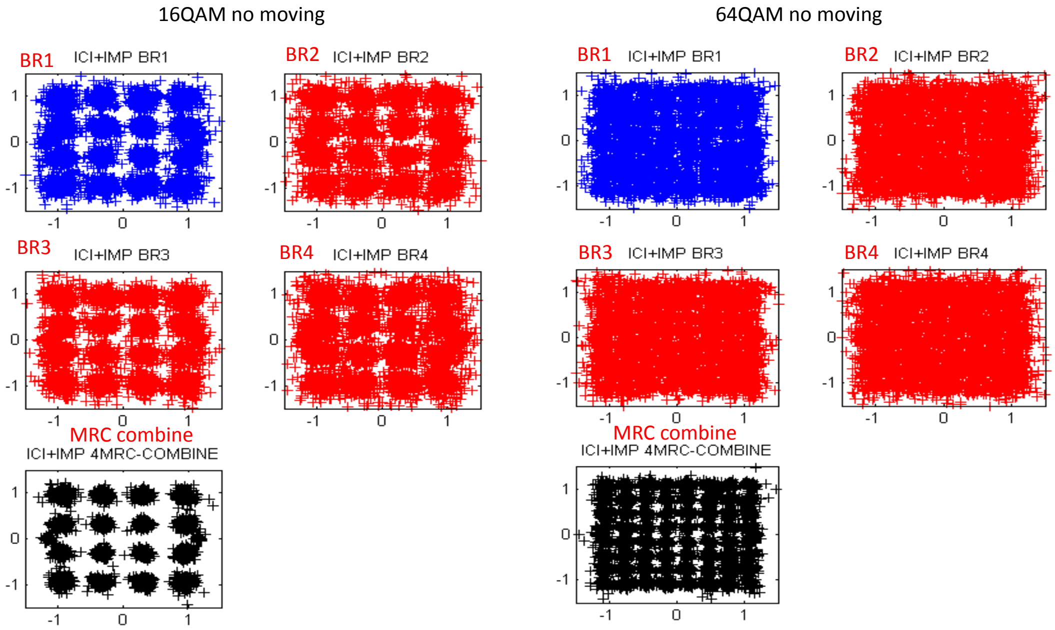

Figure 6.38: Constellation

of 16QAM, and 64QAM are shown in figure 6.37. For both 16QAM, and 64QAM cases, during frame 2, 3, and 4 the Doppler shift is nearly constant over a frame, so our method and the re-sampling method achieved quite similar performance. With frame 1, 5, and 6 the velocity changes linearly over a data frame, and our proposal slightly outperformed the re-sampling method. The performance gain is very small due to the Doppler shift is still small, and the acceleration rate also is small. Similar to simulation result, the performance gain for 64QAM is greater than for 16QAM.

The transmitter was pull toward the surface, the push toward the bottom. When the transmitter approach near the surface, or the bottom its velocity gradually reduce, then changes direction, increase velocity again. So the velocity trajectory is quite complicate as shown in figure 6.37 shows the estimation of the time varying Doppler shift over 6 frames. Our Doppler compensation provide a stable performance when the velocity changes over time. The BER are before Turbo decoding, and it is free error after decoding.

The effectiveness of the proposed Doppler compensation is shown in figure 6.39, figure 6.40, figure 6.41 for Mode 2 with QPSK, 16QAM, and 64QAM, respectively. Similarly, the results for Mode 3 with QPSK, 16QAM, and 64QAM are shown in figure 6.42, figure 6.43, and figure 6.44, respectively.

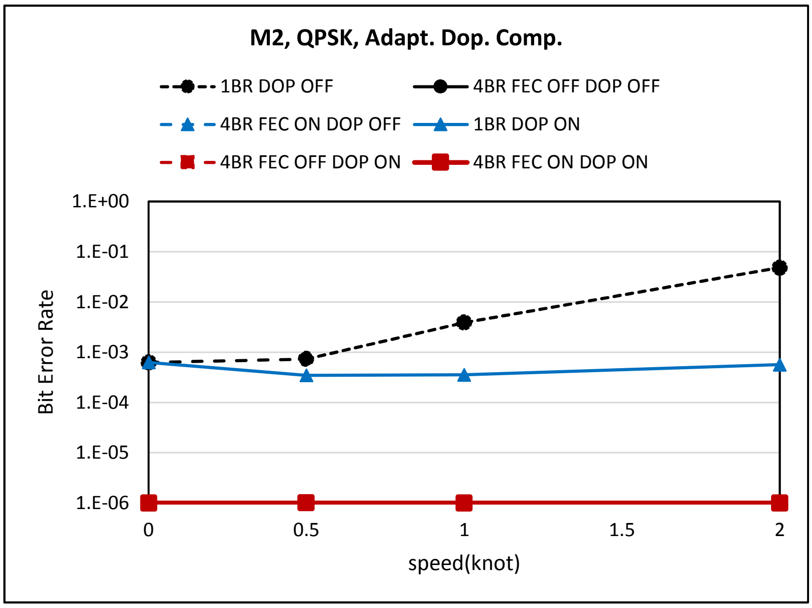

FIGURE 6.39: Shizuoka Mode2 64QAM adaptive Doppler compensation

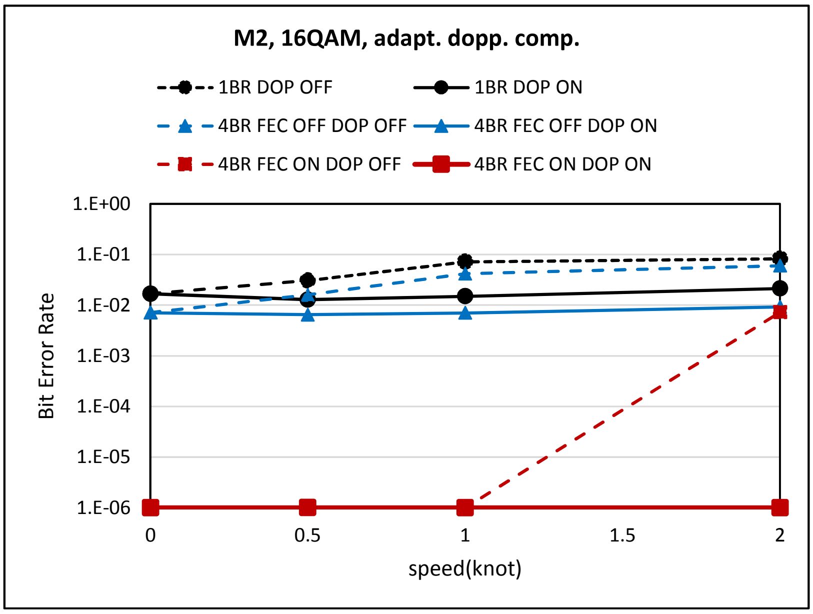

FIGURE 6.40: Shizuoka Mode2 64QAM adaptive Doppler compensation

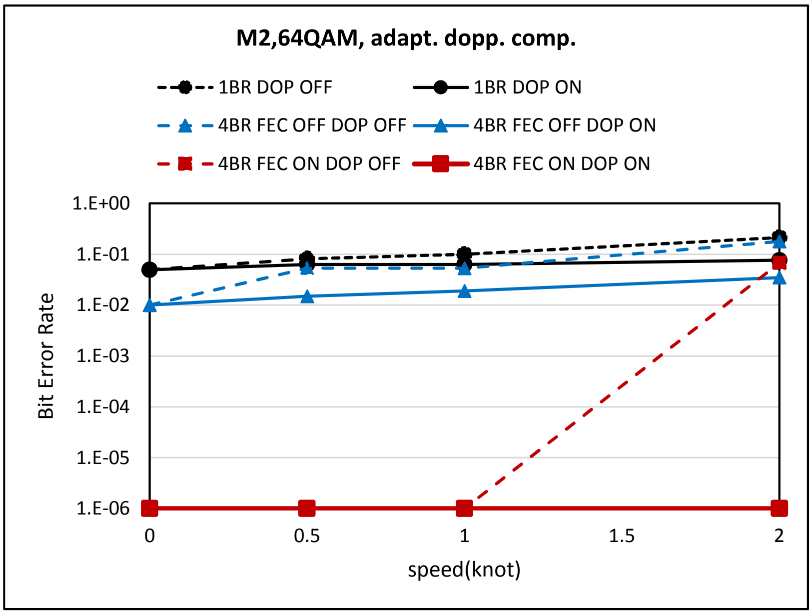

FIGURE 6.41: Shizuoka Mode2 64QAM adaptive Doppler compensation

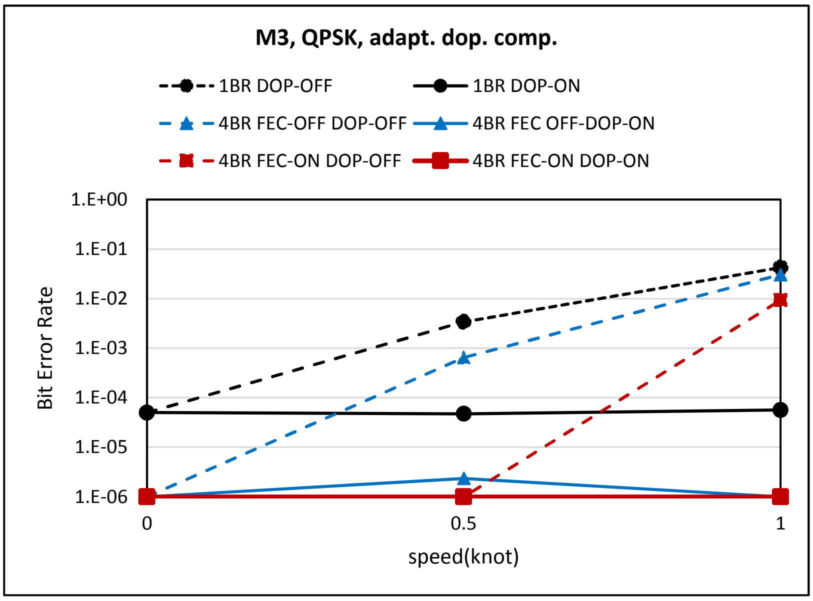

FIGURE 6.42: Shizuoka Mode3 4QAM adaptive Doppler compensation

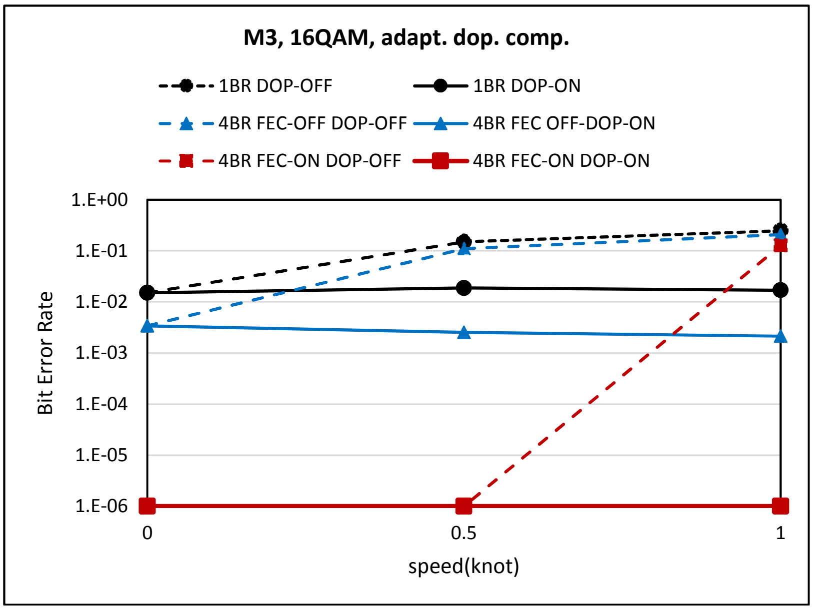

FIGURE 6.43: Shizuoka Mode3 16QAM adaptive Doppler compensation

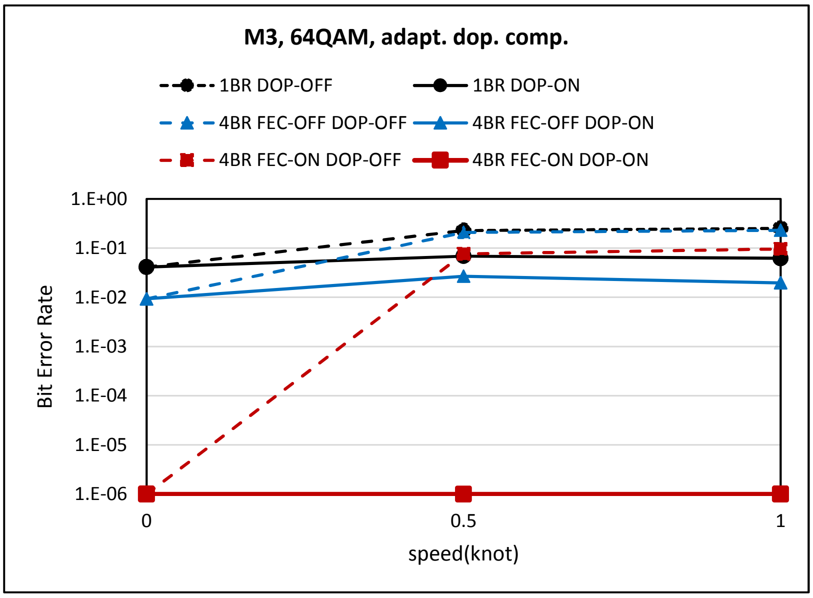

FIGURE 6.44: Shizuoka Mode3 64QAM adaptive Doppler compensation

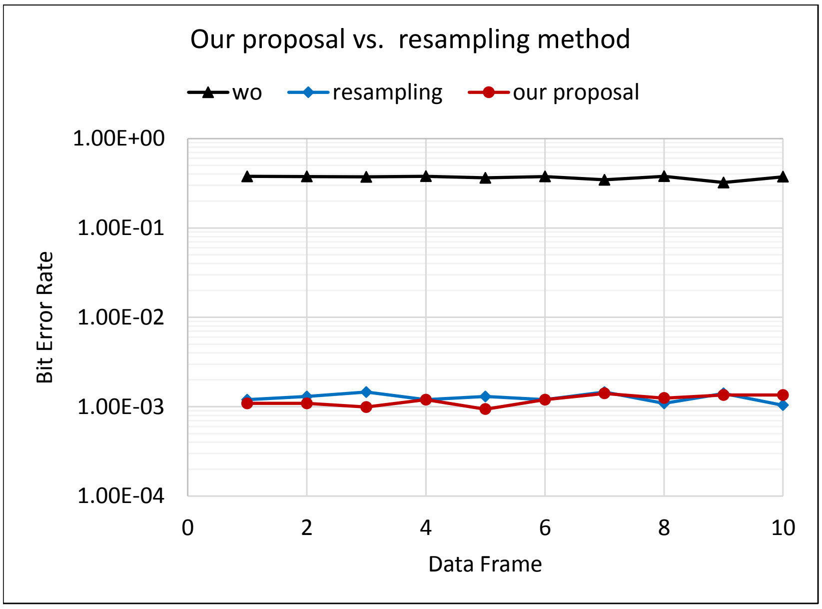

Figure 6.45: compare our non-uniform Doppler comp. vs. re-sampling

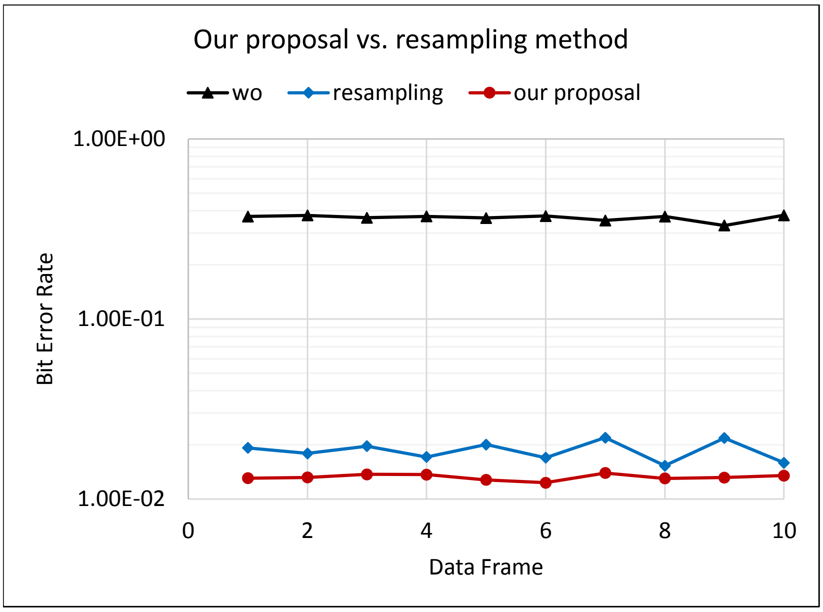

Figure 6.46: compare our non-uniform Doppler comp. vs. re-sampling

Figure 6.45 and figure 6.46 compares performance of Doppler compensation of the proposed method against the re-sampling in time domain method for 16QAM and 64QAM, respectively. For 16QAM, two methods achieve a similar bit error rate (BER), however, for 64QAM the proposed method achieve a better BER. The re-sampling method resamples the entire data frame of many OFDM symbols with a single scale. Therefore, when Doppler rate changes roughly over OFDM symbols, impacts of Doppler rate is still remained. In contrast, the proposed method is symbol-by-symbol Doppler compensation in frequency domain, so it works well even when Doppler rate changes over OFDM symbols.

Chapter 7

Conclusion

This thesis presents transceiver architecture of an acoustic OFDM system, covering from error correction coding and diversity receiver. The main contributions are proposed robust signal methods such as for acoustic OFDM, (2) disclosed experiment results taken through experiments in Okinawa and Shizuoka sea. The thesis spent great effort on algorithms to mitigate Doppler effect in acoustic OFDM systems, which is one of the greatest challenges. A method for estimating and compensating the time varying Doppler rate/shift symbol-by-symbol is proposed [17, 19]. An iterative channel estimation and ICI cancellation is proposed in [20, 21]. In addition, we further investigate methods for channel estimation under severe ICI which are SALAS de-noising improved channel estimation, and path-searching channel estimation.

In addition, the complicated time varying channel is distilled, and the relation between the slope of time varying CIR and the slope of time varying CTF is explained. Derivation of ICI (mechanism of ICI generation) is analyzed through two point of views, one is time varying channel, and the other is path-model with Doppler shifts of delay paths. Impact of ICI (SIR caused by ICI), its impact on channel estimation also is analyzed as well.

On practical aspect, the thesis shows a method for arbitrary rate re-sampling in a low complexity manner using a bank of 64 FIR filters. LMMSE channel estimation is achieved without per-knowledge about channel (the auto-correlation function), and is implemented by 4 FIR filters.

Bibliography

[1] M. A. Ainslie and J. G. McColm, “A simplified formula for viscous and chemical absorption in sea water,” *The Journal of the Acoustical Society of America*, vol. 103, no. 3, pp. 1671–1672, 1998.

[2] M. Stojanovic, “Low complexity ofdm detector for underwater acoustic channels,” in *OCEANS 2006*, pp. 1–6, IEEE, 2006.

[3] M. Suzuki, T. Sasaki, and T. Tsuchiya, “Digital acoustic image transmission system for deep-sea research submersible,” in *OCEANS’92. Mastering the Oceans Through Technology. Proceedings.*, vol. 2, pp. 567–570, IEEE, 1992.

[4] A. Kaya and S. Yauchi, “An acoustic communication system for subsea robot,” in *OCEANS’89. Proceedings*, vol. 3, pp. 765–770, IEEE, 1989.

[5] T. Shimura, H. Ochi, Y. Watanabe, and T. Hattori, “Experiment results of time-reversal communication at the range of 300 km,” *Japanese Journal of Applied Physics*, vol. 49, no. 7S, p. 07HG11, 2010.

[6] T. Shimura, Y. Watanabe, H. Ochi, and H. Song, “Long-range time reversal communication in deep water: Experimental results,” *The Journal of the Acoustical Society of America*, vol. 132, no. 1, pp. EL49–EL53, 2012.

[7] L. Freitag, P. Koski, A. Morozov, S. Singh, and J. Partan, “Acoustic communications and navigation under arctic ice,” in *Oceans, 2012*, pp. 1–8, IEEE, 2012.

[8] A. Kukulya, A. Plueddemann, T. Austin, R. Stokey, M. Purcell, B. Allen, R. Littlefield, L. Freitag, P. Koski, E. Gallimore, *et al.*, “Under-ice operations with a remus-100 auv in the arctic,” in *Autonomous Underwater Vehicles (AUV), 2010 IEEE/OES*, pp. 1–8, IEEE, 2010.

[9] A. E. Abdelkareem, B. S. Sharif, C. C. Tsimenidis, and J. A. Neasham, “Compensation of linear multiscale doppler for ofdm-based underwater acoustic communication systems,” *Journal of Electrical and Computer Engineering*, vol. 2012, p. 3, 2012.

[10] E. Valera Zorita and M. Stojanovic, "Space–frequency block coding for underwater acoustic communications," *Oceanic Engineering, IEEE Journal of*, vol. 40, no. 2, pp. 303–314, 2015.

[11] B. Li, J. Huang, S. Zhou, K. Ball, M. Stojanovic, L. Freitag, and P. Willett, "Mimo-ofdm for high-rate underwater acoustic communications," *Oceanic Engineering, IEEE Journal of*, vol. 34, no. 4, pp. 634–644, 2009.

[12] B. Li, S. Zhou, M. Stojanovic, L. Freitag, and P. Willett, "Multicarrier communication over underwater acoustic channels with nonuniform doppler shifts," *Oceanic Engineering, IEEE Journal of*, vol. 33, no. 2, pp. 198–209, 2008.

[13] evologics, "acoustic modem," 2016.

[14] teledynebenthos, "acoustic modem," 2016.

[15] aquasent, "acoustic modem," 2016.

[16] C. R. Berger, S. Zhou, J. C. Preisig, and P. Willett, "Sparse channel estimation for multicarrier underwater acoustic communication: From subspace methods to compressed sensing," *Signal Processing, IEEE Transactions on*, vol. 58, no. 3, pp. 1708–1721, 2010.

[17] T. MinhHai, S. Rie, T. Suzuki, and T. Wada, "An acoustic ofdm system with symbol-by-symbol doppler compensation for underwater communication," *The Scientific World Journal*, vol. 2016, 2016.

[18] T. M. Hai, Y. Matsuda, T. Suzuki, and W. Tomohisa, "Ultrasonic diversity ofdm transceiver architecture with impulsive noise cancelling for shallow sea communication," in *Proceedings of the UA2014-2nd International Conference and Exhibition on Underwater Acoustics*, 2014.

[19] T. MinhHai, S. Rie, S. Taisuki, and T. Wada, "A transceiver architecture for ultrasonic ofdm with adaptive doppler compensation," in *OCEANS'15 MTS/IEEE Washington*, pp. 1–6, IEEE, 2015.

[20] H. M. Tran and T. Wada, "On ici canceller for mobile ofdm dtv receivers," in *Advanced Communication Technology (ICACT), 2014 16th International Conference on*, pp. 290–297, IEEE, 2014.

[21] H. M. Tran and T. Wada, "On improvement of the ici canceller for ofdm mobile dtv receiver," in *Advanced Communication Technology (ICACT), 2013 15th International Conference on*, pp. 1134–1139, IEEE, 2013.

[22] M. Schulkin and H. Marsh, "Absorption of sound in sea-water," *Radio and Electronic Engineer*, vol. 25, no. 6, pp. 493–500, 1963.

[23] S. Coleri, M. Ergen, A. Puri, and A. Bahai, "Channel estimation techniques based on pilot arrangement in ofdm systems," *Broadcasting, IEEE Transactions on*, vol. 48, no. 3, pp. 223–229, 2002.

[24] M. Sandell and O. Edfors, "A comparative study of pilot-based channel estimators for wireless ofdm," *Div. of Signal Processing, Research Report*, 1996.

[25] H. Schulze and C. Lüders, *Theory and applications of OFDM and CDMA: Wideband wireless communications.* John Wiley & Sons, 2005, pp.181-192.

[26] M. S. Akram, "Pilot-based channel estimation in ofdm systems," *Nokia Mobile Phones white paper*, 2007.

[27] T. Suzuki, H. M. Tran, and T. Wada, "An underwater acoustic ofdm communication system with shrimp (impulsive) noise cancelling," in *Computing, Management and Telecommunications (ComManTel), 2014 International Conference on*, pp. 152–156, IEEE, 2014.

[28] R. Saotome, T. M. Hai, Y. Matsuda, T. Suzuki, and T. Wada, "An ofdm receiver with frequency domain diversity combined impulsive noise canceller for underwater network," *The Scientific World Journal*, vol. 2015, 2015.

[29] A. Abdelkareem, B. Sharif, C. Tsimenidis, J. Neasham, and O. Hinton, "Low-complexity doppler compensation for ofdm-based underwater acoustic communication systems," in *OCEANS, 2011 IEEE-Spain*, pp. 1–6, IEEE, 2011.

[30] A. E. Abdelkareem, B. S. Sharif, C. C. Tsimenidis, and J. A. Neasham, "Time varying doppler-shift compensation for ofdm-based shallow underwater acoustic communication systems," in *Mobile Adhoc and Sensor Systems (MASS), 2011 IEEE 8th International Conference on*, pp. 885–891, IEEE, 2011.

[31] A. E. Abdelkareem, "Doppler compensation algorithms for dsp-based implementation of ofdm underwater acoustic communication systems," 2012.

[32] B. Sharif, J. Neasham, O. Hinton, A. Adams, and J. Davies, "Adaptive doppler compensation for coherent acoustic communication," in *Radar, Sonar and Navigation, IEE Proceedings-*, vol. 147, pp. 239–246, IET, 2000.

[33] B. S. Sharif, J. Neasham, O. R. Hinton, and A. E. Adams, "A computationally efficient doppler compensation system for underwater acoustic communications," *Oceanic Engineering, IEEE Journal of*, vol. 25, no. 1, pp. 52–61, 2000.

[34] J.-J. Van de Beek, P. O. Börjesson, M.-L. Boucheret, D. Landström, J. M. Arenas, P. Ödling, C. Ostberg, M. Wahlqvist, and S. K. Wilson, "A time and frequency synchronization scheme for multiuser ofdm," *Selected Areas in Communications, IEEE Journal on*, vol. 17, no. 11, pp. 1900–1914, 1999.

[35] M. Speth, S. Fechtel, G. Fock, and H. Meyr, “Optimum receiver design for ofdm-based broadband transmission. ii. a case study,” *Communications, IEEE Transactions on*, vol. 49, no. 4, pp. 571–578, 2001.

[36] T. W. Kenta Nohara, “The design of frequency domain inter carrier interference (ici) canceling circuit caused by radio frequency shift for ofdm receiver,” in *The 15th Workshop on Synthesis and System Integration of Mixed Information Technologies (SASIMI 2009)*, pp. 172–176, IEEE, 2009.

[37] S. V. Zhidkov, “Impulsive noise suppression in ofdm-based communication systems,” *Consumer Electronics, IEEE Transactions on*, vol. 49, no. 4, pp. 944–948, 2003.

[38] K. Al-Mawali, A. Z. Sadik, and Z. M. Hussain, “Joint time-domain/frequency-domain impulsive noise reduction in ofdm-based power line communications,” in *Telecommunication Networks and Applications Conference, 2008. ATNAC 2008. Australasian*, pp. 138–142, IEEE, 2008.

[39] T. K. Moon, *Error Correction Coding: Mathematical Methods and Algorithms.* Wiley, 2005, pp.181-192.

[40] B. Li, S. Zhou, M. Stojanovic, L. Freitag, and P. Willett, “Non-uniform doppler compensation for zero-padded ofdm over fast-varying underwater acoustic channels,” in *OCEANS 2007-Europe*, pp. 1–6, IEEE, 2007.

[41] P. H. Moose, “A technique for orthogonal frequency division multiplexing frequency offset correction,” *Communications, IEEE Transactions on*, vol. 42, no. 10, pp. 2908–2914, 1994.

[42] M. V. Afonso, J. M. Bioucas-Dias, and M. A. Figueiredo, “Fast image recovery using variable splitting and constrained optimization,” *Image Processing, IEEE Transactions on*, vol. 19, no. 9, pp. 2345–2356, 2010.

[43] V. Fischer, A. Kurpiers, and D. Karsunke, “Ici reduction method for ofdm systems,” in *Hamburg: 8th International OFDM-Workshop*, pp. 1–5, 2003.

[44] W. G. Jeon, K. H. Chang, and Y. S. Cho, “An equalization technique for orthogonal frequency-division multiplexing systems in time-variant multipath channels,” *Communications, IEEE Transactions on*, vol. 47, no. 1, pp. 27–32, 1999.

[45] G. Leus, “On the estimation of rapidly time-varying channels,” in *Signal Processing Conference, 2004 12th European*, pp. 2227–2230, IEEE, 2004.

[46] x. ma and a. touzni, “ofdm channel estimation,” Jan. 29 2011. european patent 2070280 b1.

[47] X. Ma and A. Touzni, “Ofdm channel estimation,” Dec. 20 2011. US Patent 8,081,690 european patent 2070280 B1.

[48] Y. Mostofi and D. C. Cox, “Ici mitigation for pilot-aided ofdm mobile systems,” *Wireless Communications, IEEE Transactions on*, vol. 4, no. 2, pp. 765–774, 2005.

[49] M. Morelli and U. Mengali, “A comparison of pilot-aided channel estimation methods for ofdm systems,” *Signal Processing, IEEE Transactions on*, vol. 49, no. 12, pp. 3065–3073, 2001.

[50] T. W. Takeshi Kano, “Improvement of channel estimation for chinese dtmb sc-mode,” *The 26th International Technical Conference on Circuits/Systems, Computers and Communications (ITC-CSCC 2010),Pattaya Chonburi, Thailand*, pp. 462–465, 2010.

[51] T. W. Akio CHIMURA, “Improvement of channel estimation for 3.9g lte downlink,” *The 26th International Technical Conference on Circuits/Systems, Computers and Communications (ITC-CSCC 2011), Gyonjyu, Korea*, pp. 562–565, June 2011.

[52] M. V. Afonso, J. M. Bioucas-Dias, and M. A. Figueiredo, “An augmented lagrangian approach to the constrained optimization formulation of imaging inverse problems,” *Image Processing, IEEE Transactions on*, vol. 20, no. 3, pp. 681–695, 2011.

[53] I. Selesnick, “L1-norm penalized least squares with salsa,” *Connexions*, 2014.

[54] G. Strang, *Computational science and engineering*, vol. 1, pp.563-571. Wellesley-Cambridge Press Wellesley, 2007.

[55] Z. Hong, L. Zhang, and L. Thibault, “Channel estimation and ici cancellation for ofdm,” Aug. 9 2011. US Patent 7,995,688.

[56] Z. Hong, L. Zhang, and L. Thibault, “Iterative ici cancellation for ofdm receiver with residual carrier frequency offset,” in *Vehicular Technology Conference (VTC Fall), 2011 IEEE*, pp. 1–5, IEEE, 2011.